Dynamique interne des flavoprotéines étudiée par spectroscopie femtoseconde

Lipsa Nag

▶ To cite this version:

Internal dynamics of flavoproteins studied using femtosecond spectroscopy

LIPSA NAG

Composition du Jury :

Stephen Meech
School of Chemistry, University of East Anglia   Président

Thomas Gustavsson
LIDYL, CEA Saclay   Rapporteur

Catherine Berthomieu
LIPM, CEA Cadarache   Rapporteur

Joanna Brazard
IPCMS, University of Strasbourg   Examinateur

Marten H. Vos
LOB, Ecole Polytechnique   Directeur de thèse

Ursula Liebl
LOB, Ecole Polytechnique   Co-directeur de thèse

যদি তোর ডাক শুনে কেউ না আসে তবে একলা চলো রে॥

রবীন্দ্রনাথ ঠাকুর

Acknowledgements

"Clouds come floating into my life, no longer to carry rain or usher storm, but to add colour to my sunset sky."- Rabindranath Tagore

Firstly, my sincere gratitude to François Hache for accepting my application to work towards a PhD at the LOB. I am forever indebted to my supervisor Marten Vos for his steadfast scientific direction and support and without whom this thesis would not have been possible. My sincere thanks to Ursula Liebl for co-supervising my thesis and for many interesting biology discussions. I would also like to give special thanks to my jury: my reviewers Thomas Gustavsson and Catherine Berthomieu, examiner Johanna Brazard and the jury's president Stephen Meech. Their insightful reports and questions made the joy of finishing my dissertation even sweeter.

Our work on TrmFO progressed with immense help from Pierre Sournia and Mayla Salman, who were always available to answer all my questions. I am grateful to Jean-Christophe Lambry for molecular dynamics simulations which helped us understand this work in depth. I am also thankful to Hannu Myllykalio for his valuable suggestions throughout this work.

I am glad to have had the opportunity to work on an interesting and rewarding scientific project for three years. My scientific journey became more vibrant thanks to my wonderful colleagues at LOB who filled my life with colour. Thank you Emilie, Laura, Marco, Mayla, Olga, Pierre and Xiujun. Thank you also to Hélène, Joséphine, Guillaume, Lamiae, Thuy, Paul and Lien for making our office so lively! I'm grateful for the many friends I have made here, which makes this parting bittersweet.

No amount of words are enough to express my gratitude towards my parents. It wouldn't have been possible to embark upon my scientific adventure without their unfailing support. Thank you to my sister and brother, who are both my strength and the cause of my undoing. Lastly, thank you to Dhruv for always living up to his name.

Abstract

Nature employs charge transfer reactions in many biological functions. Redox-active cofactors like flavins (FAD and FMN) are often implicated in such reactions. Long-range charge transfer in proteins often proceeds via formation of radical intermediates. The aromatic amino acids tyrosine (TyrOH) and tryptophan radicals are thought to play important roles as intermediates in intra- and interprotein charge transfer reactions. Tryptophanyl radicals, in their protonated cation and deprotonated neutral form, have been observed and characterized before. However, tyrosyl radicals had only been characterized in the neutral form, and were thought to be formed by concerted electron extraction and deprotonation of tyrosine. Short-lived intermediates are often difficult to observe directly in biochemical reactions, but may be populated when they can be photochemically formed using short light pulses.

In this work, we have characterized intermediates in non-functional charge transfer reactions in flavoproteins using femtosecond time-resolved fluorescence and absorption spectroscopy. With the initial aim to study active site flexibility, excited states and product states formed in the wild type and mutant forms of the methyltransferase flavo-enzyme TrmFO from Thermus thermophilus were investigated. In the active site of this enzyme, a tyrosine (Tyr343), is closely stacked on the flavin isoalloxazine ring and a cysteine (Cys51) can form a highly fluorescent adduct with the flavin. In the mutant C51A fluorescence of FAD_{ox} is strongly quenched by electron transfer from the tyrosine in $\sim$1 ps. The resulting product state displayed a distinct spectral feature, a strong absorption band at $\sim$490 nm that did not correspond to any previously characterized radical species. It was assigned to the radical cation of tyrosine (TyrOH$^{\bullet+}$) which had never been observed before. The FAD$^{\bullet-}$ TyrOH$^{\bullet+}$ intermediate, is very short-lived as it decays in $\sim$3 ps, back to the initial state by charge recombination. An important general conclusion of the work on this model system is that, despite the very low pKa of TyrOH$^{\bullet+}$, electron transfer from tyrosine can take place without concomitant proton transfer.

We also performed polarization photoselection experiments to estimate the dipole moment direction for this new transition. The resultant angle between the excited FAD_{ox} transition and the probed TyrOH$^{\bullet+}$ transition in C51A TrmFO was $31° \pm 5°$.

This result sets limits to the orientation of the dipole moment of the transition in the molecular frame of the phenol ring. Moreover, the finding of distinct directions for the excited flavin transition band and the 490 nm transition provides a valuable confirmation of their origin in different molecular enitities.

Based on the above results from TrmFO, we reinvestigated the photochemistry in the model flavoprotein glucose oxidase (GOX) with transient absorption and fluorescence spectroscopy. Here, both tryptophan and tyrosine residues are located in the vicinity of FAD and the photoproduct evolution on the picosecond timescale is more complex. Distinct phases of excited state decay with time constants of 1 ps and $\sim$4 ps were observed, as well as phases of $\sim$4 ps, $\sim$37 ps and a longer-lives phase for product state evolution. Analysis of these phases resulted in a comprehensive model for the involvement of tyrosine and tryptophan radicals, as well as the different FAD redox states, in the light-induced charge separation and recombination in GOX. To account for the ensemble of data, partial involvement of the TyrOH$^{\bullet+}$ radical cation, showing similar spectral properties as in C51A TrmFO, was required for the 4-ps and 37-ps phases. This result explains previous enigmatic features and indicates the involvement of TyrOH$^{\bullet+}$ in a variety of protein systems.

So far, only the deprotonated tyrosyl radical TyrO$^{\bullet}$ has been observed as a functional intermediate in systems such as ribonucleotide reductase, photosystem II and certain photolyases. The visualization of a TyrOH$^{\bullet+}$ radical cation in TrmFO C51A and GOX suggests the possibility of its intermediate formation as a precursor of TyrO$^{\bullet}$ in functional biochemical reactions, light-driven or not-light driven.

Finally, in TrmFO the construction of variants altered at several positions with site-directed mutagenesis was initiated with the aim to identify systems suitable for studying active-site flexibility using electron transfer rates as conformational markers. Further experimental and modeling work is required to pursue this goal.

Résumé en français

La nature utilise des réactions de transfert de charge (TdC) dans de nombreuses fonctions biologiques. Les cofacteurs à activité redox, comme les flavines (FAD et FMN), sont souvent impliqués dans ces réactions. Le TdC à longue distance dans les protéines s'effectue souvent par la formation d'intermédiaires radicalaires. Les acides aminés aromatiques tyrosine (TyrOH) et tryptophane sont considerés à jouer un rôle important en tant qu'intermédiaires. Les radicaux tryptophanyle, avaient été observés et caractérisés auparavant dans leurs formes cation protoné et neutre déprotoné, Cependant, les radicaux tyrosyles n'avaient été caractérisés que dans la forme neutre et on pensait qu'ils étaient formés par extraction électronique et déprotonation concertée de la tyrosine. Les intermédiaires à courte durée de vie sont souvent difficiles à observer directement dans les réactions biochimiques, mais peuvent être peuplés s'ils sont formés photochimiquement par de courtes impulsions.

Ici, nous avons caractérisé des intermédiaires dans des réactions non-fonctionnelles de transfert de charge dans des flavoprotéines en utilisant la spectroscopie femtoseconde de fluorescence et d'absorption. Dans le but initial d'étudier la flexibilité du site actif, des états excités et produits formés dans le type sauvage et des formes mutantes de la flavo-enzyme méthyltransférase TrmFO de Thermus thermophilus ont été étudiés. Dans le site actif de cette enzyme, une tyrosine (Tyr343) est empilée sur le cycle isoalloxazine de la flavine, et une cystéine (Cys51) peut former un adduit avec la flavine très fluorescent. Dans le mutant C51A, la fluorescence du FAD_{ox} est fortement quenchée par transfert d'électrons de la tyrosine dans $\sim$1 ps. L'état produit résultant présentait une caractéristique spectrale distincte, une forte bande d'absorption à $\sim$490 nm qui ne correspondait à aucune espèce radicalaire précédemment caractérisée. Il a été attribué au cation radical de la tyrosine ($TyrOH^{\bullet+}$) qui n'avait jamais été observé auparavant. L'intermédiaire $FAD^{\bullet-}$ $TyrOH^{\bullet+}$, est de très courte durée car il retombe, en $\sim$3 ps, vers l'état initial par recombinaison de charge. Une conclusion générale importante de ces travaux est que, malgré le très bas pKa de $TyrOH^{\bullet+}$, le transfert d'électrons à partir de la tyrosine peut avoir lieu sans transfert concomitant de proton.

Nous avons aussi réalisé des expériences de photosélection par polarisation pour estimer l'orientation du moment dipolaire de la nouvelle transition. L'angle établi entre les transitions FAD_{ox} et $TyrOH^{\bullet+}$ dans le TrmFO C51A était de 31° ± 5°. Ce résultat pose des limites pour l'orientation du moment dipolaire au sein du cycle phénolique. De plus, la découverte de directions distinctes pour la bande de transition de la flavine excitée et la transition à 490 nm confirme leur origine dans différentes entités moléculaires.

Sur la base des résultats de TrmFO, nous avons réexaminé la photochimie dans la flavoprotéine modèle glucose oxydase (GOX). Ici, des résidus de tryptophane et de tyrosine sont situés proche du FAD et l'évolution du photoproduit à l'échelle picosecondes est plus complexe. Des phases distinctes de déclin de l'état excité avec des constantes de temps de 1 et $\sim$4 ps ont été observées, ainsi que des phases pour l'évolution de l'état produit de $\sim$4 ps, $\sim$37 ps et une phase plus longue. L'analyse a abouti à un modèle complet de la séparation des charges et la recombinaison photo-induites dans GOX impliquant, des radicaux de tyrosine et de tryptophane, ainsi que des différents états redox du FAD. Pour tenir compte de l'ensemble des données, pour les phases de 4 ps et de 37 ps une implication partielle du cation radical TyrOH$^{\bullet+}$, avec des propriétés spectrales similaires à celles du C51A TrmFO, était requise. Ce résultat explique des caractéristiques énigmatiques connues et indique l'implication de TyrOH$^{\bullet+}$ dans divers systèmes protéiques.

Jusqu'à présent, seul le radical tyrosyle déprotoné TyrO$^{\bullet}$ a été observé comme intermédiaire fonctionnel dans des systèmes tels que la ribonucléotide réductase, le photosystème II et certaines photolyases. La visualisation d'un radical cation TyrOH$^{\bullet+}$ dans TrmFO C51A et GOX suggère la possibilité de sa formation intermédiaire en tant que précurseur de TyrO$^{\bullet}$ dans des réactions biochimiques fonctionnelles, déclenché par la lumière ou non.

Finalement, dans TrmFO, la construction de variantes modifiées à plusieurs endroits par mutagénèse dirigée a été initié dans le but d'identifier des systèmes appropriés pour étudier la flexibilité du site actif en utilisant la vitesse de TdC comme marqueur conformationnel. D'autres travaux sont nécessaires pour poursuivre ce voie.

Contents

Chapter 1

Introduction

Charge transfer reactions involve the movement of electrons and/or protons from donor to acceptor molecules. Many biological functions rely greatly on charge transfer reactions. Such processes include photosynthesis, mitochondrial respiration (cytochrome c oxidase), DNA repair (photolyase), light sensing (BLUF domain, cryptochrome), among many others. Charge transfer proteins routinely employ specialized redox cofactor molecules. Biochemical charge transfer can be inter- or intraprotein in nature and often involves intermediates to form bridges in the charge transfer pathway between the redox centres. Visualization and characterization of intermediates formed during charge transfer reactions can shed light on their role in the function of proteins.

As charge transfer reactions involve the movement of small entities, they are often very rapid in nature. Short-lived intermediates in functional biochemical reactions can therefore be challenging to characterize. In this work, we have studied non-physiological charge transfer reactions triggered by impulsive perturbation with light using time-resolved spectroscopy in non-light activated proteins. Here, the electronic excited state created by the absorption of a photon by a coloured cofactor, flavin, acts as an electron acceptor for close-lying electron donors. This allows for the real-time characterization of the ensuing radical pair intermediates prior to their recombination.

Tyrosine (Tyr) and tryptophan (Trp) residues frequently act as reaction intermediates in biological charge transfer reactions. While tryptophanyl radicals have been characterized in both their protonated and neutral form, at the start of this thesis tyrosyl radicals had only been characterized in the neutral form. Moreover, the protonated tyrosyl radical (TyrOH$^{\bullet+}$) had been suggested to not form due to concomitant proton transfer. The main aim of this work was to characterize short-lived radical intermediates involving Tyr. Light-triggered charge transfer reactions were therefore investigated in the flavoproteins TrmFO (from the bacterium *Thermus thermophilus*, *Tt*TrmFO) and glucose oxidase (from the fungus *Aspergillus niger*, GOX), both of which harbour a Tyr residue close to the flavin active site. For the first

time, the TyrOH$^{\bullet+}$ radical has been observed to form and has been characterized in both systems.

Chapter 2 starts with a description of the evolution of studies on biological charge transfer. The roles of different protein components involved in these reactions are also explained. The use of light to trigger charge transfer reactions in proteins has been justified as well as its role as a probe to observe reaction intermediates. The prevailing theory of charge transfer, used in the context of biochemical reactions is also summarized in this chapter. Finally, some relatively well-studied charge transfer systems are briefly introduced to the reader as examples of the role of intermediates biological charge transfer reactions.

This thesis describes studies performed on flavoproteins. **Chapter 3** introduces the reader to flavoprotein photochemistry. The different redox and protonation states of flavins have been elucidated. The advantages of specifically flavoproteins in observing intermediates of Tyr and Trp is explained. Furthermore, this chapter describes the current state of the art in the characterization of radicals of Tyr and Trp.

Chapter 4 briefly summarizes the early motivation for this work, which was based on flexibility studies performed on the active site of the flavoprotein ThyX from *Thermotoga maritima*. Since TrmFO is a functional homologue of ThyX and both proteins were discovered by members of the Laboratoire d'Optique et Biosciences, studies on the flexibility of the active site of *Tt*TrmFO were a natural progression. This chapter also describes the change in the primary aim of this work to the identification and characterization of the properties of the FAD* quencher Tyr343 in *Tt*TrmFO.

The experimental techniques used in this work have been described in **Chapter 5**. The molecular biological and biochemical techniques to express and purify wild type and genetically modified TrmFO proteins are briefly introduced. Time-resolved pump-probe spectroscopy is used extensively in our measurements and a brief general description of this method has been provided. Subsequently, the time-resolved fluorescence and absorption setups have been described extensively.

Figure 1.1 shows a graphical representation of the visualization of light-triggered electron transfer in *Tt*TrmFO- the major focus of **chapter 6**. In this chapter, the main results obtained on electron transfer in *Tt*TrmFO have been presented in detail. The reasons for focussing on mutant TrmFO C51A are elucidated. Time-resolved fluorescence was performed to visualize the excited state FAD in TrmFO and its mutants. Time-resolved absorption was performed in tandem to visualize both excited and product states formed in TrmFO mutants. Subsequently, deconvolution of a decay
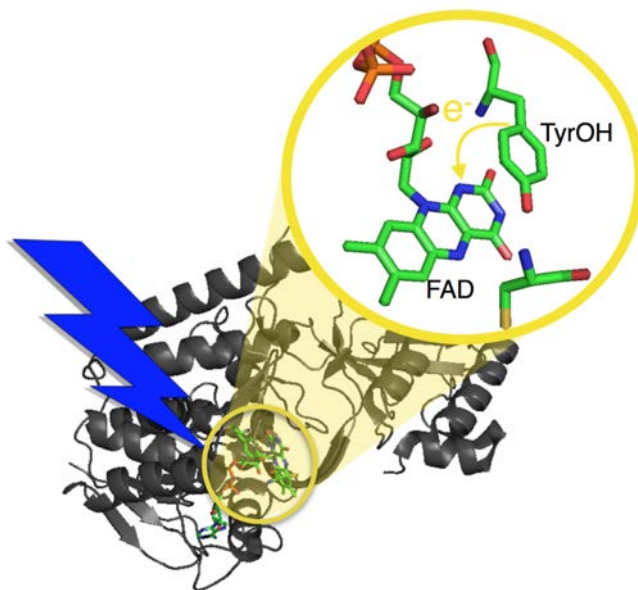
Figure 1.1: *Light-triggered electron transfer in TrmFO from Thermus thermophilus.*[1]

associated difference spectrum leads to the identification and characterization of the TyrOH$^{\bullet+}$ intermediate. Furthermore, the direction of the transition dipole moments were studied using polarization photoselection experiments.

Chapter 7 describes similar experiments (as above) on the model flavoprotein GOX. TyrOH$^{\bullet+}$ was observed in two decay phases of in the transient absorption spectra of GOX. Through spectral deconvolution, the spectrum of TyrOH$^{\bullet+}$ was calculated for each phase and compared with that observed for TrmFO C51A. Finally, a kinetic model was proposed for the charge transfer processes in light-triggered GOX.

Overall conclusions and perspectives of this work are presented in **chapter 8**.

Chapter 2

Charge transfer in biological systems

2.1 Overview

Redox charge transfer reactions are ubiquitous in biological systems. They involve the movement of electrons and protons, which are sometimes coupled. They can play an important role in energy transduction pathways in living organisms like photosynthesis[2] and respiration.[3] They are also associated with processes like signalling[4] or catalysis.[5] Charge transfer proteins are of interest to a wide community of researchers as understanding them can shed light on fundamental biological phenomena which are relevant for designing biocatalysts[6] and artificial photosynthesis systems[7,8] among others.

Movement of small charged entities (electrons and protons) is often very rapid. High speed of charge-transfer steps can often be advantageous in biological systems because it prevents them from being rate-limiting in protein-substrate interaction processes. Conversely, this often makes pure redox intermediates elusive and difficult to characterize in enzymatic catalysis.

A major reason for the initiation of the wide range of studies in the field of charge transfer came from the development of instrumentation which enabled the study of rates of rapid chemical reactions. Electron transfer reactions are among the fastest to occur in nature. Some of the earliest experiments were performed using rapid mixing technology (stopped flow) on inorganic chemical model systems and charge transfer was observed with a time-resolution in the order of milliseconds.[9] With the advent of lasers and the concurrent development of newer spectroscopic technologies, it has become possible to visualize faster electron transfer processes, eventually down to the picosecond and sub-picosecond regime, for cases where the reaction can be initiated by light. This has proven to be particularly useful in the case of light-driven biological systems, as electron transfer has been observed to occur over a wide range of timescales:

starting from microseconds/milliseconds (timescale typical for catalytic turnover) going down to femtoseconds.

In mixing methods, the protein is modified by binding of external molecules. Here, the technology-limited mechanical mixing speeds, or intrinsic binding rates, limit the local perturbation created in the protein. Hence, the first electron transfer steps are often too fast to be observed by stopped flow techniques. Laser-based technologies have proved to be especially useful for observing charge transfer in biological systems. Pulsed lasers are able to create flash perturbations (down to femtosecond duration since the 1980s) within the protein. This can induce electron transfer in the protein which is often orders of magnitude slower than the impulsive light perturbation, making its signal easy to resolve. Electron transfer reactions can be characterized by measuring various parameters like rates, activation energy, temperature dependence. In order to determine rates, we measure changes in the physical properties of the donor and acceptor moieties, in particular their optical absorption and emission spectrum. It is therefore convenient to also use light for this purpose, as it can monitor changes in the redox state of the sample with high time resolution. Incidentally, many biological redox partners are coloured as they consist of cyclic extended π-conjugated systems that absorb in the visible region. As will be emphasized below, such approaches are limited to (not necessarily naturally) light-activatable proteins.

Productive long-range biological electron transfer can occur either between different proteins or between multiple redox centres located within the same protein. Electron transfer proteins appear to be naturally designed to contain robust redox centres to facilitate their function (even when exposed to limited thermal fluctuations and genetic modifications).[10] In 1951 Michaelis, in the context of oxidoreductase protein design, wrote that "proteins must bring redox centres together".[11] At the time, initial models to describe electron transport within proteins were still under development. In 1956, Chance and Williams realized that a rigid structure with immobilized redox centres would require the encapsulating polypeptides to act as electron conductors or semiconductors.[12,13] As these requirements could not be reconciled with the actual properties of enzymes, they suggested that thermally promoted conformational changes could lead to the encounter of redox cofactors. Also in 1956, Marcus first wrote about electron transfer theory. Initially, this was in the context of pure chemical reactions. Ultimately the theory has been widely used in various forms for decades in biochemical studies.[14,15]

2.2 Electron transfer theory

As interest in reaction kinetics and electron transfer grew after 1945, the field was characterized by a strong cooperation between theory and experiments.[16] With increased availability of isotopes after the second world war,[17] electron transfer reactions were studied extensively using isotope exchange reactions. This approach proved useful in observing simple electron transfer in homogeneous inorganic chemical systems.[9,17,18] Such reactions were of the type:

$$Fe^{2+} + Fe^{*3+} \rightleftharpoons Fe^{3+} + Fe^{*2+} \tag{2.1}$$
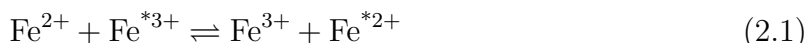
where * designates the labelled isotope.

These reactions are relatively straightforward to interpret as the reactants are the same as the products (but for the isotope substitution) thus eliminating the need to account for the relative thermodynamic stability of reactants and products. More generally, electron transfer reactions represent the simplest class of reactions in chemistry as no bonds are broken or made in an elementary electron transfer process.

Several theories have been proposed to describe such reactions.[14,19,20] The most successful among them appeared to be the one proposed by Marcus for calculating rates in outer-sphere electron transfer reactions in 1956,[14] coincidentally at the same time as Chance and co-workers (section 2.1) were experimentally studying electron transfer. In later years, Marcus extended the application of this theory to include biological systems.[15] This is perhaps the simplest among the theories to describe electron transfer. For this reason, it has also gained a wide-ranging support from researchers, including biologists.

The initial molecular events in light-based perturbations, the absorption of photons by coloured entities, are extremely fast. They consist of electronic transitions within the molecule from the ground state to an excited state. According to the Franck-Condon principle, these transitions can be regarded as occurring in a stationary nuclear framework i.e., they would be vertical in energetic diagrams such as those of Fig.2.1.

Marcus implemented a slight variation to the Franck-Condon principle. He proposed that thermal fluctuations (including those for surrounding solvent molecules) of the nuclei of reactants and products bring the system in a configuration favourable for barrier crossing to occur on a much longer timescale than the electron displacement from donor to acceptor itself. Fig. 2.1 shows the reactant and product Gibbs energy surfaces represented as parabolas characteristic of harmonic oscillators as a function of reaction coordinate (which accounts for nuclear coordinates). The geometry of these parabolas can be used
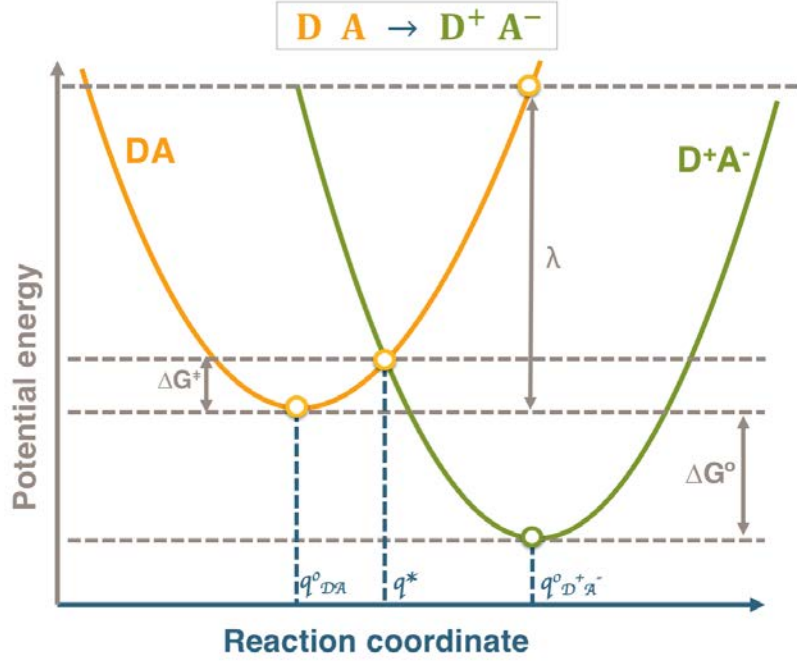
Figure 2.1: *Potential energy curves assuming harmonic oscillators of the reactants (D + A) and products (D⁺+A⁻), where D is donor and A is acceptor. In the plot, q^0_{DA} and $q^0_{D^+A^-}$ represent the position of the potential energy minima of the reactants and products respectively. The two parabolas intersect at q*. Gibbs energy of activation ($\Delta G^‡$), standard Gibbs energy ($\Delta G°$) and reorganizational energy (λ) have also been represented.*

to predict reaction rates and kinetic barriers. The electronic and nuclear terms can then be regarded separately while calculating the rate:

$$k_{ET} = \frac{2\pi}{\hbar}(EC)(FC) \tag{2.2}$$

where EC is the electronic coupling term and FC is the (nuclear) Franck Condon term.

Electron transfer can occur when thermal fluctuations bring the reaction coordinates of the reactants to q* (Fig. 2.1), where the parabolas for reactants and products intersect. The potential energy minima of the reactants and products are represented by q^0_{DA} and $q^0_{D^+A^-}$ respectively (Fig. 2.1). Gibbs energy of activation ($\Delta G^‡$) is the energy required by the reactants to go from q^0_{DA} to q*, and is the energy required for self-exchange reactions (described in Equation 2.1).

It can be inferred from Equation 2.2 that the probability of electron transfer depends on the probability of the reactants to reach the $q*$ configuration and on the probability of moving to the product energy surface after this, which itself depends on the electron coupling between the DA state and the D⁺A⁻ state. The reorganizational energy (λ) is an energy change resulting from the molecular rearrangement that occurs as the charge distribution is altered in the donor-acceptor complex in the (protein)

14

medium as well as in the surrounding solvent molecules. The driving force of the reaction, ΔG°, has also been indicated in Fig. 2.1.

For one-step reactions, the main mechanism of electron transfer is tunnelling through the potential energy barrier. For efficient tunneling, there needs to be an overlap between the wavefunctions of the reactants and products. The electronic coupling term, EC, within a homogeneous medium has been described by Hopfield[21] in 1974 as proportional to the square of the coupling hamiltonian energy H_{DA} which can be written as

$$EC = \langle H_{DA}\rangle^2 = \langle H_{DA}{}^0\rangle^2 e^{-\beta r} \tag{2.3}$$

where r is the edge-to-edge distance between the donor and acceptor and β is a constant reflecting the speed at which the exponential wavefunctions of donor and acceptor decrease within the medium. $\langle H_{DA}{}^0\rangle$ stands for the electronic coupling matrix element when the donor and acceptor are in contact ($r = 0$). In this formalism, the electronic coupling between donor and acceptor decreases exponentially as the distance (r) between them increases.

In the classical limit, the rate of electron transfer from donor to acceptor can be described by

$$k_{ET} = \frac{2\langle H_{DA}\rangle^2}{h}\left(\frac{\pi^3}{4\lambda RT}\right)^{1/2} e^{-\Delta G^\ddagger/RT} \tag{2.4}$$

Furthermore, from Equation 2.4, the Gibbs energy of activation ($\Delta G\ddagger$) can also be represented in terms of the driving force (ΔG°) and the reorganizational energy as (λ)

$$\Delta G^\ddagger = \frac{(\Delta G^\circ + \lambda)^2}{4\lambda} \tag{2.5}$$

It can be seen intuitively that with the disposition of the parabola in Fig. 2.1, the rate increases as the driving force (ΔG°) increases. Fig. 2.2 shows the dependency of the rate of electron transfer on the driving force (ΔG°). It can be inferred that electron transfer becomes more efficient when ΔG° becomes negative in the normal Marcus region. At $\Delta G^\circ \approx -\lambda$, $\Delta G^\ddagger \approx 0$ and electron transfer is barrierless. In the third case, as the driving force is increased further, electron transfer enters the Marcus inverted region and the rate decreases again. The three regions have been indicated in Fig. 2.2. All this indicates that for optimal electron transfer, nuclear rearrangements accompanying electron transfer must be compensated for by the reaction driving force. Gray and Winkler suggest that this balance between ΔG° and λ is a direct consequence of protein structure.[13] They suggest that biological electron transfer over long distances is possible because protein folds create a suitable balance between ΔG° and λ, as well as adequate coupling between redox centres.
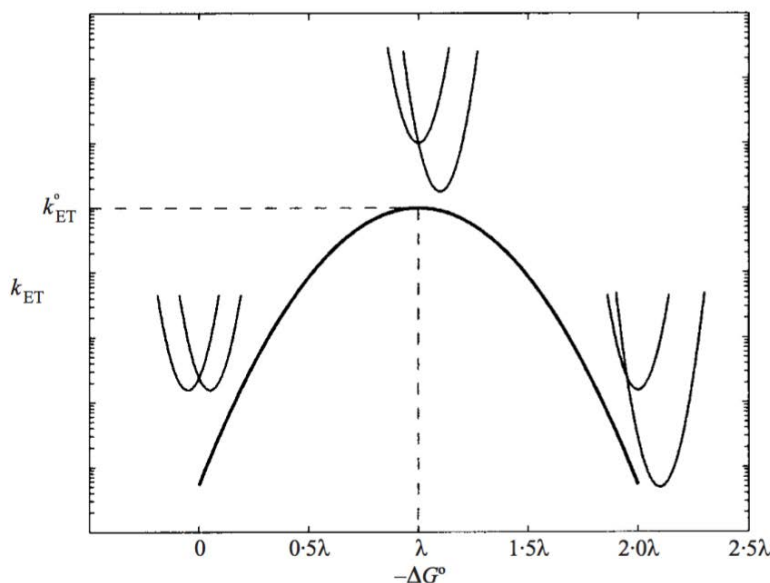
Figure 2.2: *Dependence between the rate of electron transfer k_ET and driving force $\Delta G°$ as derived from equations 2.4 and 2.5. Rates keep increasing (from left to right) with driving force until they reach the barrierless electron transfer regime (where $\Delta G° \approx -\lambda$). Following this, electron transfer rates keep decreasing as $\Delta G°$ continues to increase. This is the inverted region. (Source: Gray and Winkler[13])*

It must be noted that the above relations are at the semi-classical limit of Fermi's Golden rule and are valid only when nuclear motions can be treated classically. This is possible at high temperatures and when electronic coupling between the donor and acceptor is weak (below a few tens of cm^{-1}).[22] At low temperatures, in principle, quantization of the energy levels has to be taken into account. At the adiabatic limit, coupling between DA and D$^+$A$^-$ states is very strong and surface hopping at q^* has a high probability. Thus, for strongly coupled systems, electron transfer depends on the rate of reaching $q*$.

The coupling term proposed by Hopfield[21] is applicable for weakly coupled systems. The formalism implies that the donor and acceptor are separated by a homogeneous medium, and therefore electronic coupling decays exponentially with distance (Equation 2.3). As mentioned earlier, the decay of this electronic coupling is represented by the constant β in Equation 2.3. On representing the medium by a single constant β, it is assumed that it is homogeneous. However, the nature of the medium of electron transfer proteins has long been a subject of debate.

The simplest view advocated by Dutton and co-workers is to assume homogeneity of the protein medium through the uniform-barrier model. In this analysis, they take β to be the same for all electron transfer reactions at am empirical value of $\beta = 1.4 \mathring{A}^{-1}$.[10,23]

To a first order approximation, they described the rate of electron transfer at room temperature is given by:[10]

$$\log k_{ET} = 13 - 0.6(r - 3.6) - 3.1\frac{(\Delta G^\circ + \lambda)^2}{\lambda} \tag{2.6}$$

The assumption of a uniform β presupposes that biological electron transfer is independent of the nature and structure of the biological medium. This view is likely quite valid for very long-range reactions, where the atom-level details of the intervening media are effectively averaged. However, at shorter distances, small variations from this average value of β can lead to large changes in rate constants of biological electron transfer. Hence, structural dependencies of β have been invoked.[13] The packing density model introduced by Page, Dutton *et al.*[10] is another way to introduce structure dependent variation of β.

Interpreting the protein medium as heterogeneous, overall electronic coupling has been described by Gray and Winkler in the tunneling pathway model as arising from a combination of parallel pathways each consisting of distinct steps through covalent bonds, through hydrogen bonds and through space. The total coupling of a single pathway is given as a repeated product of coupling decays of individual links in the pathway.

Interpretations of β by uniform- barrier and tunneling pathway models are at odds for specific systems.[24] In many of these cases, there is a debate concerning the usage of edge-to-edge distances for calculation of electron transfer rates. As mentioned earlier, small changes in β can lead to larger changes in rates. In other cases, differences arise due to the method by which β was deduced. Ideally, values of β can be determined from electron transfer reactions at several donor-acceptor distances in the barrierless regime (See Fig. 2.2). The barrierless regime is not always determined, as it is not straightforward to construct a Marcus curve. Consequently, β is extracted from electron transfer reactions that are activated. This makes it difficult to disentangle the distance dependence of tunneling from that of the activated ET processes. Therefore, in our studies and interpretations, the edge-to-edge distances between donor and acceptor are linked qualitatively to the rate of electron transfer.

As the earlier work of Chance and Williams (see section 2.1), Page, Dutton *et al.* have described the fundamental design of electron transfer in proteins as "two catalytic sites connected by redox chains".[23] Catalytic sites have been described as multi-electron redox centres or groups of single-electron redox centres that communicate with substrates and behave as donors and/or acceptors of electrons. Chains are described as groups of single-electron redox centres containing wider separation among them, with fewer near-neighbours. Catalytic sites can be located within a single protein or placed

sufficiently close to each other to allow electron transfer without a connecting chain. Frequently, proteins contain one catalytic site linked to a redox cofactor chain. These chains link the catalytic site to those in other proteins or to the solvent. Common examples of "catalytic sites" are oxidizable or reductible metal cations like Cu^{2+}, Mg^{2+}, Fe^{2+} etc. They can also include organic cofactors of proteins like FAD, FMN, heme, chlorophyll, etc. some of which also harbour metal atoms. In the last decades it has also become apparent that examples of participants in the redox chain also include radical-forming amino acids such as tyrosine and tryptophan.

It has been observed that the edge-to-edge distance between the donor and acceptor in many natural electron transfer proteins extends from the point of van der Waal's contact to about 14 Å[10] for rates to be in a physiologically relevant regime. Generally for distances greater than 14Å, functional "long-range" charge transfer reactions between donor and acceptor redox centres are thought to be facilitated by such redox chains (bridges). The role played by the bridge entities has been considerably debated as the bridge-state energy is expected to have a marked influence on the ET mechanism.[25] Two electron transfer mechanisms have been suggested - superexchange and hopping. According to the superexchange mechanism, electron transfer proceeds directly from the donor to the acceptor without creating real intermediates among the bridge molecules.[26] Contrarily, when the orbital wavefunctions of the bridge molecules overlap with the donor and acceptor, the bridge molecules are directly involved as intermediates in electron transfer between the donor and acceptor. This mechanism is called hopping. Electron hopping involves multiple tunneling steps, often to promote charge separation within and between proteins, which is essential for instance in energy storage and conversion.[27]

In several studies, it has also been observed that electron transfer over very long distances occurs with the formation of charged bridge molecules as reaction intermediates[28,29] (lending credence to the hopping mechanism). An evaluation of the redox potentials of prospective chain elements is helpful in determining the possibility of formation of oxidized or reduced bridge intermediates. In proteins with a single redox cofactor, side-chains provide opportunities for multistage tunneling. While the redox potentials required to oxidise and reduce polypeptide side chains are generally high, the side-chains of certain amino acids (tyrosine and tryptophan) have redox potentials which are potentially suited to them[30–33] (See chapter 3).

In our study, we have performed fluorescence and absorption time-resolved spectroscopy on several flavoproteins. Through these techniques, we have deduced the rates of electron transfer from the neutral ground state amino acid donor to excited state acceptor. We have also discussed these rates in relation to the distance between

donor and acceptor entities. Analysis of electron transfer rate and distance relationships is facilitated by a consistent definition of the donor-acceptor distance. As FAD is a $\pi-$aromatic molecule, we have taken edge-to-edge distances using the shortest distance between the $\pi-$conjugated rings of the donor and acceptor.

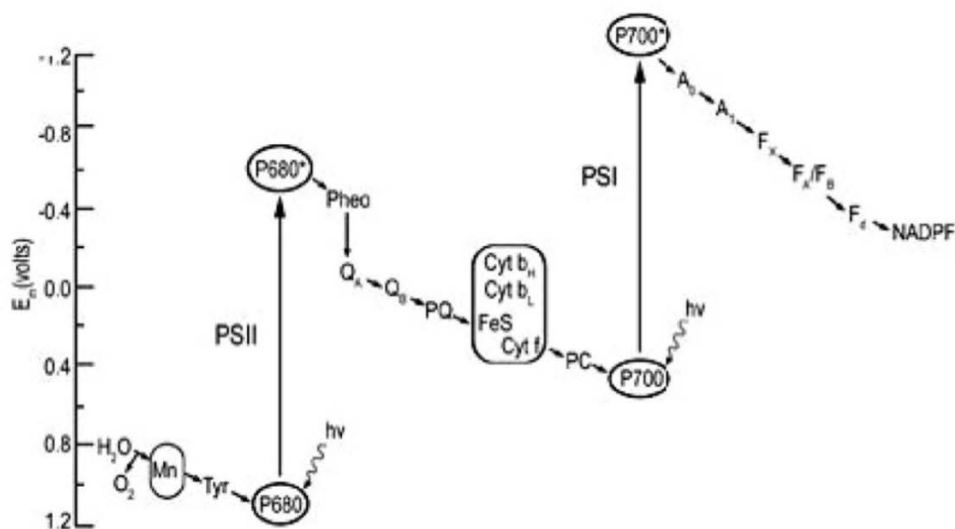## 2.3   Well-studied biological charge transfer systems

Figure 2.3: *Z-scheme of oxygenic photosynthesis showing the electron flow and the potentials of redox partners involved. Note: the tyrosine residue is involved in a charge transfer relay between P680 and Mn in the oxygen evolving complex of PSII.*[34,35]

Conversion of light energy to electrical energy to chemical energy has been famously studied in photosynthetic reaction centres.[2] In the initial stages for this process, photons are acquired from sunlight to induce charge separation in a membrane-protein complex. This creates an electric potential and a proton gradient over the membrane which ultimately drives ATP synthesis. Photon absorption is enhanced by well-optimized antenna systems which funnel the excitation energy to the reaction centres (as seen in Fig. 2.3). This phenomenon occurs widely in green plants, algae and cyanobacteria. In plants, two reaction centres are used in series - photosystem II and photosystem I (Fig. 2.3). Among these, photosystem II (PSII) is unique as it catalyses the four-electron oxidation of two water molecules to O_2 in the oxygen evolving complex (Fig. 2.3). In fact, PSII is the only enzyme known to perform this function. In the oxygen-evolving complex, tyrosine plays an important role. Each charge separation event here proceeds via the reduction of the photo-oxidized chlorophyll dimer primary electron donor P680 by the nearby redox-active tyrosine ($\sim$ 20-200 ns)[36] and the

subsequent re-reduction of the tyrosyl by Mn ($30\mu s \sim 1ms$) range.

Oxygenic photosynthesis is the phenomenon in which water is oxidized using photons to yield O_2, four electrons and four protons. Reversely, respiration is the (non light-active) process in which O_2 is reduced using four electrons and four protons. Cytochrome c oxidase (CcO) is another prototypical protein in the study of biological charge transfer, and is an enzyme implicated in the mitochondrial (and bacterial) respiration process. During this process, it accepts electrons from one side of the mitochondrial membrane and protons from the other, thus creating an electrochemical proton gradient across the membrane. Although CcO is not functionally light-active, it has been studied using light to visualize the electron transfer pathways involved.[37] CcO contains four redox-active cofactors, two "a"-type hemes, and two copper centres, and accommodates four electrons in its fully reduced form.[37] The complex mechanism of O_2 reduction to H_2O in CcO mobilizes a number of redox carriers and is notably thought to involve a Tyr structuring the active site. This Tyr is cross-linked to a histidine residue, itself coordinating another redox carrier, a Cu atom. The formation of transient product states is linked to the proton pumping function of the enzyme.

Apart from photosynthetic and signalling proteins, there is a small group of "true" enzymes where the catalytic reactions are driven by light. These so-called photoenzymes use light as a substrate and therefore,require a continuous supply of light (of a certain energy) for their function. They contain cofactors which are chromophores and absorb the light. There are only three known classes of "true" photoenzymes - Photolyases,[38] Light-Dependent NADPH: Protochlorophyllide Oxidoreductases (LPORs) and the recently discovered fatty acid photodecarboxylase (FAP).[39] The light-activation of photolyase has been well studied and is described below.

DNA photolyase is an enzyme implicated in the light-induced repair of UV-damaged DNA in bacteria, plants and certain animals. Apart from photocatalysis involving electron transfer from the reduced flavin FADH$^-$ to the substrate, the protein performs a second photoreaction: preparing the catalytic state FADH$^-$ from the resting state FADH$^\bullet$. The latter reaction involves a triple tryptophan chain, which constitutes one of the best examples of redox-active components bridging a donor and acceptor. Here, the two redox centres are the solvent-exposed terminal tryptophan and the flavin radical cofactor FADH$^\bullet$. Electron transport through the protein is initiated by light absorption which creates the excited state of the flavin radical. An electron is then extracted from a nearby Trp (W382, Fig. 2.4) in $\sim$ 30ps. Subsequently, electrons move along the bridge of tryptophans (as shown in Fig 2.4) to stabilize the catalytically active FADH$^-$ in $\sim 30ps$. The latter processes occurs faster than the initial charge separation, leading to an effective overall trans-protein charge transfer in 30 ps.[40]
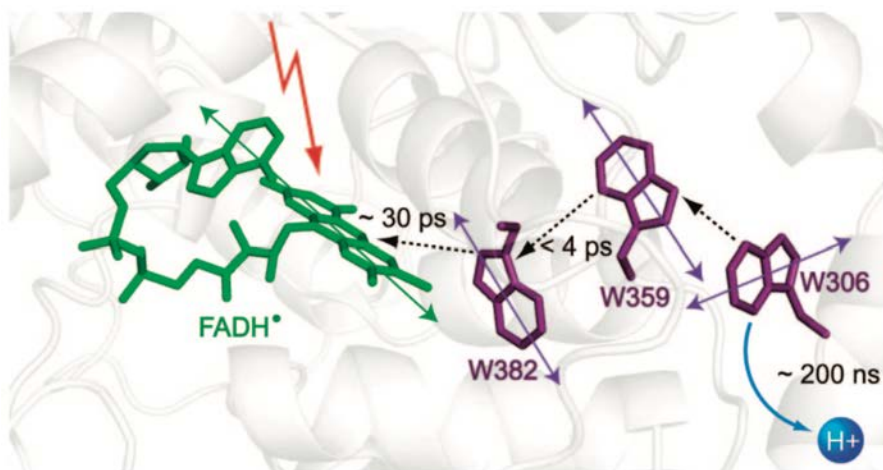
Figure 2.4: *Scheme of electron and proton transfer reaction chain in DNA photolyase from E. coli by Lukacs et. al..[40] The FADH• cofactor is excited and charge separation occurs as electrons hop through a chain of tryptophans.*

This reaction itself is challenging to study as the three bridge entities are chemically identical tryptophans. Complementary molecular biology and biophysical techniques such as site-directed mutagenesis and polarization photoselection[41] have aided in the experimental study of such systems. In the particular case of DNA photolyase, the reaction was studied by changing each tryptophan one-by-one in the chain to redox-inert phenylalanine.[40–43] It has subsequently been demonstrated that this tryptophan chain in DNA photolyase (Fig. 2.4) effectively acts as a "wire" within the protein to facilitate long-range electron transfer.[40]

While photoenzymes require continuous exposure to light to function, there are other enzymes which use light for signalling. They are called photoreceptors as they "receive" photons to signal a reaction. Many organisms in nature have developed light-sensing proteins to optimize certain functions. Mechanisms utilizing blue light have been observed to be involved in various biological functions[44] and are frequently mediated by proteins containing a flavin cofactor (see chapter 3). Flavin-binding blue-light photoreceptors can be categorized based on their structure and photochemistry into three distinct groups:

- light-oxygen-voltage (LOV) photoreceptors,

- sensors of blue-light using flavin adenine dinucleotide (FAD) (BLUF photoreceptors) and

- cryptochromes (CRYs)

Other classes of photoreceptors (not involving flavins) include rhodopsins (with the chromophore retinal),[45] phytochromes (with phytochromobilin), photoactive yellow

protein (with p-coumarin) and the UV sensor UVR8 (with 14 tryptophan residues).[46]

LOV domains are blue-light photoreceptors that contain a non-covalently bound flavin mononucleotide (FMN) or in some cases flavin adenine dinucleotide (FAD), which acts as a sensor for environmental stimuli such as light or oxygen.[47,48] This non-covalently bound flavin chromophore senses blue light in the 400-470 nm range. Upon light activation, it undergoes a reversible photocycle, what can be observed looking at the steady state spectra: under blue light illumination the structured 447 nm peak of the flavin disappears and a single non-structured band will rise around 390 nm. Due to the blue light irradiation flavin is promoted to the excited singlet state, which undergoes intersystem crossing to the excited triplet state. This is followed by adduct formation between the C4a atom of the flavin cofactor and the sulphur atom of the neighbouring cysteine.[49,50] In the dark, the flavin-cysteinyl adduct degrades slowly, on a time-scale from minutes to hours. This reverts the LOV domain to the ground state and concludes its photocycle. Natural systems utilize blue-light sensing of LOV domains to pass this information to the nearby effector domain that they are linked to.[51] This mechanism, that does not involve an electron transfer reaction, is used in phototropism,[52] stomatal opening and temporal circadian rhythms among others.

Proteins containing BLUF domains are responsible for photoadaptive responses of many prokaryotes and a few eukaryotes.[53,54] They are implicated in various reactions including phototaxis[55,56] and photosynthetic gene regulation[57,58] in phototrophic organisms, biofilm formation[59] along with virulence in pathogenic bacteria.[60,61] BLUF domains contain a non-covalently bound FAD as the light-absorbing cofactor. Like the LOV domain, the BLUF domain passes through a light and dark state during its photocycle. The light state of BLUF has been observed to be almost identical to the dark state, with spectra resembling that of oxidized FAD, except for a 10-15 nm shift of the 447nm peak to the red.[57,62] This red-shifted photoproduct relaxes to the dark state within seconds to minutes.[62,63]

Mechanisms of the BLUF domain proteins can differ from one organism to another. In AppA – the most studied BLUF domain protein – the protein initially forms a complex with a transcription factor (PpsR). Absorption of blue light would lead to larger structural change resulting in the release of PpsR, preventing the biosynthesis of the photosynthetic genes.[64] The mechanism which leads to this large structural movement and to the dissociation of the AppA-PpsR complex is still not completely elucidated and the mechanism of photoactivity changes in different BLUF domain proteins. In Pixd (Slr1694), which controls phototaxis in the cyanobacterium *Synechocystis* sp. PCC 6903 a proton coupled electron transfer was observed between the well conserved Y8 tyrosine and FAD.[65,66] Light absorption initially triggers the

formation of the anionic flavin radical, which is protonated in a few picoseconds (most probably by the tyrosine) forming the neutral flavin radical (see chapter 3 for flavin redox states). As the close tyrosine residue is well conserved – replacement with other amino acid abolishes the photoactivity of the protein – in all BLUF domain proteins it was proposed that a similar mechanism is responsible for the function of these photoactive flavoproteins. A similar mechanism was found to be present indeed in PapB where formation of the neutral semiquinone decays to the red shifted signaling state, in AppA however, the role of radical intermediates in the photocycle is debated and continues to be explored.[67] It has been suggested that the formation of radical intermediates is not necessary for BLUF domain activity.[67] Lukacs et al. have proposed a non-radical pathway for BLUF domain function which proceeds via keto-enol tautomerization.[67]
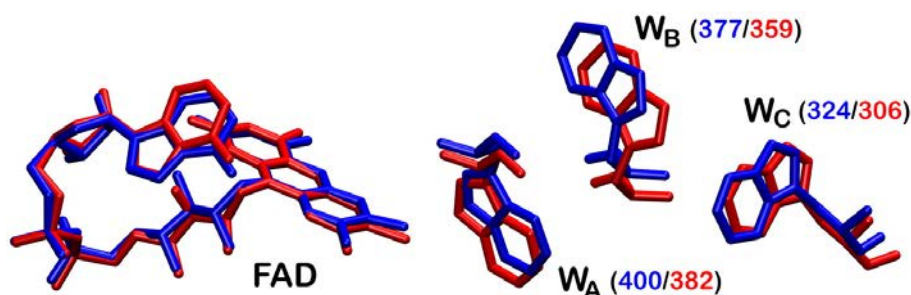

Figure 2.5: *Active site of cryptochrome from Arabidopsis thaliana[68] (in blue, PDB: 1U3D) overlaid with that of E. coli photolyase (in red, PDB: 1DNP). The electron is transported through a triad of tryptophans in cryptochrome similar to the mechanism in DNA photolyase. It has been proposed that magnetic sensitivity in cryptochrome is induced by radical formation of the FAD and the terminal tryptophan residue W_C.*

Electron transfer proved to be crucial in the function of *E. coli* photolyase which repairs the UV induced lesions in the DNA strand. In catalytically active photolyase the flavin is in its fully reduced form and upon blue light absorption an electron is ejected to the pyrimidine dimer thus breaking the bond. It is interesting that after purification in the majority of photolyases, FAD is in the neutral semireduced radical form, but it can be reduced by using visible light. In this process also ET takes place via a well conserved tryptophan triad.[69] Despite being homologous to photolyases, cryptochromes are involved in very different processes like the regulation of the hypocotyl growth in plants and entrainment of circadian rhythm in animals.[70] They have also been suggested to be sensors for the geomagnetic field to assist many animals in long-range navigation.[71,72] The formation of the signaling state in cryptochrome involves blue light-induced electron transfer to the FAD cofactor from a tryptophan triad (W400, W377, W324). These tryptophans are highly conserved among cryptochromes from many species and bridge the space between flavin and the protein surface (Fig. 2.5). The sequence of electron transfer steps result in an increased separation among the

radical pair, eventually leading to the formation and stabilization of the signaling state of cryptochrome (reported to be FADH⁻). It is interesting to note the similarity between the mechanisms of electron transfer in the homologous proteins DNA photolyase and cryptochrome, as they both proceed through a conserved tryptophan triad (Fig. 2.5).

Redox intermediates have also been observed, or inferred to form, in catalytic proteins which are photo-inactive. Class 1a ribonucleotide reductase (Class 1a-RNR) is an example of such a system. Ribonucleotide reductases (RNR) catalyse the reduction of nucleotides to 2'-deoxynucleotides, which are essential for the *de novo* synthesis of deoxyribonucleotides. As deoxyribonucleotides are precursors to DNA, RNRs are important for maintaining the precision of DNA replication and repair. They are found in all organisms and are classified based on the metal cofactor used to initiate catalysis.

Class 1a RNR contains a diferric-tyrosyl radical (TyrO$^{\bullet}$) as "cofactor". The prototypical class 1a RNR from *E. coli* is comprised of two subunits, $\alpha2$ and $\beta2$, and functions actively as an $\alpha2\beta2$ complex.[73] The $\beta2$ subunit contains the diferric-TyrO$^{\bullet}_{122}$ cofactor. The TyrO$^{\bullet}_{122}$ species is observed to show high stability, atypical for redox intermediates of amino acids, as it has a lifetime of 4 days. TyrO$^{\bullet}$ in solution has a lifetime of milliseconds, but the longer lifetime of TyrO$^{\bullet}_{122}$ in class 1a RNR is likely due to the fact that it is positioned in a hydrophobic pocket within the protein along with its position between the two Fe atoms. Additionally, it has also been proposed that a specific charge transfer pathway exists across the $\alpha2\beta2$ complex which contains four tyrosines involved in long-range charge transfer over 35 Å.[73] The individual charge transfer steps are linked to the RNR function of nucleotide reduction, and several TyrO$^{\bullet}$ intermediates have been visualized for these steps aided by protein engineering.
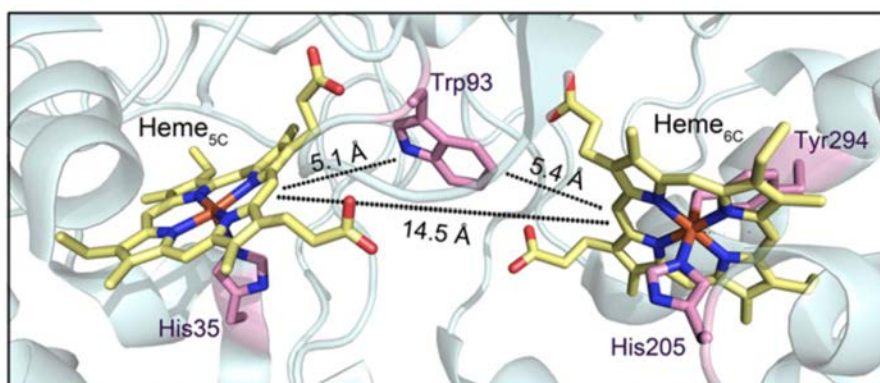

Figure 2.6: *Relative orientation of hemes and the intervening tryptophan residue (PDB: 3L4M) in the diheme center of MauG. The edge-to-edge distances between the indole side chain of Trp93 and each heme porphyrin ring, and between the two heme porphyrin rings have been indicated.*[74]

MauG is another protein whose main catalytic function is enabled by the formation of redox intermediates involving an aromatic amino acid residue. MauG is a diheme enzyme that catalyzes the final steps in the biosynthesis of the catalytic tryptophan tryptophenylquinone (TTQ) cofactor of methylamine dehydrogenase. It has been observed to contain an electron transfer chain containing two protein-bound hemes and a tryptophan residue.[74] Fig. 2.6 shows the diheme centre of MauG. The distances between the two hemes as well as their distances from Trp93 have been shown. This Trp-93 resides midway between the hemes, and each Fe(IV) heme (as shown in Fig. 2.6) has been noted to be a sufficiently strong oxidant for Trp$^\bullet$.

It has been proposed by Geng *et al.* that the charge equilibration proceeds through hole hopping via Trp93 without Trp radicals getting accumulated.[74] Their model supposes that rapid and reversible electron transfer occurs between the two hemes and the intervening Trp93 in the hopping site. It can be inferred that Trp93 intermediates form and decay rapidly within the MauG system. Such a "charge resonance" system between the two hemes has been suggested to be the basis of the stability of the *bis*-Fe(IV) species in MauG which is an intermediate in its catalytic reaction.

The systems that have been studied in this work, the t-RNA methyltransferase TrmFO from *Thermus thermophilus* and glucose oxidase (GOX) from *Aspergillus niger*, are also not naturally photoactive. They are flavoproteins involved in the catalysis of different biological reactions (see chapter 6 and chapter 7). In both systems, like the flavoprotein systems described above, FAD excitation with blue light leads to subsequent charge transfer steps involving neighbouring residues. This has allowed us to visualize previously unobserved intermediate states in both systems, particularly those of close-lying redox active residues tyrosine and tryptophan. In several examples mentioned above, tyrosine (TyrOH in the neutral ground state) is actively involved in bridging electron transfer. The nature of the intermediates formed by tyrosine has been debated, generally assumed to include the deprotonated TyrO$^\bullet$ neutral radical. The radical cation form TyrOH$^{\bullet+}$ has also been proposed to be involved in charge transfer, but had never been characterized.[75] A major aim of this thesis is to investigate this issue. The subsequent chapter will introduce the background of this work in greater detail.

Chapter 3

Flavoprotein photochemistry and aromatic amino acid radicals

3.1 Flavins and flavoproteins

Proteins containing flavins as redox cofactors have unique properties, as they are able to participate in both 1 e$^-$ and 2 e$^-$ transfer reactions and/or hydride exchange reactions. This enables them to participate in a wide range of redox reactions. They are found abundantly in nature as they are estimated to account for up to 2% of all proteins.[76] As seen from the examples given in the previous chapter, the optical properties of flavoproteins enable a limited number of them to act as "photoswitches" through light-triggered reactions. However, a large proportion of flavoproteins, whilst participating in functional electron transfer processes, are not naturally photoactive. In this section, we will discuss the general redox properties of flavins to understand their role in electron transfer processes.

Riboflavin, isolated from cow milk by Blyth in 1879,[78] was the first flavin to be discovered. Fig. 3.1 shows the structure of riboflavin. It contains a conjugated ring system (isoalloxazine) which is linked to a ribityl chain. Riboflavin is present in various food items including milk, eggs and cereal. While bacteria, fungi and plants can produce riboflavin, other organisms like humans do not have the ability to synthesize it.[79] Interestingly, flavins in animal tissues are rarely present as free riboflavin. They are mostly present as flavin mononucleotide (FMN) or flavin adenine dinucleotide (FAD) bound to flavoenzymes. Riboflavin is a precursor to FMN and FAD in such systems. As seen in Fig. 3.1, the structure of FMN is similar to that of riboflavin with the addition of a phosphate group. On addition of an adenosine group to FMN, it becomes FAD. Riboflavin is an important dietary component and is known commonly today as vitamin B$_2$ which is a popular dietary supplement. Its deficiency has been linked to neuromuscular and neurological disorders, cancer and a predisposition to *Listeria*
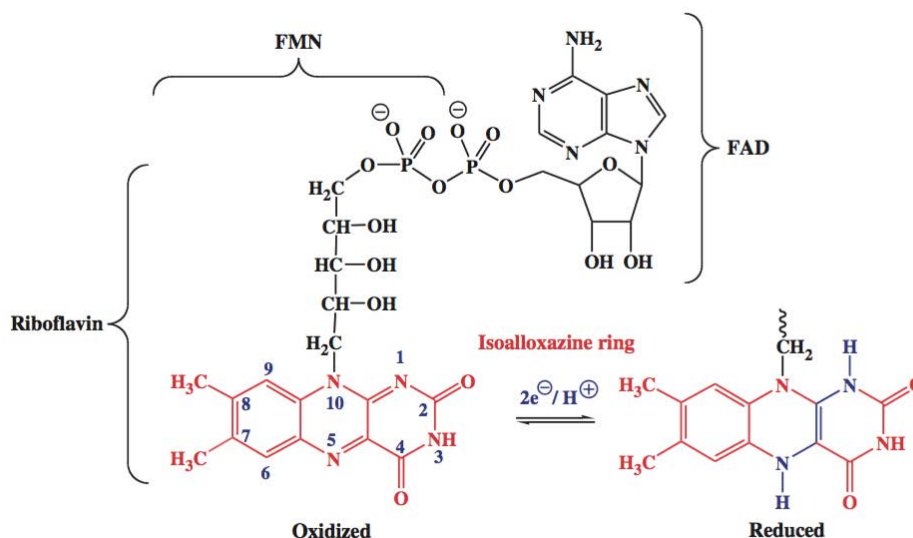
Figure 3.1: *Structures of riboflavin, flavin mononucleotide (FMN) and flavin dinucleotide adenine (FAD). The isoalloxazine ring has been shown in its oxidised and two-electron reduced state. Additionally, the numbering scheme for the isoalloxazine ring is indicated. Image taken from ref [77].*
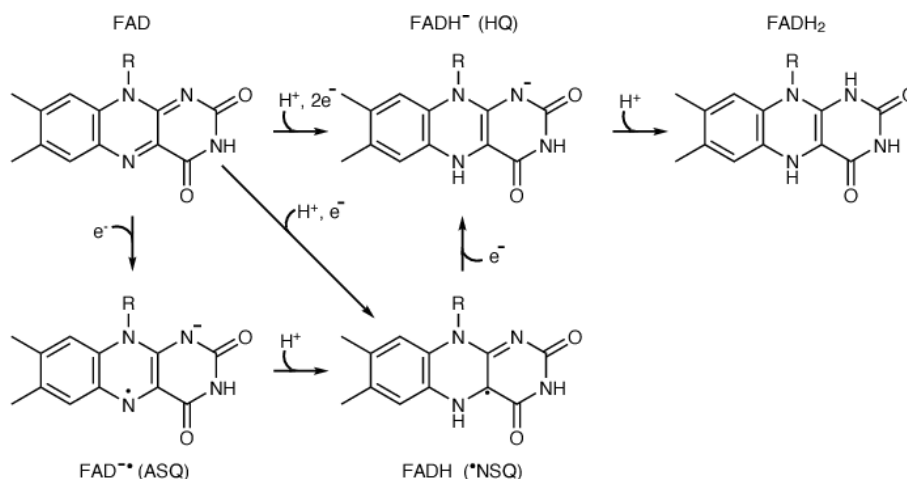
infection.[80,81]

Figure 3.2: *Different redox states of FAD : the oxidized form FAD_{ox} (designated FAD here), the anionic semiquinone form $FAD^{\bullet-}$, the neutral semiquinone form $FADH^{\bullet}$, the hydroquinone form $FADH^{-}$ and the fully reduced form $FADH_2$. These are the five physiologically relevant states of FAD. Other states can also be produced outside physiological conditions. Image taken from ref [82].*

More than 90% of the known flavin-dependent enzymes are classified as oxidoreductases, and the remaining enzymes are classified as transferases, lyases, isomerases and ligases.[77] The immense biochemical utility of FMN and FAD is due to their redox-active isoalloxazine ring system which is capable of being involved in one-

27

and two-electron, proton and/or hydride transfer reactions. Consequently, FMN and FAD can exist in several physiologically relevant redox states: oxidized (FAD_{ox}), one-electron reduced anionic semiquinone ($FAD^{\bullet-}$), one-electron reduced protonated ($FADH^{\bullet}$), two-electron reduced protonated ($FADH^-$) and two-electron reduced bi-protonated ($FADH_2$) (as shown in Fig. 3.2). In addition, the oxidized flavin molecule is susceptible to nucleophilic attack at positions N5 and C4a of the isoalloxazine ring. The ability of FAD and FMN to exist in various redox states makes them versatile enzyme cofactors for numerous biochemical reactions, most of all in oxidoreductases, which participate in biological redox reactions.
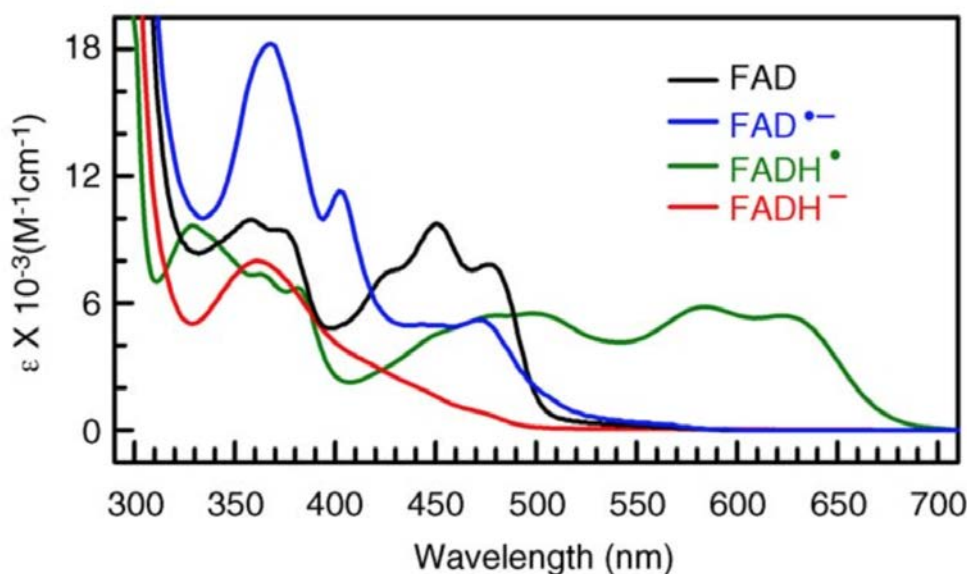

Figure 3.3: *Spectra of four different redox states of FAD.[83] FAD here refers to oxidized FAD. The $FADH_2$ spectrum, not included here, slightly resembles that of $FADH^-$ with a more gradual incline and lower extinction in the blue region. The FAD and $FAD^{\bullet-}$ spectra are from mosquito cryptochrome AgCRY1. The $FADH^{\bullet}$ and $FADH^-$ spectra are from E. coli photolyase.*

As stated before, flavins (FAD and FMN) are among the few known redox coenzymes (like quinones) that can participate in both one-electron and two-electron transfer processes.[84] Furthermore, they prove to be suited to spectroscopic studies as all five redox states of flavins absorb in the visible region with distinctly different spectral signals. Fig. 3.3 shows the steady state absorption spectra of four relevant redox states of FAD.[83] The oxidized form FAD_{ox}, the resting state for many flavoproteins, has a distinct absorption band at $\sim 450 nm$. This yellow form is the one with the highest extinction in the visible part of the spectrum. The reduction of FAD_{ox} can be visualized spectrally by the absorption decrease in the 450 nm region. For the one-electron reduced forms, this is additionally accompanied by an absorption increase in the red for $FAD^{\bullet-}$, a small signal in the ~ 510 nm region and for $FADH^{\bullet}$, a stronger signal

extending over the entire visible spectrum (it is the only FAD redox state to absorb significantly beyond 530 nm). The two-electron reduced forms absorb weakly in the visible region; the $FADH_2$ spectrum resembles that of the $FADH^-$ spectrum in Fig. 3.3, with a more gradual incline in the blue region and with lower absorptivity (extinction coefficients).

Flavins have lower extinction coefficients compared to many of the coloured cofactors which participate in charge transfer reactions like chlorophyll and hemes (See Fig. 3.3). The molar absorption coefficient for the long-wavelength absorption maximum of chlorophyll a (ε_{419}) is $\sim 90 mM^{-1}cm^{-1}$[85] and for hemes up to $\sim 200mM^{-1}cm^{-1}$[86] whereas the corresponding value for oxidized flavin (for example, FAD[87]) at 450 nm is only 12 mM^{-1}cm^{-1}. Intermediates formed during biological redox reactions are of considerable interest (see section 2.3). Using flavoenzyme systems to monitor such intermediates may facilitate characterizing them and evaluating their role in biological charge transfer reactions. In this context, flavoenzymes provide a unique advantage as their extinction coefficients are lower than that of other systems where intermediates have been proposed to participate. They have extinction coefficients of the same order of magnitude as the Tyr and Trp redox intermediates (see section 3.2) making it easier to distinguish the latter's signal. In systems containing chlorophyll or hemes as cofactors, the absorption signal of these Tyr and Trp redox intermediates would be much smaller than the signal of the corresponding cofactor redox state. This makes flavoproteins especially suited to visualize charge transfer intermediates.

3.2 Charge transfer intermediates involving amino acid residues

Biological systems are often naturally optimized to conduct long-range charge transfer between redox sites. The mechanism of charge transfer between a donor and acceptor frequently involves electron hopping via bridging amino acid residues (see section 2.2). These bridge amino acid residues have in turn been observed to form functionally relevant radical intermediates in many systems such as photosystem II,[36] cytochrome c oxidase,[88] DNA photolyase,[40,42,89] cryptochrome,[71,72] among others.

In most biological systems where charge transfer has been studied, amino acid residues involved in redox reactions and formation of intermediates are tyrosine and tryptophan. The redox potentials of the constituents of the amino acid side chains are generally extremely high.[13] However, tyrosine (Tyr) and tryptophan (Trp) have been observed to have redox potentials more relevant for physiological reactions.[30,31,94] This is
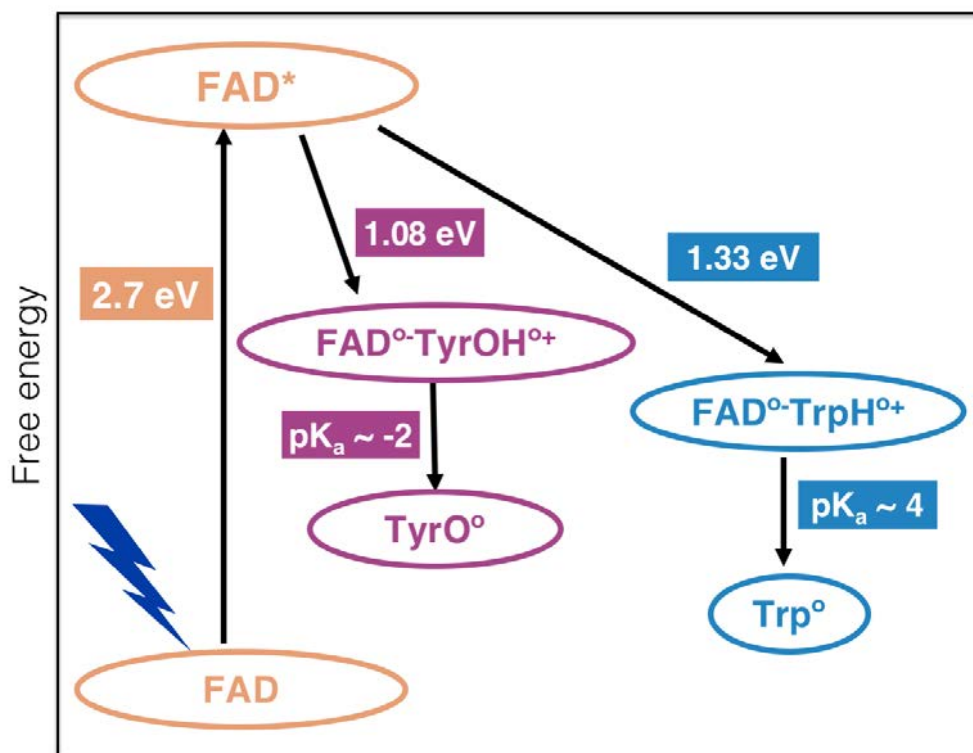
Figure 3.4: *Schematic representation of the electron transfer from a photoexcited FAD to a nearby Tyr/Trp and the subsequent intermediates formed. The 2.7eV represents the excitation of FAD from ground state to FAD*. Free energies have been indicated for the formation of product states FAD$^{\bullet-}$TyrOH$^{\bullet+}$ (1.08 eV) and FAD$^{\bullet-}$TrpH$^{\bullet+}$ (1.33 eV) which have been calculated using redox potentials.[90,91] The pK$_a$ values for the deprotonation of radical cations have also been given. TyrOH$^{\bullet+}$ has been proposed to be less likely to be observed as it is highly unstable (pK$_a \sim -2$).[92] On the other hand, TrpH$^{\bullet+}$ is a more stable radical cation as it has a pK$_a \sim 4$.[93]*

illustrated in the scheme in Fig. 3.4 for the case of light-induced reactions with FAD. The relative free energies of product states formed $FAD^{\bullet-}TyrOH^{\bullet+}$ (1.08 V) and $FAD^{\bullet-}TrpH^{\bullet+}$ (1.33 V) have also been indicated. The free energies have been calculated using the redox potentials for the pairs $FAD/FAD^{\bullet-}$ (-0.22 V),[91] $TyrOH^{\bullet+}/TyrOH$ (1.4 V)[90] and $TrpH^{\bullet+}/TrpH$ (1.15 V).[90] The pK_a values for $TyrOH^{\bullet+}$ and $TrpH^{\bullet+}$ are ~ -2[92] and ~ 4[93] respectively. $TyrOH^{\bullet+}$ has been proposed to be less likely to be observed[75] as it is highly unstable ($pK_a \sim -2$)[92] and is expected to undergo rapid proton transfer to form $TyrO^{\bullet}$. On the other hand, $TrpH^{\bullet+}$ is a more stable radical cation as it has a $pK_a \sim 4$.[93]

In DNA photolyase, both protonated ($TrpH^{\bullet+}$) and deprotonated ($Trp^{\bullet}$) radicals of tryptophan have been observed to form sequentially at different timescales.[69] On the other hand, in a model compound containing a Trp-analogue, the latter species was inferred to be formed by concerted proton and electron transfer in aqueous solution.[95] Together, these studies indicate that while Trp radicals can be formed by concerted electron and proton transfer, this is not always the case.

Tyrosine radicals have markedly different characteristics compared to tryptophan radicals. Since the pK_a of $TyrOH^{\bullet+}$ is ~ -2, it is expected to be highly unstable if it is formed at all. At the start of this thesis, it had not yet been observed as a reaction intermediate and was spectrally uncharacterised. In the prototypical photosynthetic system PSII (described in section 2.3), the secondary electron donor to the photo-oxidized chlorophyll dimer P_{680} is a tyrosine. Here, the electron transfer ($\sim 20 - 200$ns) occurs concomitant to proton transfer and therefore, no $TyrOH^{\bullet+}$ intermediates have been observed. For several of the examples discussed in section 2.3, like cytochrome c oxidase, BLUF domain and ribonucleotide reductase, Tyr was indicated to form a $TyrO^{\bullet}$ intermediate, a form that has been characterized.[96] Tyr has also been observed to form radical intermediates in photolyase from the cyanobacterium *Anacystis nidulans*.[89] For tyrosine-containing photoactivatable model compounds in aqueous solution, a stepwise mechanism with electron transfer preceding proton transfer has been invoked.[97] However, in this case $TyrOH^{\bullet+}$ deprotonation is much faster than its formation, prohibiting its visualization and characterization.

Tyr and Trp radicals have been characterized spectroscopically in many systems. Interestingly, in the neutral ground state, both Tyr and Trp absorb in the UV region of the spectrum. However, their characterized intermediates have distinctive spectra in the near-UV to the visible spectral range. Fig. 3.5 shows the characteristic spectra of known Tyr and Trp intermediates. Both the Trp radicals - neutral and cation - have been spectrally characterised. While the spectrum of $TrpH^{\bullet+}$ contains a broad band centred ~ 570 nm, the spectrum of $Trp^{\bullet}$ contains a similarly broad band but centred at
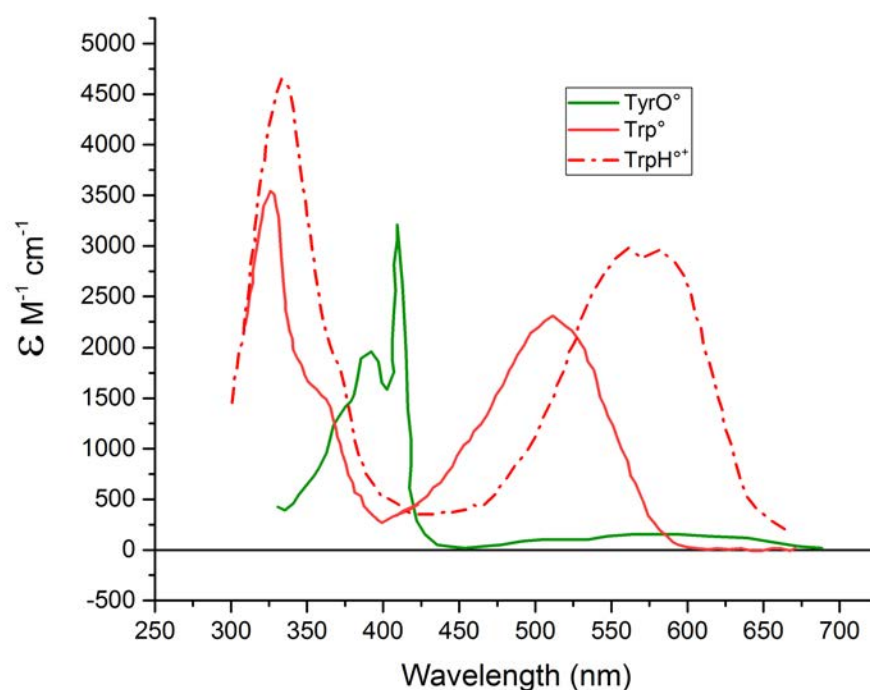
Figure 3.5: *Spectra of known intermediates of tyrosine and tryptophan. The tyrosine intermediate has been shown in green.[96] The tryptophan intermediates have been shown in red.[98] These spectra have been obtained using pulse radiolysis and photolysis.*

$\sim$ 500 nm. On the other hand, the spectrum of TyrO$^\bullet$ is distinctly different with a
sharp band at $\sim$ 410 nm. All radical intermediates have distinctly lower extinction
coefficients compared to typical protein cofactors like chlorophyll and even FAD$_{ox}$. Yet,
the extinction coefficients of Tyr and Trp radical intermediates are comparable to those
of FAD radicals. This reiterates that flavoenzymes are well-suited for visualizing and
characterizing intermediates of amino acid residues in proteins.

The evidence for the involvement of a certain amino acid residue in a charge transfer
reaction can be gauged by replacing said residue with one which is redox-inactive.
Site-directed mutagenesis has frequently been used to substitute redox-active residues
like Tyr and Trp by a redox-inactive aromatic residue like phenylalanine (Phe). In the
case of DNA photolyase, the three tryptophans in the redox chain are *a priori*
spectrally indistinguishable. To understand their role in the charge transfer pathway,
each Trp was mutated to Phe.[42] As Phe is an aromatic residue, substitution of a Trp
with a Phe residue reduces the possibility of large steric effects due to the mutation.
Electron transfer between solvent-exposed Trp and the photo-excited FADH$^\bullet$ is orders
of magnitude slower on mutating a redox-active bridge Trp to Phe, as seen by Byrdin *et
al.*.[42]

Polarization photoselection is another way, without protein modification, to
distinguish between the three Trp residues in the redox chain of DNA photolyase. Here,
a linearly polarized pump is used for preferentially exciting the FAD cofactors which
have transition dipole moments parallel to the pump polarization direction.[41] This
photoselection induces a transient anisotropy in the previously isotropic sample. In
principle, as the three Trp residues have different spacial orientations with respect to
the FAD cofactor within the protein, they can be distinguished by probing with
polarized light. In our studies, we have used a similar method along with site-directed
mutagenesis to implicate residues involved in charge transfer reactions.

Spectrally characterising Tyr and Trp radicals in model systems helps in spectral
deconvolution and in the assignment of the intermediate and final photoproducts formed
in complex charge transfer pathways in proteins. In systems like photolyase and RNR,
such approaches have led to the characterization of intermediates. Among flavoproteins,
electron transfer photoproducts have been unequivocally spectrally characterized in only
few systems like photolyase, cryptochrome and BLUF domains (except for attempts in
glucose oxidase by Lukacs *et al* in 2012[100]). Often, charge transfer reactions are not
straightforward and proceed with the existence of multiple charged species at each stage
of decay. Brazard *et al.* have analysed such a system in new cryptochrome/photolyase
type FAD-based photoreceptors.[99] Due to the presence of FAD$_{ox}$ rather than FADH$^\bullet$, as
in *E. coli* photolyase, the primary photoreaction is ultrafast (few hundred fs) in this
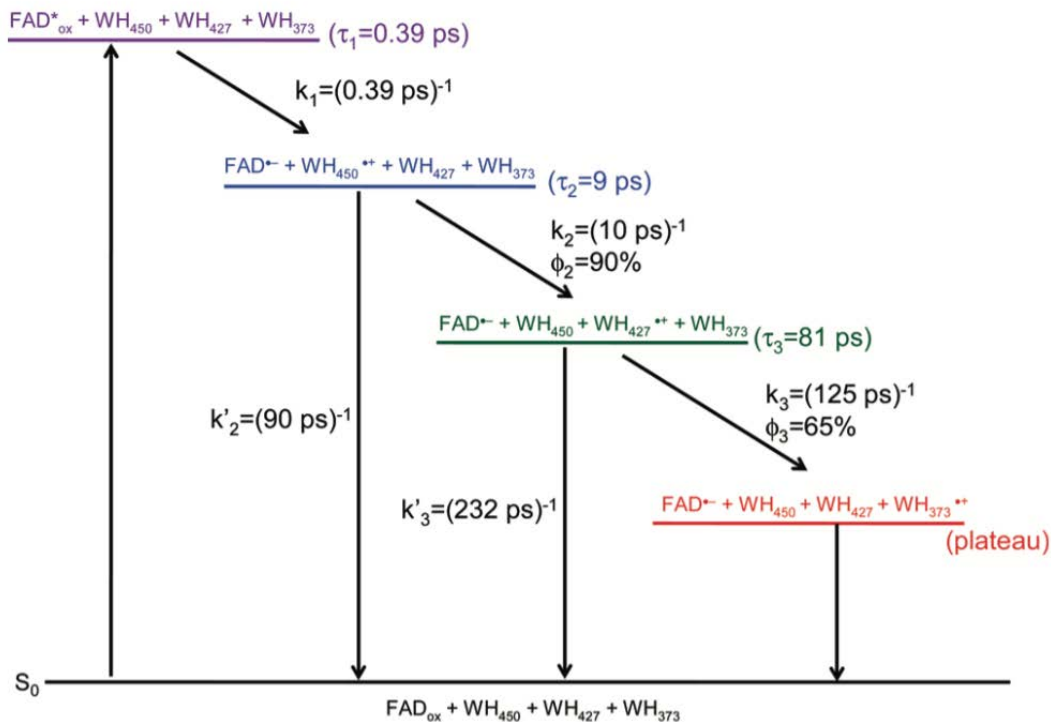
Figure 3.6: *Kinetic model proposed to describe the photoactivation of FAD_{ox} in the algal photoreceptor OtCPF1. In chapter 7, a similar model has also been proposed for glucose oxidase decay after photoexcitation.*[99]

system and subsequent kinetic steps can be resolved. Using polarization photoselection, they have been assigned to a cascade of electron hopping reactions along a chain of three conserved tryptophan residues (Fig. 3.6). The kinetic model proposed for OtCPF1 (3.6), not unlike the kinetic scheme of photosynthesis (Fig. 2.3), accounts for competition between forward electron hopping (along the tryptophan chain) and charge recombination at each kinetic step. Such a model has also been used by us to describe electron transfer in glucose oxidase (see chapter 7).

Chapter 4

Motivation for this work

4.1 Conformational flexibility in ThyX

Initial motivation for this thesis project arose from the work on configurational flexibility of the flavoenzyme thymidylate synthase (ThyX) in 2013.[101] ThyX is a homotetrameric enzyme which is essential for *de novo* synthesis of the DNA precursor 2'-deoxythymine-5'-monophosphate (dTMP) in many bacterial systems. ThyX is not structurally homologous to thymidylate synthase ThyA that is used by most eukaryotes.[102] ThyX, which is absent in humans, is used by various pathogenic bacteria and is considered an antimicrobial target.[103] During its reaction cycle, it converts deoxyuridine monophosphate (dUMP) to dTMP using N^5,N^{10}-methylene-5,6,7,8-tetrahydrofolate (MTHF) and nicotinamide adenine dinucleotide phosphate (NADPH) as carbon and electron donor, respectively. Since it interacts with three substrates during its reaction cycle, at least two of which should simultaneously be accommodated in the active site, it is also an attractive candidate for studies on conformational flexibility.

ThyX is not a light-active flavoenzyme. Sub-picosecond fluorescence spectroscopy was performed on ThyX from the hyperthermophilic bacterium *Thermotoga maritima* (*Tm*ThyX) in the presence and absence of substrate dUMP to probe the active site. It was found that wild type ThyX exhibits a long multiphasic fluorescence decay which reflects dynamic conformational changes. A nearby Tyr91 residue was observed to be the primary quencher of FAD* fluorescence in *Tm*ThyX, indicating that electron transfer occurs from Tyr91 to FAD*. The substrate dUMP is also an FAD* fluorescence quencher in ThyX, suggesting that closely bound dUMP could be an electron donor to FAD*.

The FAD* decay in ThyX was observed to be multiphasic, spanning three orders of magnitude in time. The corresponding continuous lifetime distribution in ThyX
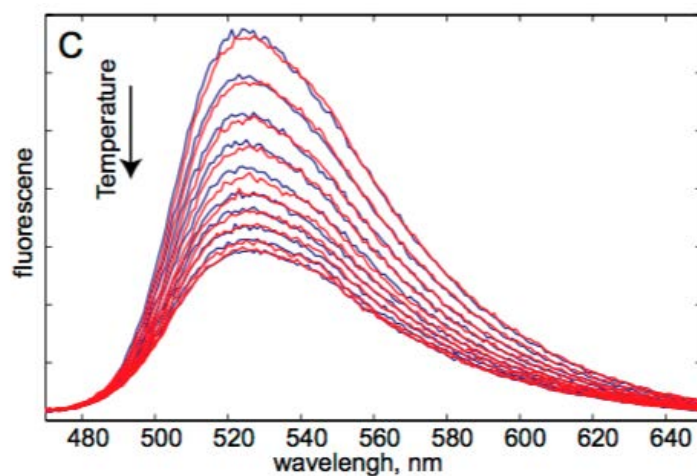
Figure 4.1: *Steady-state fluorescence of WT TmThyX upon 400 nm excitation at different temperatures between 25° and 70° upon warming (blue) and cooling (red).*[101]
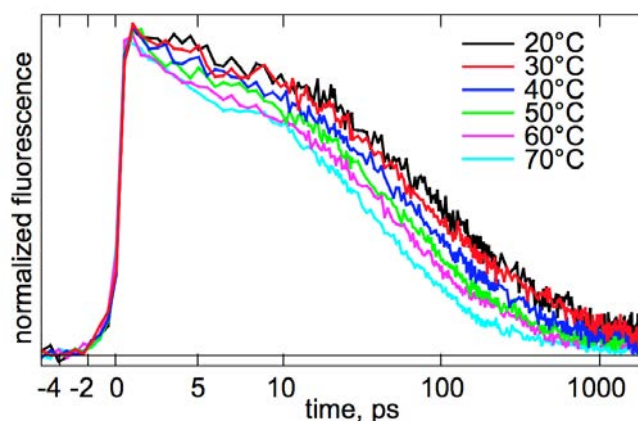

Figure 4.2: *Temperature dependence of amplitude-normalized fluorescence decay of wild type TmThyX at 520 nm.*[101] *Excitation at 395 nm. The time axis is linear until 10 ps and logarithmic thereafter.*

fluorescence was attributed to conformational heterogeneity in the active site. To obtain more insight into the conformational flexibility of TmThyX, the fluorescence properties were measured as a function of temperature. These experiments were facilitated by the fact that TmThyX is stable at very high temperatures (Fig. 4.1). The total fluorescence was observed to decrease with increasing temperature and was fully reversible on cooling. This indicated that, even at high temperatures, FAD remains bound to the protein. From the observation that the slower decay phases were specifically suppressed on warming (Fig. 4.2), it was concurred that this multiphasic decay does not (only) reflect static heterogeneity, but that extremely rapid (down to the picosecond timescale) large scale conformational changes occur in the active site.
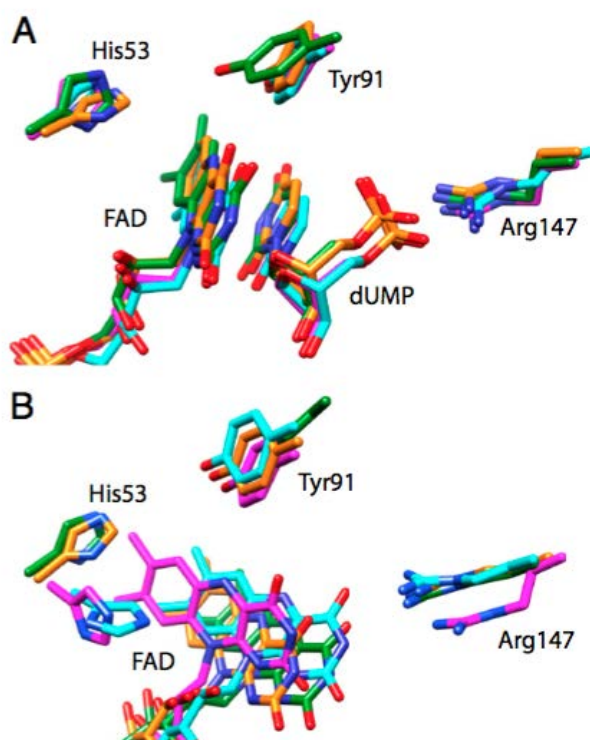

Figure 4.3: *Superimposed structures of elements of the four active sites in ThyX, time averaged over the last 500 ps of 2.5 ns free trajectories of MD simulations in the presence (A) and absence (B) of dUMP.[101] The superposition is on the entire backbone of each subunit. The carbon atoms are colour-coded with the respective subunits.*

To complement the experiments, molecular dynamics (MD) simulations were also performed and a large variation in active site configurations was indeed observed. In the MD simulations (Fig. 4.3 A), of wild type ThyX, especially the flavin, was observed to be more flexible in the absence of substrate dUMP (Fig. 4.3 B). A significant variation in distance between FAD and the Tyr-91 quencher was observed accompanied by unusually large fluctuations (up to ~ 4 Å) occurring infrequently on a timescale of up to several nanoseconds.[101] This flexibility was not observed in the presence of dUMP

substrate (Fig. 4.3 B). Thus both experiments and simulations indicated extremely high flexibility and very rapid changes in active site conformation in this enzyme.

4.2 Motivation and aim of the thesis

The original motivation for this thesis was to investigate whether active site flexibility is a general feature for multi-substrate nucleic acid-processing proteins. We started studies similar to those performed on ThyX[101] on its functional analogue TrmFO.[104] TrmFO, also a flavoprotein, is a methyltransferase which catalyzes the post-transcriptional formation of m^5U_{54} in tRNAs and is required for structural stabilization of crucial RNA molecules. Like ThyX, it also interacts with three substrates during the catalysis: MTHF, NADPH and tRNA (which is much larger than dUMP - the substrate of ThyX). While there is no structural homology between these enzymes, this made it an equally interesting system for studies on conformational dynamics.

TrmFO also has a tyrosine residue (Tyr-343 in *T. maritima*) lying very close to the FAD cofactor which, like Tyr-91 in *E. coli* ThyX, is the primary quencher of FAD* fluorescence (discussed in chapter 6). The active site also contains a close-lying cysteine (Cys) residue (C51 in *Thermotoga maritima*) which likely forms an adduct with FAD. This adduct is different from the one formed between Cys and FAD in LOV domain (See section 2.3). In LOV domains the FAD has to be in the excited triplet state to form an adduct with Cys, whereas in TrmFO an adduct between Cys and FAD can be observed in the ground state. However, this adduct is not visualized in X-ray crystallographic structures of TrmFO and its nature remains debated.[105]

In wild type TrmFO, the Cys-FAD adduct is highly fluorescent. To visualize the underlying active site dynamics in an adduct-less *Tm*TrmFO, the cysteine residue at position 51 was mutated to an alanine. Time-resolved fluorescence and absorption experiments were then performed on this C51A mutant. The fluorescence was quenched within ∼ 1ps. The emphasis of the thesis changed as we realized that the fast fluorescence quenching in TrmFO made it an interesting system to characterize redox intermediates involving Tyr radicals. It is inherently difficult to characterize product states in ThyX as its excited state decays in a large range of timescales. The Tyr343 in *Tm*TrmFO lies very close to the FAD isoalloxazine, and the FAD excited state is completely quenched rapidly. Through time-resolved absorption experiments we serendipitously visualized the elusive and short-lived (∼ 3ps) TyrOH$^{•+}$ radical intermediate which had never been seen before, and characterized it spectrally (see subsection 6.2.2).[1]

The double mutant C51A/Y343F of TrmFO was observed to have a long fluorescence decaying over three orders of magnitude (from ps to ns). This similarity between the double mutant and ThyX made it the next candidate for flexibility studies (see section 6.6). However, the distribution of donor-acceptor configurations sampled in C51A/Y343F did not change during the time-period sampled, and further experiments to elucidate potential quenchers of FAD in the C51A/Y343F TrmFO mutant are yet to be performed.

Many natural redox systems have Tyr and Trp residues positioned near the active site. TrmFO is one of the few systems where product states of intermediates have been visualized. The identification of the "yet unseen" redox intermediate $TyrOH^{\bullet+}$ in TrmFO C51A paved the way to investigate whether this state can also be visualized in other systems where it had been speculated to be formed. One such system is glucose oxidase (GOX) from *Aspergillus niger*, which has been widely used as a model system in spectral studies[100,106,107] and where transient product states had not yet been thoroughly characterized (see chapter 7). GOX contains several Tyr and Trp residues in proximity of the active site FAD, and has been observed to have a more complex excited state decay than TrmFO C51A. In our work, we have successfully identified the formation of $TyrOH^{\bullet+}$ intermediate in GOX and have spectrally characterized it. The spectra for $TyrOH^{\bullet+}$ obtained from GOX and C51A TrmFO have also been compared and are observed to be similar, thus opening the way to investigate the role of this state in a broader class of proteins.

Chapter 5

Experimental methods

5.1   Protein procurement and handling

During this thesis, expression and purification of wild type TrmFO from *Thermus thermophilus* and certain mutant proteins - C51A, C51A Y343F, etc. was carried out. Glucose oxidase from *Aspergillus niger* used in these experiments was ordered in lyophilized form from Sigma.

5.2   Expression of TrmFO variants

The plasmid pQE80L was used for cloning and expression of the *trmFO* gene. It also allowed the expression of protein upon induction with isopropyl β-D-1 thiogalactoside (IPTG) in *E. coli* BL21DE3.

Individual *E. coli* colonies were resuspended in 10 mL of Lysogeny Broth (LB) growth medium with 100 μg/ml ampicillin and incubated for 18 hours at 37°C with shaking. Subsequently, the culture was scaled up to 500 ml of LB growth medium with 100 μg/ml ampicillin and incubated at 37°C with shaking at 180 rpm for $\sim$2 hours. Once the exponential phase was reached (OD at 600 nm = 0.6 - 0.8), the protein expression was induced by 1 mM IPTG final concentration for 3 h. The culture was centrifugated for 30 min at 5000 rpm and the pellet was resuspended in 5 ml of lysis equilibrium wash buffer (LEW: 50 mM NaH_2PO_4, 300 mM NaCl, pH 8.0). This suspension was stored at -80°C until the purification step.

5.3   Purification of TrmFO variants

The bacterial re-suspensions were treated for 30 minutes on ice with DNase and lysozyme (one tip of spatula each for 5 ml of bacterial suspension) and shaken at 180

rpm. Subsequently they underwent 5 cycles of 20 seconds of sonication (in an ice bath). The samples were left on ice to complete the lysis for a few minutes.

In order to optimize the holoenzyme / apoenzyme ratio, FAD was added to the lysate to a final concentration of 100 μM and left for 10 min on ice to promote its fixation on TrmFO. This was followed by centrifugation for one hour at 13,200 rpm which enables the recovery of the soluble fraction of the proteins in the lysate, containing the protein of interest.[105]

For purification, the soluble fraction (ca. 4.5 mL) was deposited on a *Protino*® Ni-TED Resin 2000 column (Macherey Nagel) pre-equilibrated with 5 mL of LEW buffer. It was then washed with 25 mL of LEW buffer following which the protein was eluted in 3 mL of elution buffer (LEW + 250mM imidazole).

This last step was carried out after the column had been washed with 5 mL of LEW buffer with the soluble protein fraction recovered. The eluted protein was desalted using exclusion chromatography on Econopac 10DG polyacrylamide column (Bio-Rad) and collected in 4 mL of HEPES buffer (50 mM HEPES, 300 mM NaCl , pH 8.0). The protein was concentrated using 30kDa AMICON® concentrators.

In order to evaluate the purity of the different TrmFO mutants, the purified proteins were subjected to a migration of 30 min at 100V on 10% acrylamide gel under denaturing conditions (SDS-PAGE), and subsequently coloured using instantBlue (Expedeon).

For experiments to study the presence of hydrogen bonding in the active site of TrmFO C51A, the protein solution was washed several times with a similar HEPES buffer but made with D_2O to minimize the presence of H_2O in solution.

5.4 Pump-probe spectroscopy

Pump-probe spectroscopy is a group of widely used techniques for studying ultrafast phenomena. Figure 5.1 shows a simplified scheme of a typical pump-probe setup. The pump and the probe are derived from a single source after which they are split up. A delay line is used to create a time difference in arrival of the probe beam with respect to the pump at the interaction volume, typically a sample cell but not necessarily (see Section 5.5). The time resolution is created by translating the mechanical delay line, where a change in the delay line position of 150 μm corresponds to a time delay of 1 ps. The experiment is repeated at different set delay times to construct the kinetics point
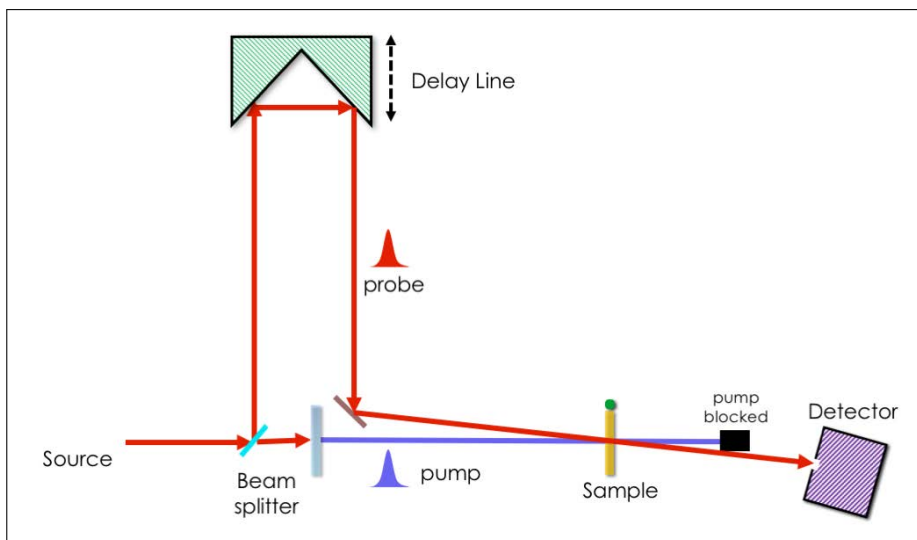
Figure 5.1: *Principle of pump-probe spectroscopy. The pump and probe are derived from the same short-pulse source and separated. One if them (the probe in this figure) is passed through a movable delay line to create a time difference.*

by point.

The detector measures the total intensity and/or spectra shape of the probe pulse. The time resolution of experiments is limited by the pulse length ($\approx 150 fs$ here) and not by the response time of the detector. The time window (the longest time that can be measured) is determined by the physical limitation of the delay line (maximum $\approx 4ns$).

The following sections describe the two different pump-probe techniques used in the experiments: femtosecond time-resolved fluorescence using Kerr gating and femtosecond time-resolved absorption spectroscopy.

5.5 Femtosecond time-resolved fluorescence spectroscopy

Time-resolved fluorescence spectroscopy can be used to probe the excited state decay of flavin in flavoproteins. The decay and spectra are highly sensitive to the protein environment as specific amino acid residues close to the flavin can influence the timescale of its fluorescence decay by acting as fluorescence quenchers. Additionally, the change in shape of fluorescence spectra can yield information regarding motions and relaxation processes of the flavin in the excited state. Therefore, we will use a method that has both high temporal resolution and the ability to measure full spectra.
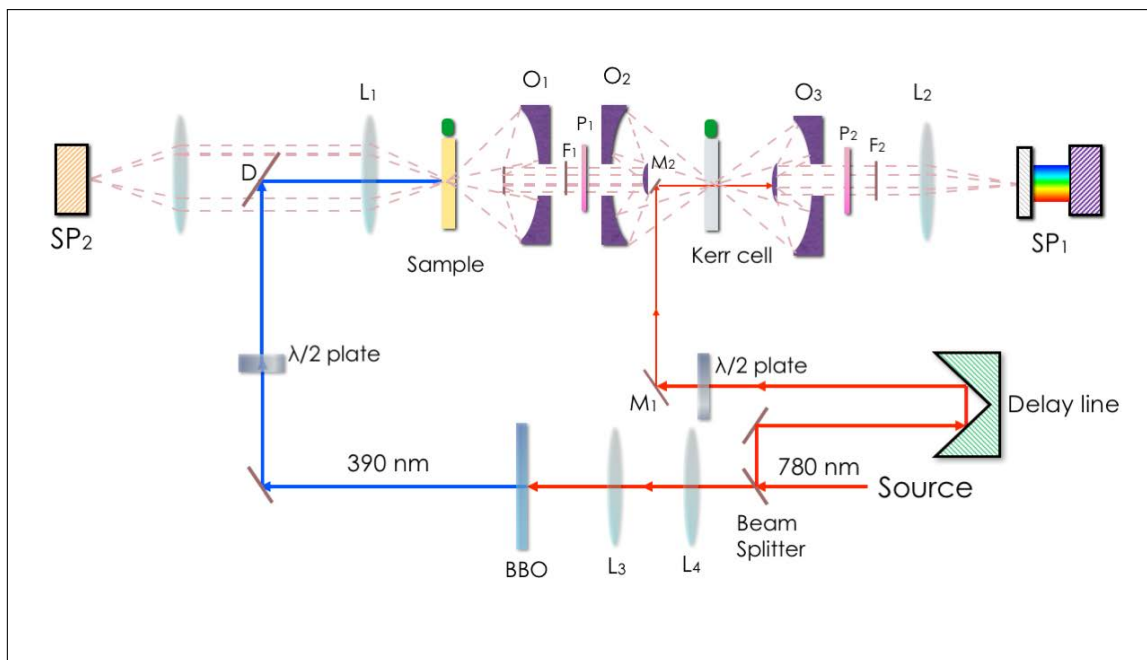
Figure 5.2: *Diagram of the Kerr-gated spectrofluorometer used for all time-resolved fluorescence measurements. The setup is based on Kerr gating to simultaneously obtain high spectral and temporal resolution. Temporal resolution and sensitivity can be adapted by switching between suprasil, benzene and CS_2.*

There are several types of experimental methods that provide combined time and spectral resolution: streak camera,[108,109] broadband upconversion,[110,111] and Kerr gating.[112,113] The femtosecond time-resolved fluorescence setup used in these experiments incorporates Kerr gating. This method has a relatively better time resolution than streak cameras (that are not a pump-probe technique and are limited by the response of the camera) and is more straightforward in operating than broadband upconversion.

Kerr gated setups can have a high time resolution going down to the length of the pulse used ($\approx 150 fs$), which is especially useful for observing short-lived excited states of flavins. Kerr- based setups use fluorescenece gating. When a polarized intense gate pulse interacts with the Kerr medium, its refractive index changes and it becomes temporarily birefringent. The Kerr medium is placed between two crossed polarizers. The polarization of the fluorescence beam that passes the Kerr medium while this induced birefringence persists will be changed. Therefore, part of the fluorescence light passes through the second polarizer to reach the detector and the shutter is opened. The Kerr effect is a molecular phenomenon and depending on the time-resolution required, different Kerr media (with distinct response times and response amplitudes) have been used for obtaining the time-resolved fluorescence data in these experiments: suprasil ($\approx 200 fs$), benzene ($\approx 300 fs$) and CS_2 ($\approx 1 ps$). The response amplitudes of these Kerr media are in inverted order. Therefore, depending on the experiment, a

compromise between time resolution and signal to noise ratio can be chosen.

Figure 5.2 depicts a scheme of the Kerr gated fluorometer used for time-resolved experiments. The light source is a Ti:sapphire laser/amplifier system (Quantronix Integra-C) centered at $\approx 780nm$ with a 1 kHz repetition rate providing an energy of $\approx 1mJ$. The $\approx 100fs$ pulse is split into two parts: the first part is frequency doubled using a β Barium Borate (BBO) crystal yielding pulses centered at 390 nm; the second part is passed through the delay line and is used as the gate pulse at 780 nm.[114]

The sample in its excited state can give rise to polarization effects due to anisotropy. To avoid this, the polarization of the pump pulses are set at *magic angle* (54.7°) with respect to the polarization direction of the first polarizer ($\lambda/2$ plate). The pump pulse is directed into the sample and focused to ~ 150 μm by a lens (L_1). This lens transmits at the excitation wavelength as well as the emission spectral range. The fluorescence emitted in the backward direction is transmitted through L_1 and the dichroic mirror (D) and focused into a fiber optics spectrometer (SP_2) in order to monitor fluctuations in total fluorescence. The intensity of the pump and gate beams is adjusted with variable neutral density filters.

The sample exhibits fluorescence in all directions upon excitation. Reflective objectives are used to collect the emitted light in the forward direction, to avoid a strong dispersion. The fluorescence is collimated by a Cassegrain-type reflective objective (RO)(Fig. 5.2, O_1). A vertically oriented thin polarizer (P_1) is placed in the collimated beam. The linearly polarized fluorescence is then refocused by a second RO (O_2) and overlapped with the gate beam inside the Kerr medium (Fig. 5.2, Kerr cell). After the Kerr medium, a third RO (O_3) is used to re-collimate the fluorescence beam. A horizontally oriented polarizer (P_2) is placed after this RO to enable the gate-polarized fluorescence to pass. This *gated* fluorescence is directed through the entrance slit of a polychromator and the resulting dispersed beam is imaged onto the nitrogen- cooled CCD camera (SP_1) which is configured as an array-detector.

The sample is contained in a 1 mm quartz cell. To avoid photobleaching and sample degradation, the cell (Fig. 5.2, Sample) is rotated continuously during the experiment so that a new volume of the sample is excited in every shot.

5.6 Time-resolved Absorption Spectroscopy

Transient fluorescence spectroscopy is useful for obtaining information exclusively about excited states and the lifetimes of their decay. To visualize the subsequent processes
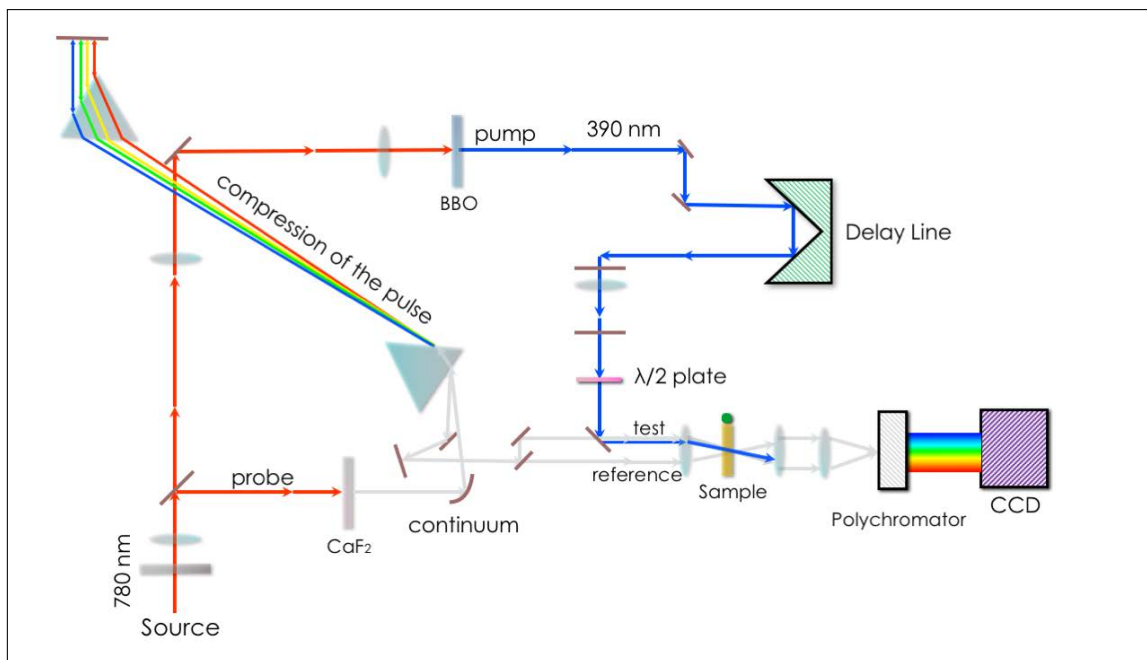
Figure 5.3: *Diagram of the transient absorption setup used for all time-resolved absorption measurements with the repetition rate set at 500 Hz. The 780 mn-source is split into pump and probe pulses. The pump is doubled to 390 nm and the probe focused on a CaF_2 plate for continuum generation. After compression using a prism pair, the probe is split to test and reference pulses. It is to be noted that the beams going in and coming out of the compression prism overlay in practice, but have been shown here at slightly different angles for clarity.*

following flavin excitation, femtosecond time-resolved absorption spectroscopy was performed. This enabled the visualization of the ensemble of transiently populated excited and product states formed. Additionally, it is useful to correlate the transient absorption data with those obtained from transient fluorescence spectroscopy.

The laser source for the setup used for time-resolved absorption experiments is the same as the one for fluorescence experiments. The setup is a standard setup for transient absorption experiments with the repetition rate set at 500 Hz. This repetition rate is limited by the read-out time of the CCD camera. For the above-described fluorescence setup, the acquired data are integrated over many shots whereas the difference absorption spectra are acquired on a shot-to-shot basis for signal to noise reasons.

As in the fluorescence setup, the source is split into two as shown in Fig. 5.3. One part is passed through a Barium Borate crystal to generate a 390 nm pump pulse. This part is passed through the delay line to create a temporal delay with respect to the probe pulse. The second part of the beam is focused on a continuously translated CaF_2 plate for continuum generation. The resultant white pulse is then compressed using two

prisms. Following this, the continuum is passed through another beam splitter to have separate test and reference beams to correct for shot-to-shot variations of the probe beam. The pump beam is overlapped with the test beam within the 1mm quartz sample cell. The test and reference beams are spectrally dispersed in a polychromator so that data over the whole spectrum can be collected by a CCD camera configured as a dual array detector. As in the fluorescence setup, the sample is contained in a 1 mm quartz cell which is moved continuously using a lissajous scanner. The excitation wavelength was 390 nm for all time-resolved measurements.

Conventionally, the polarization is kept at magic angle (54.7 °) to avoid anisotropy effects. During this work, additional photoselection experiments have been performed on all samples. This was done by changing the polarization of the pump beam to be either parallel or perpendicular to the polarization of the probe beam. To do this, a half-wave plate is placed in the path of the pump beam before it is focused into the sample cell.

The photoselection experiments enable the calculation of anisotropy spectrum, $r(\lambda)$ for the samples. This is defined by the equation

$$ r = \frac{\Delta A_{\parallel} - \Delta A_{\perp}}{\Delta A_{\parallel} + 2\Delta A_{\perp}} \tag{5.1} $$

For pumping and probing single transitions at angle β[41]

$$ r = \frac{3\cos^2 \beta - 1}{5} \tag{5.2} $$

The value of r can vary between 0.4 (for $\beta = 90°$) and -0.2 (for $\beta = 0°$). The value of r can be outside this range if multiple overlapping transitions are probed, as is the case in our experiments.

5.7 Raw Data and Analysis

In Fig. 5.4 and Fig. 5.5 typical examples of averaged raw data obtained during the experiments are displayed. In all three figures, the x-axis stands for the wavelength of fluorescence or absorption and the y-axis indicates the time delay between the pump and the gate/probe pulse. The colours in the 3D plot signify the amplitude of the fluorescence/absorption signal, with the blue indicating low or negative signal and red indicating high or positive signal. The data with an acquisition scheme comprising
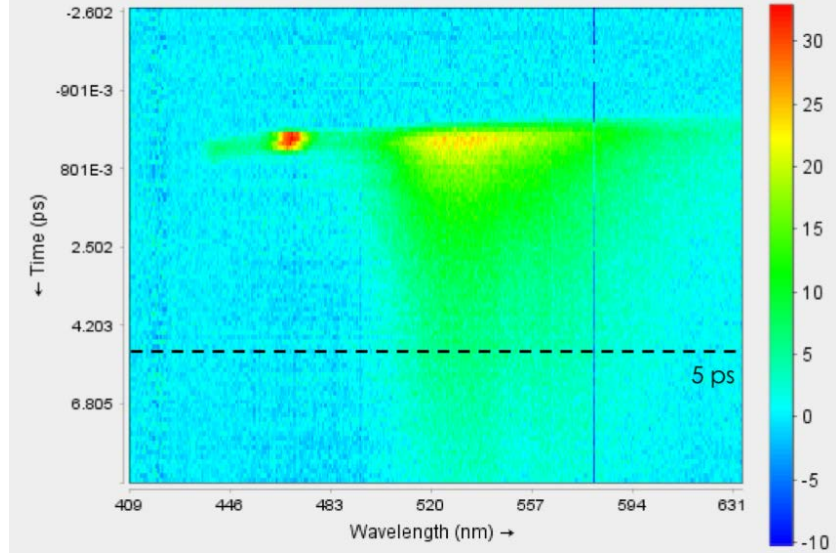
(a) Time-resolved fluorescence with suprasil
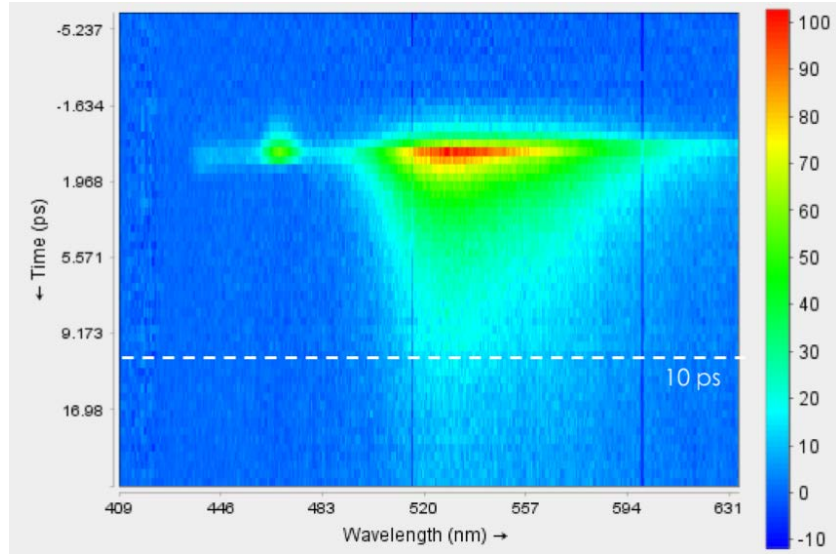
(b) Time-resolved fluorescence with CS$_2$. Note the different timescales in (a) and (b).

Figure 5.4: *False-colour 2D plots of averaged raw data obtained with glucose oxidase from A. niger over the course of the experiments. The spectra have been corrected for background. Figures (a) and (b) show time-resolved fluorescence data with suprasil and CS$_2$ Kerr gates respectively acquired till 12 ps and 24 ps respectively.*
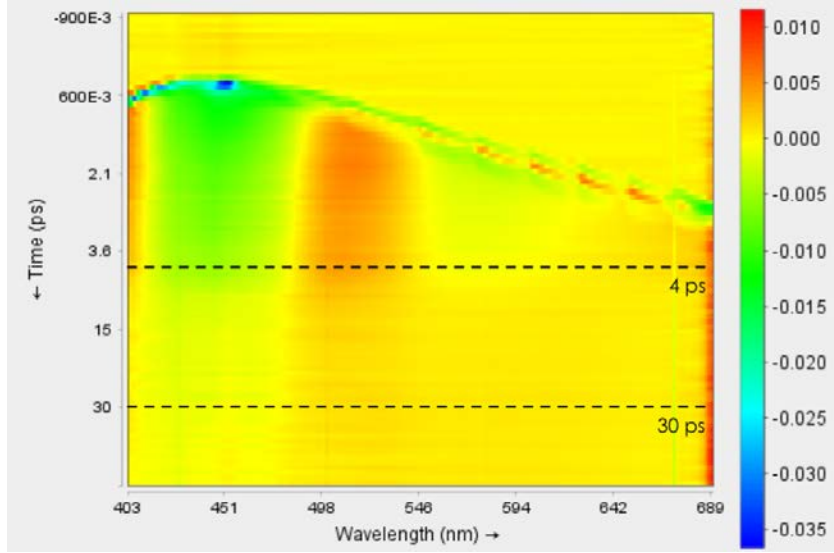
Figure 5.5: *False-colour 2D plots of averaged raw data obtained with glucose oxidase from A. niger during time-resolved absorption experiments. Data have been acquired till 100 ps. The dotted lines indicate the time point at which a change in time step occurs.*

different time windows with progressively longer time steps in each window.

As an example, Fig. 5.4 (*a*) and (*b*) show time-resolved fluorescence data of glucose oxidase with different Kerr media - suprasil and CS_2 respectively. The sharp peak at 440 nm around t=0 is due to Raman scattering of the aqueous solvent from excitation at 390 nm. Several Kerr media have been used in tandem for all time-resolved fluorescence experiments to get an overall picture of the fluorescence decay. In the case of glucose oxidase, the fluorescence decay is multiphasic with a very rapid (1 ps) initial decay and with a peak at 530 nm. With the CS_2 Kerr gate where data was acquired up to 24 ps with a minimum time step of 400 fs. Subsequently, the experiment was done under the same conditions with a suprasil Kerr gate to better elucidate the early stage of decay with time steps of $100 fs$. The amplitude of response of the Kerr medium is higher in CS_2 than suprasil, and therefore the CS_2 data have better signal-to-noise. The data obtained using each Kerr media have been combined for all the decay time traces shown in the subsequent sections.

In the transient absorption experiments the intensity I of the transmitted light is recorded, as a function of wavelength, by the detector. This is converted to absorption using Beer-Lambert law which is given by

$$A = -\log(\frac{I}{I_0}) \tag{5.3}$$

where I_0 is the initial intensity of light. At low concentrations of the sample, the absorption relates to the molecular extinction coefficient ε according to Beer Lambert

law which is given by

$$A = b\varepsilon\,c \tag{5.4}$$

where b is the path length of light in the sample (1mm), ε is the extinction coefficient and c the concentration of the sample.

As the beam splitter separating the rest and reference beam is not completely 50:50 over the whole spectral range and as both test and reference pass through the sample, I_0 is not determined in this experiment and the results are expressed as a difference in absorption ΔA. This ΔA is a superposition of n_{comp} contributions of various components and can be expressed as

$$\Delta A(t, \lambda) = b \sum_{i=1}^{n_{comp}} c_i(t)\Delta\varepsilon_i(\lambda) \tag{5.5}$$

Figure 5.5 shows the time-resolved absorption data over the full spectrum for glucose oxidase. The 3D plot shows the bleaching ($-\Delta A$, in blue and green, left), induced absorption ($+\Delta A$, in red, centre) and stimulated emission ($-\Delta A$ arising from FAD* emission, in green, centred around 560 nm) parts of the signal. In this case, spectral evolution with time can be seen distinctly in the raw data itself.

Also it is clear that the t=0 point varies with wavelength due to the dispersion of the probe beam. Furthermore, around t=0 relatively strong signals are observed due to the cross phase modulation artifact. These signals complicate the possibility of extracting ΔA signals on the time scale of the pulse duration.

The data from the time-resolved experiments were analyzed in terms of multi-exponential functions using the open-source software Glotaran[115] for global analysis. Through singular value decomposition, the number of parameters required to describe the system can be estimated. The analysis takes the instrument response function(IRF) and dispersion into account. The IRF is modeled as a Gaussian whereas the program fits the dispersion as a polynomial of variable order.

The data are accumulated as matrices $S(\lambda, t)$. Global analysis is based on the superposition principle, which itself is based on the assumption that the measured data can be described by a linear combination of n components $S'(\lambda, t)$, each with a distinct time profile and spectrum. This is represented mathematically as

$$S'(\lambda, t) = \sum_{i=1}^{n} c_i(t)a_i(\lambda) \tag{5.6}$$

where n is the number of components, $c_i(t)$ and $a_i(t)$ are the time and spectral profile of any component i. The kinetic scheme where n components decay independently and mono-exponentially in parallel results in Decay Associated Spectra (DAS), one for every component. In this case, equation 5.6 is adjusted as

$$S'(\lambda, t) = \sum_{i=1}^{n} c_i^{DAS}(t) DAS_i(\lambda) \tag{5.7}$$

Further, the simplest interpretation of the DAS consists of a kinetic scheme where the components decay sequentially in an unbranched, unidirectional manner with increasing lifetimes ($A \rightarrow B \rightarrow \ldots \rightarrow n$). In this scenario the first compartment A gets populated by an input excitation pulse and subsequently forms the second component. The second component decays into the third compartment and so on, until finally the n$^{\text{th}}$ component decays to the ground state. This is called the sequential model. The spectra calculated from this scheme are called the Species Associated Spectra (SAS) and reflect the spectra of the intermediate species.

In the subsequent chapters, the terms DAS and SAS will both be used frequently to describe the results of the analysis. When used in the context of time-resolved absorption, the terms to Decay Associated Difference Spectra (DADS) and Species Associated Difference Spectra (SADS) will be used as all transient absorption spectra are essentially difference spectra.

Chapter 6

Femtosecond spectroscopy of *wild type* TrmFO and mutants

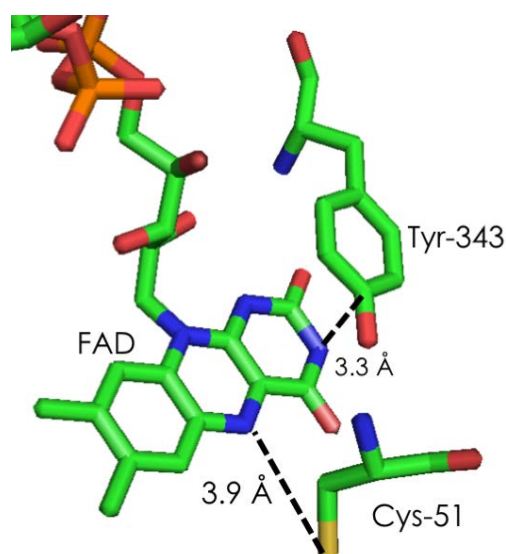## 6.1 Experiments on Wild type TrmFO and mutation of Cys51

Figure 6.1: *Active site of wt TrmFO as seen in the crystal structure (PDB:3G5Q). Selected distances between the FAD and the nearest amino acid residues have been given.*

While most of our work on TrmFO concerns modified variants, in this section we will first report results from steady state and ultrafast time-resolved measurements on *wild type* TrmFO. Subsequently, we will explain the effect of the mutation of a specific cysteine residue.

Fig. 6.1 shows the active site of wt TrmFO as seen in the crystal structure (PDB 3G5Q).[117] The amino acid residues, which will be discussed most in this chapter, are the ones closest to the isoalloxazine ring of the FAD cofactor- cysteine at position 51
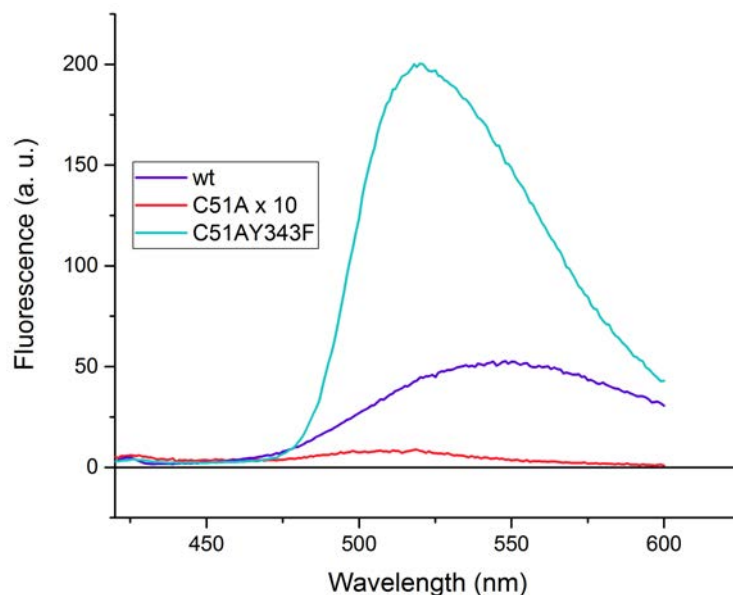
Figure 6.2: *Steady state fluorescence of wt TrmFO and mutants C51A and C51A/Y343F. The spectra have been normalized at excitation wavelengths- 380 nm for wt and C51A/Y343F and at 400 nm for C51A. The wt fluorescence is intense and centred at 550 nm. The mutants have a typical fluorescence spectrum centred at 520 nm. Fluorescence is much lower in amplitude for mutant C51A compared to the wild type and C51A/Y343F.Intense fluorescence of C51A/Y343F is probably due to the absence of quencher Tyr343.*

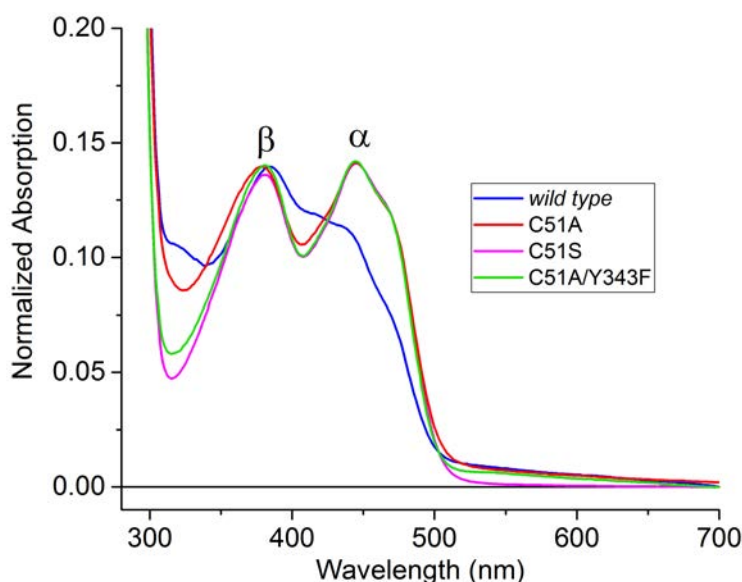Figure 6.3: *Steady state absorption spectra of wild type TrmFO (in blue) and mutants C51A (red), C51S(pink) and C51A/Y343F(green). The wt spectrum is different from that of typical flavoproteins due to the adduct which has a distinct band at 400 nm. The absorption spectra of the mutants are typical for flavoproteins and the absorption bands for α and β transition moments[116] have been indicated.*
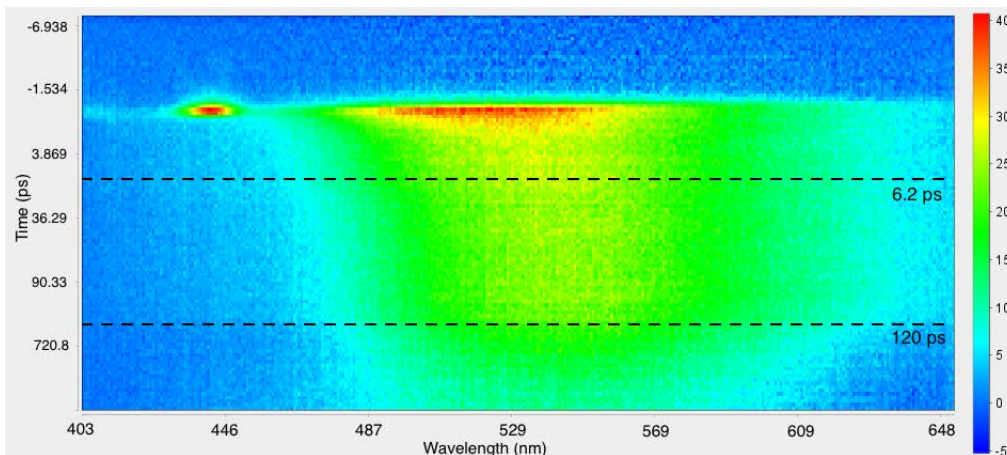
Figure 6.4: *Raw data of time-resolved fluorescence experiments on wt TrmFO with CS_2 as a Kerr medium. Starting at 7 ps before t=0, points have been acquired every 0.3 ps till 6.2 ps, every 3 ps till 120 ps and every 75 ps thereafter until 2 ns. Different time windows have been indicated.*

(Cys51, 3.9 Å   distance between the S atom and N5 of the isoalloxazine ring)[1] and tyrosine at position 343 (Tyr343, closest ring-to-ring distance of 3.3 Å). In solution, wt TrmFO partially forms an adduct with Cys51.[118] This adduct is thought to be a dormant reaction intermediate that can be activated by binding of tRNA. As the adduct is not visualized in the crystal structure, its structure has been debated and has been suggested to be an iminium adduct.[105] In *Bacillus subtilis* TrmFO at physiological pH, this adduct dissociates within hours after purification.[119] By contrast, in the purified *T. thermophilus* enzyme, we found that this adduct is stable and does not convert to regular oxidized FAD (FAD_{ox}), even at elevated temperatures.[1] However under white light illumination, the spectrum of this adduct changed significantly, whereas it remained constant when the protein was kept in the dark.[105]

Fig. 6.3 shows the steady state absorption spectra of wt TrmFO and the C51A, C51S and C51A/Y343F mutants. The wt spectrum is unusual for a flavoprotein and superimposed on a regular FAD spectrum, an additional broad absorption around 400 nm is observed. This broad absorption band is a distinct marker of the adduct.[105] Since Cys51 is involved in the adduct formation, its replacement renders the protein adduct-less and the resultant absorption spectra (for C51A, C51S and C51A/Y343F) are typical for flavoproteins. The cysteine has been mutated to alanine which has a $-CH_3$ side chain in place of cysteine's $-CH_2SH$, making it smaller in size and *a priori* avoiding steric hindrance in the active site caused by the mutation. Cys51 was also mutated to serine. Here, the $-CH_2SH$ side chain is replaced by a sterically similar $-CH_2OH$ moiety. The mutants C51A and C51S can thus be regarded as the closest models of the wt without the adduct. The absorption bands corresponding to α (at 450 nm) and β (at 380 nm) transition dipole moments[116] in these mutants have been

indicated. For ultrafast studies, the proteins are excited at 390 nm which is between the α and β transition dipoles.

The FAD-Cys51 adduct absorbing around 400 nm causes wt TrmFO to be highly fluorescent as shown in Fig 6.2. The spectra have been normalized to the absorption at the excitation wavelength. Wt fluorescence is centred at 550 nm and is red-shifted by 20-30 nm compared to typical flavoproteins. By contrast, in the mutants C51A and C51A/Y343F, the adduct is not formed and their steady state fluorescence spectra are typical for flavoproteins, with peaks at 520 nm. The fluorescence of TrmFO C51A is highly quenched, to about 100 times lower compared to wt, possibly due to the presence of a quencher (Tyr343). Overall fluorescence in C51A/Y343F is observed to be much higher than in C51A, presumably due to the absence of the potential electron donor Tyr343.
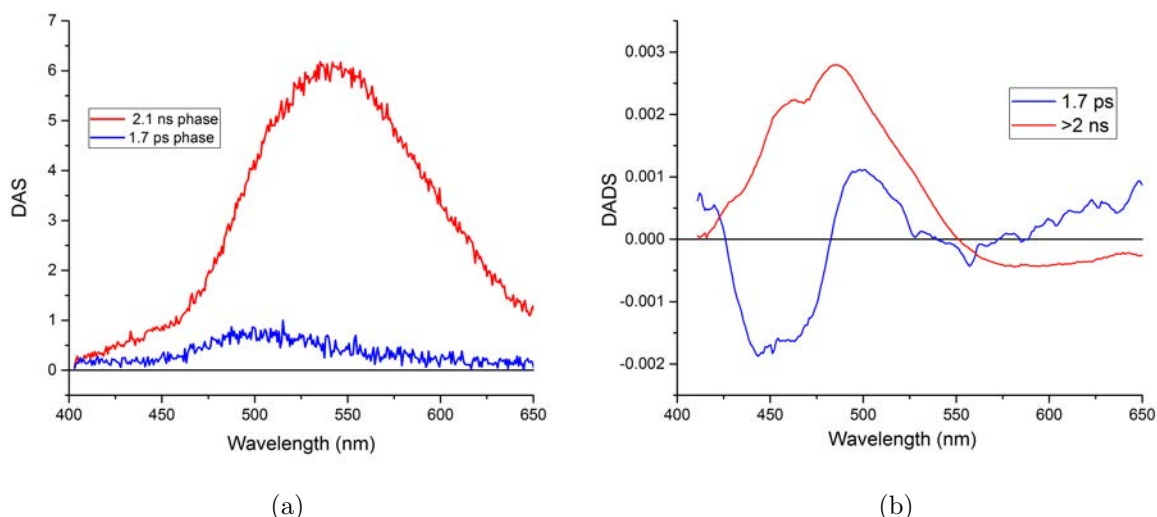

(a)

(b)

Figure 6.5: *(a) Decay associated spectra (DAS) from the femtosecond time-resolved fluorescence spectroscopy measurements on wt TrmFO. (b) Decay associated difference spectra (DADS) from the femtosecond time-resolved absorption spectroscopy of wt TrmFO.*

Results of the preliminary time-resolved experiments were performed on wt TrmFO have been shown in Fig. 6.5. The fluorescence DAS (Fig. 6.5 (a)) are dominated by the strong long-lived component with a decay time of $\sim$2 ns and a maximum at $\sim$550 nm. This component is assigned to the adduct. A much smaller fast phase centred at $\sim$500-520 nm with a time constant of $\sim$1.7 ps is also observed. However, due to the strong fluorescence of the $\sim$2 ns phase, the decay associated with this component is more difficult to resolve and possibly additional sub-picosecond decay also occurs (see Chapter 5). The short-lived fraction is assigned to the portion of non-adduct FAD in wt TrmFO. These assignments are supported by the analysis of the time-resolved absorption measurements on wt TrmFO in terms of decay associated difference spectra

(DADS, Fig. 6.5 (b)). The 1.7 ps phase resembles the excited state spectra of flavoproteins with typical bleaching (at 450 nm) and stimulated emission bands (at 550 nm). The stimulated emission feature of the $\sim$2 ns phase is red-shifted.

As will be discussed more extensively below for mutant TrmFO, the short lifetime of the fluorescence of regular FAD can be assigned to quenching by electron transfer from the close-by Tyr343. Such quenching does not appear to occur in the adduct. This finding may be related to the large Stokes shift in fluorescence of the adduct, which implies a much stronger relaxation in the excited state. Thus, the excited state potential energy minimum lies much lower in the adduct than in non-adduct FAD, leading also to a lower driving force ($\Delta G°$) for electron transfer initiated by excited state formation. A quantitative estimation of the driving force in wt TrmFO is complicated by the lack of knowledge on the redox potential for the FAD adduct complex.

A rough estimate indicates that the observed time constant of 1.7 ps is in the region expected for electron transfer from Tyr343 to FAD*. As mentioned above, the ring-to-ring distance between the FAD isoalloxazine ring and the tyrosine phenol ring is 3.3 Å. Using the model from Dutton and coworkers[23] (see section 2.2) that assumes homogeneity in the protein using a uniform-barrier model, the expected rate constant of electron transfer is $1.3 \times 10^{13} s^{-1}$ if the reaction would be barrierless (see equation 2.6). The found rate constant is only one order of magnitude lower than this, in agreement with the notion that this equation is near-barrierless[120] (see section 6.6). Indeed, using Eqn. 2.6 and the observed rate one can estimate the activation energy at $\sim$ 0.1 eV, much lower than the driving force estimated in the order of -1.08 eV (see section 3.2). In this exercise, the reorganizational energy would be $\sim$ 1.06 eV, so $\lambda \approx -\Delta G$. We emphasize that this reasoning should be considered only as a check of general agreement; for such short distances, the hypothesis of protein homogeneity is likely not completely accurate.

The heterogeneity in wt TrmFO arises due to the presence of the adduct and the corresponding strong signals. To avoid complications, in the remaining sections we will study modified TrmFO proteins in which the adduct does not form, mostly by replacement of Cys51.
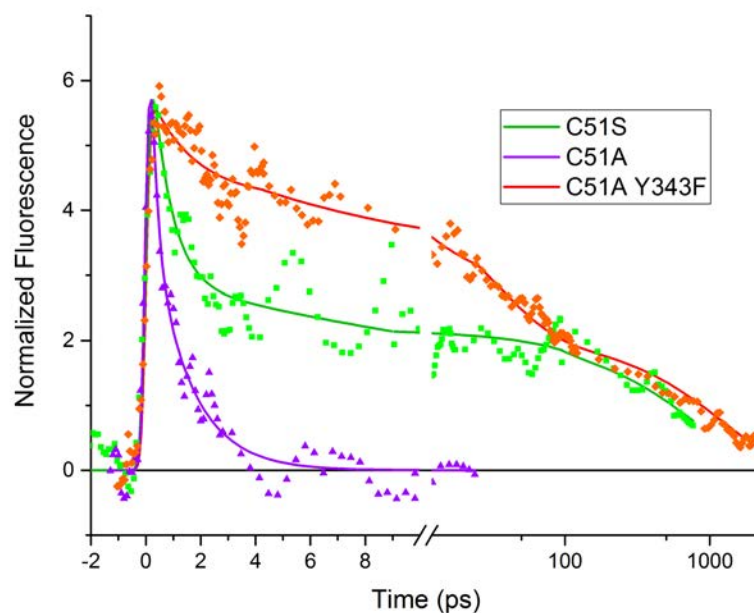
Figure 6.6: *Timetraces at 520 nm of the TrmFO mutants C51A, C51S and C51A/Y343F observed using time-resolved fluorescence. The scale is linear till 10 ps and logarithmic thereafter. The traces have been smoothened using a Savitzky-Golay method in Origin.*

| (a) | (b) |
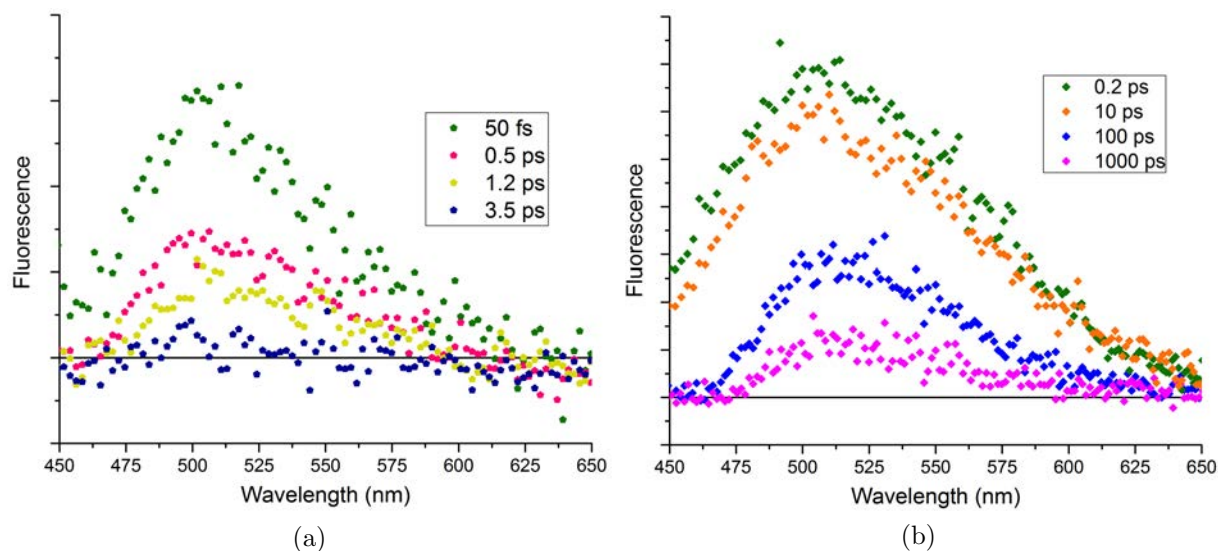
Figure 6.7: *Time-resolved fluorescence spectra of TrmFO mutants (a) C51A, where decay is over within 3.5 ps, and (b) C51A/Y343F, where fluorescence remains even after 1 ns.*

(a)

(b)

(c)

Figure 6.8:   *Decay Associated Spectra of TrmFO (a) C51A, (b) C51S and (c)
C51A/Y343F fluorescence. Signal-to-noise is lower for the 0.7 ps phase in C51S due
to use of suprasil as Kerr medium to resolve sub-picosecond kinetics (see chapter 5).*

6.2 Experiments on TrmFO mutants

6.2.1 Results from ultrafast fluorescence measurements
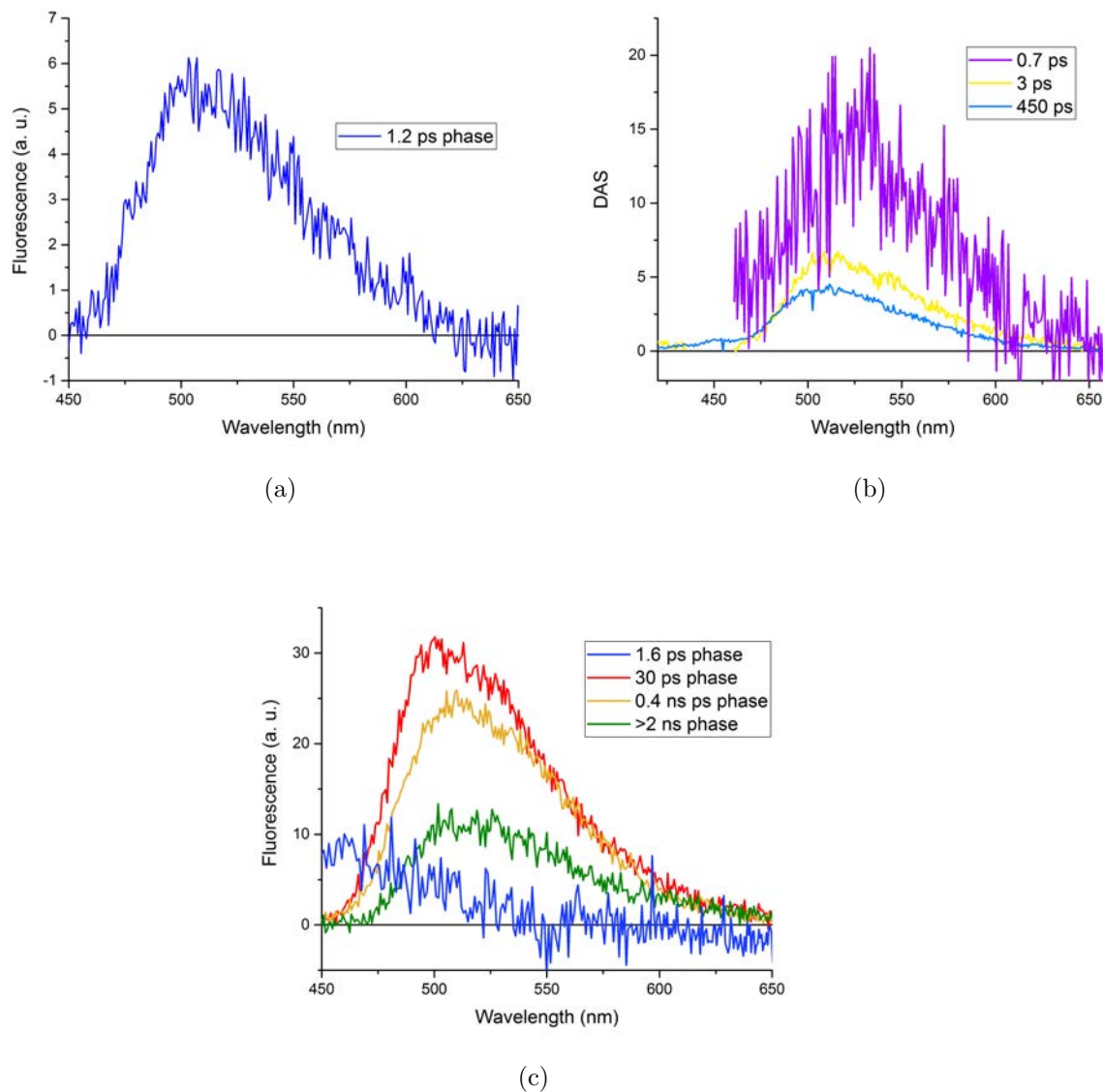
Figure 6.6 shows the fluorescence time-traces at 520 nm of the major mutants of TrmFO that have been studied. As mentioned in section 6.1, Cys51 was mutated to alanine and serine. The alanine mutation C51A yielded a fluorescence decay that was completed within a few picoseconds, consistent with the low total fluorescence observed (Fig. 6.5 (b)). In the C51S mutant, a similarly fast decay phase is observed, but also significant slower phases, indicating a more heterogeneous flavin environment, possibly due to steric hindrance. The ultrafast fluorescence decay of the C51A mutant also indicates the presence of an efficient nearby FAD* quencher. Tyr343 was hypothesized to be the primary quencher as the fluorescence decay of the C51A/Y343F mutant was much slower than the single mutant C51A or C51S. Furthermore, the decay of C51A/Y343F is predominantly faster than the open conformation of FAD in solution[121] indicating the presence of a secondary quencher. The Trp214 residue lying on a flexible loop in TrmFO is a candidate to be the secondary quencher. These results will be discussed quantitatively and in more delail in the following sections.

To explore the role of Tyr343 as a fluorescence quencher, the time-resolved fluorescence spectra of TrmFO C51A and C51A/Y343F have been compared in Fig. 6.7. TrmFO C51A undergoes ultrafast fluorescence decay which is completed within 3.5 ps whereas C51A/Y343F undergoes a multiphasic decay predominantly occuring on much longer timescales and which continues beyond 1 ns. This finding leads to the conclusion that Tyr343 is responsible for the very fast fluorescence decay in C51A TrmFO. The precise role of Tyr343 will be explored by studying the product states after the rapid fluorescence quenching in C51A through time-resolved absorption spectroscopy (see Section 6.2.2).

Global analysis of the data in Fig. 6.7(a) indicated that the fast decay of C51A could be described by a single exponential with a time constant of 1.2 ps. The DAS of this phase in C51A (Fig. 6.8 (a)) is centred around 520 nm, confirming that it corresponds to the FAD* fluorescence. As indicated above (see Fig. 6.6), the decay of C51S was multiphasic. Here, three phases were obtained from the fit, with time constants of 0.7 ps, 3 ps and 450 ps (Fig. 6.8(b)). While the two fastest phases for C51S are in the same time-range as the decay of C51A (suggesting a similar quenching mechanism by Tyr343), the presence of a significant slower phase indicates substantial heterogeneity in the configuration of the active site. Therefore, for simplicity, the analysis of the role of Tyr343 will be further studied based on the cysteine to alanine substitution.

We also note that the fluorescence decay in C51A TrmFO is very similar to that of the fraction of wt TrmFO assigned to regular (non-adduct) FAD (see Section 6.1). This indicates that fluorescence quenching by Tyr343 also occurs in the wild type protein. Thus, C51A TrmFO appears a suitable model system for studying the dynamic properties of FAD in TrmFO, given the complications of the presence of the adduct in wt TrmFO.

The fluorescence decay of C51A/Y343F requires four exponentials to be fit in a multiexponential model, with time constants of 1.6 ps, 30 ps, 0.4 ns and >2 ns. The DAS corresponding to the first 1.6 ps phase (Fig. 6.8 (b)) is blue-shifted and lacks the typical FAD fluorescence characteristics, much like the 1.5 ps phase in wt ThyX.[101] This phase is ascribed to vibrational cooling. We note that a separate vibrational cooling phase is not found from the analysis of C51A fluorescence decay (Fig. 6.8(a)) as it occurs in the same timescale as the fluorescence decay (time constant 1.2 ps). The slower phases in C51A/Y343F and C51S describe their multiphasic fluorescence decay indicating that multiple configurations of flavin-electron donor pairs coexist, like in the flexible enzyme ThyX which catalyzes a similar reaction[114] (see chapter 4). This makes them *a priori* interesting candidates for flexibility studies(section 6.6).
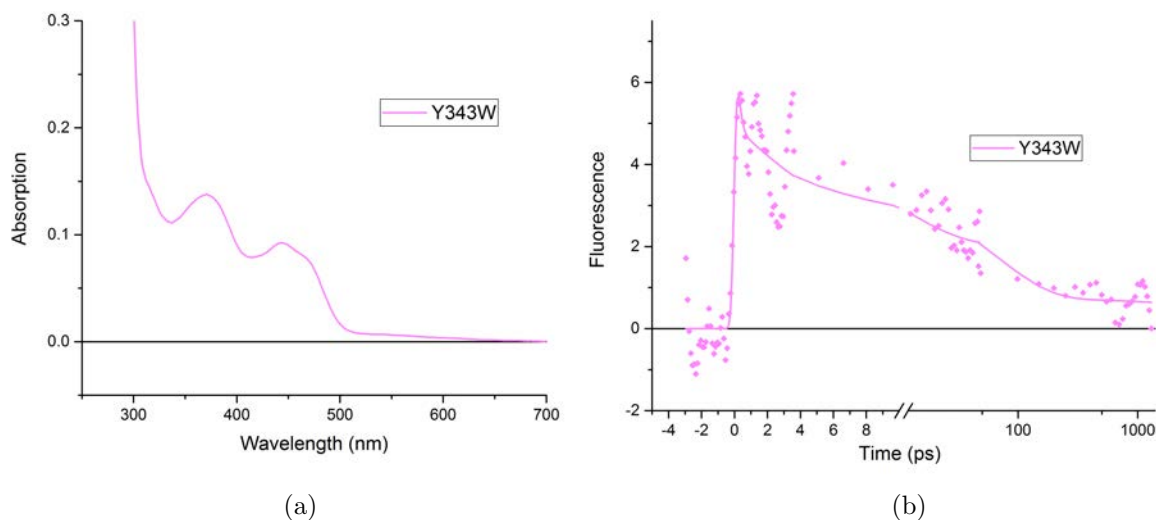
Figure 6.9: *(a) Steady state absorption of Y343W TrmFO. (b) Timetrace of TrmFO Y343W mutant fluorescence at 520 nm in lin-log scale.*

Additionally, Tyr343 was mutated to tryptophan (without the Cys51 mutation) to compare the efficiency of FAD* quenching. As seen from the steady state absorption spectrum(Fig. 6.9(a)), the adduct (at 400 nm) is not formed in this mutant presumably because Tyr343 is required for the positioning of the adduct.[105] Fig. 6.9 (b) shows the fluorescence decay of Y343W at 520 nm. The time constants obtained from its fit were -

7 ps, 75 ps and > 2 ns.

The driving force for electron transfer from Trp to FAD* is throught to be higher than for Tyr and it has, therefore, been argued that Trp is more efficient in a quenching system where the donor is sandwiched between Trp and Tyr.[120] However, in TrmFO Y343W, it is observed that FAD* quenching by Trp343 is less efficient compared to Tyr343 (in wt and C51A). For Tyr radicals, electron transfer is essentially barrierless (see section 6.1). Furthermore, the isoalloxazine ring of the FAD and the phenyl ring of Tyr343 are observed to be in a semi-stacked position in the crystal structure, an organization that could facilitate electron transfer from Tyr343 to FAD*. The substitution of tyrosine with tryptophan likely causes a significant change in the protein environment, as the double-ring Trp is bulkier than Tyr, leading to less favourable positioning of the residue for electron transfer (and to heterogeneity), which may explain the slower decay kinetics. In this context, we note that this mutant was less stable than the other TrmFO variants studied here, as also reflected in the scattering feature in the absorption spectrum (6.9 (a)). This decreased stability also precluded reliable transient absorption measurements on this mutant.

6.2.2 Results from time-resolved absorption measurements

(a)   (b)
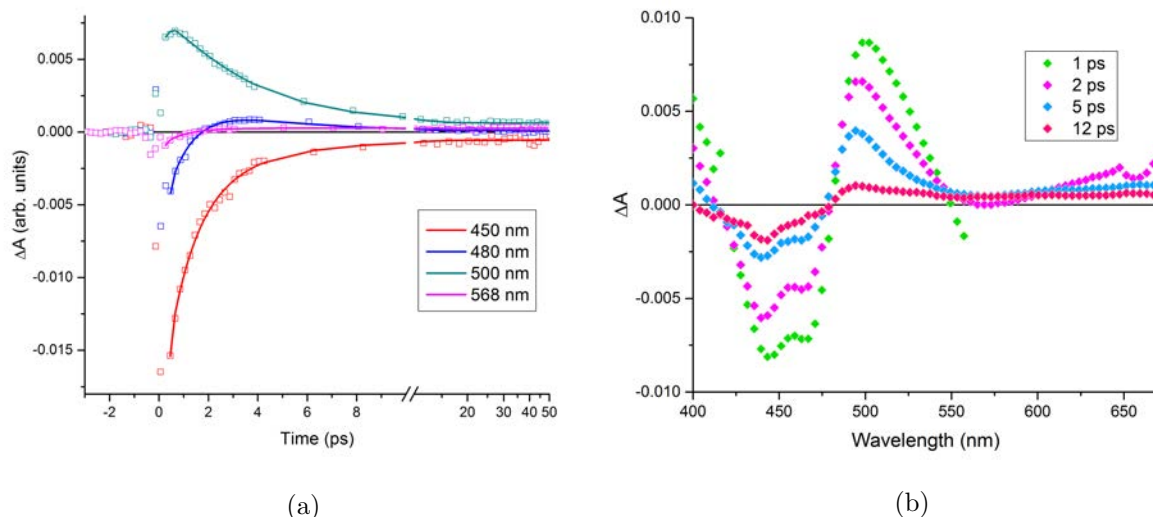
Figure 6.10: *(a) Time-traces at various wavelengths and (b) difference absorption spectra at certain time delays for TrmFO C51A. The spectra are not corrected for chirp.*

To characterize the photoproducts of the TrmFO C51A, transient absorption spectroscopy was performed. Fig. 6.10 shows the transient absorption kinetics and spectra. The kinetics at 450 nm (peak of the ground-state absorption) and at 568 nm (in the stimulated emission region) are dominated by a phase of ∼1 ps. The time

(a)   (b)

Figure 6.11:   *Decay Associated Difference Spectra of TrmFO (a) C51A and (b) C51A/Y343F.*

constant of this phase is similar to that of the fluorescence decay, and therefore this phase can be assigned to FAD* decay. However at 500 nm, an induced absorption that decays substantially slower is observed, indicating the presence of a distinct product state.

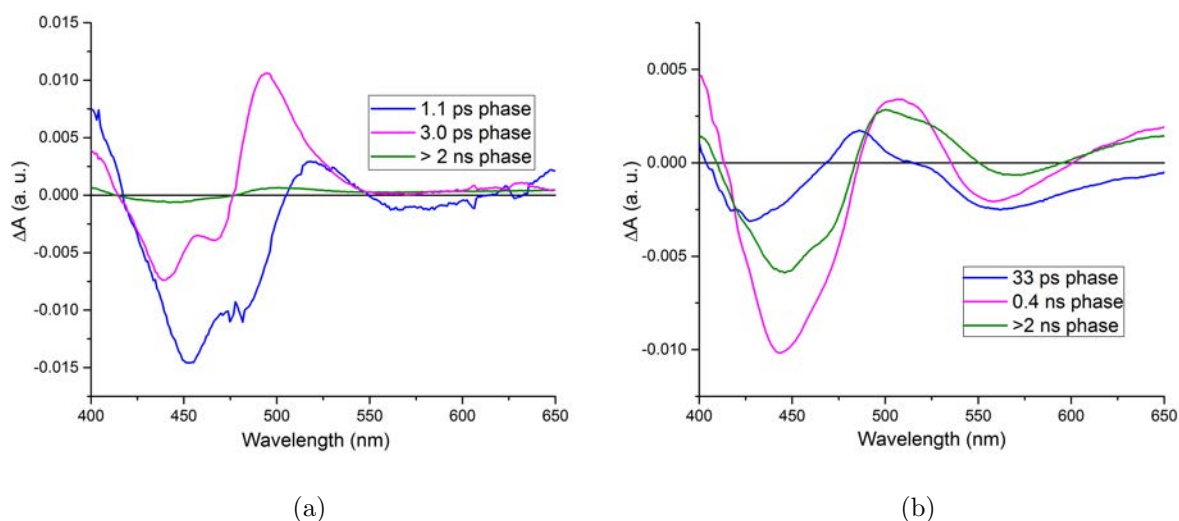Full analysis of the data in terms of DADS is given in Fig. 6.11. Two distinct kinetic phases, with time constants of 1.1 and 3.0 ps, are required to fit the data. The 1.1 ps phase, ascribed to decay of the excited-state FAD*, contains bleaching features in the FAD_{ox} absorption region and further negative absorption above 550 nm that is assigned to stimulated emission. This 1.1 ps phase also contains induced absorption features around 400 and 520 nm that are assigned to excited-state absorption. The FAD* decay in 1.1 ps gives rise to the product state decaying partly very fast (faster than it is formed) and partly in 3.0 ps (Fig. 6.12 (a)) . The 3.0 ps phase lacks stimulated emission features. It contains a strong induced absorption band centered at 490 nm that has significantly higher amplitude than the corresponding bleaching band at 450 nm. The 490 nm band is much larger and very uniquely shaped compared to any absorption expected for the anionic and neutral flavoquinone forms $FAD^{\bullet-}$ and $FADH^{\bullet}$ in this region (see section 6.3).

Fig. 6.12 (b) shows the SADS of TrmFO C51S which are consistent with the analysis of C51A. Here, two phases are observed - 0.7 ps and 3 ps. The 0.7 ps phase resembles a typical FAD* excited state spectrum, with the aforementioned bleaching (450 nm) and stimulated emission (560 nm) bands. Additionally, the 3 ps phase resembles the 3 ps phase obtained from C51A adding consistency to our analysis.
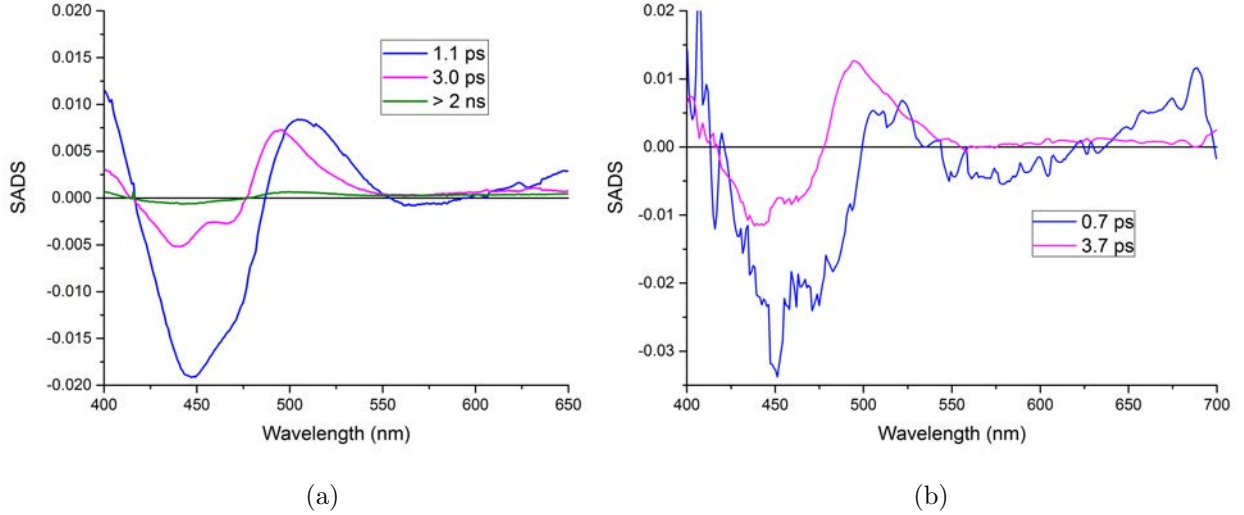
61

(a)   (b)

Figure 6.12: *(a) Species Associated Difference Spectra (SADS) corresponding to the DAS of Fig. 6.11(a). These spectra correspond to a model in which the DAS are interpreted in terms of a model $A \rightarrow B \rightarrow C$. The difference spectrum A corresponds to the initially formed state, here FAD* minus FAD_{ox} ; B an intermediate state formed in 1.1 ps and C a final state formed in 3.0 ps. As the final spectrum of C is very small, the spectrum of B (3.0 ps SADS) is very similar to the 3.0 ps DAS discussed in the text and assigned to $FAD^{\bullet -}\ TyrOH^{\bullet +}$ minus FAD_{ox}. The 1.1 ps SADS contains bleaching features in the FAD_{ox} absorption region and further negative absorption above 550 nm which is assigned to stimulated emission. Furthermore, the induced absorption features around 400 nm and 520 nm are assigned to excited state absorption. The larger bleaching in the 1.1 ps SADS with respect to the 3.0 ps SADS indicates that the 3.0 ps phase corresponds to only part of the initially excited FAD, presumably because a substantial part of the product state formed in 1.1 ps recombines to the ground state on a timescale faster than its formation. Precise quantification of the yield of the product state is complicated by the compensating excited state absorption (1.1 ps SADS) and $FAD^{\bullet -}$ (3.0 ps SADS, see Fig. 6.13) bands superimposing the ground state absorption region. We estimate this yield at roughly 20-40% C. (b) DADS of TrmFO C51S. The fast 0.7 ps phase has poorer signal to noise than the 3 ps phase (see Section 5). Only the fast components of decay have been shown in this figure.*
.

As Tyr343 is the electron donor responsible for quenching FAD*, we assign the 3 ps phase to a tyrosyl radical. As the tyrosine is protonated in the neutral state (TyrOH), the initial photoproduct is expected to be TyrOH$^{\bullet+}$, but if deprotonation occurs along with electron transfer, then TyrO$^{\bullet}$ will be formed. The latter state has been characterized well spectrally, and absorbs at 400-410 nm[93,122] (Fig. 6.14).Therefore the feature at 490 nm is assigned to TyrOH$^{\bullet+}$ and it was inferred that in this protein system, the tyrosyl cation radical can be formed as a distinct species without concomitant proton transfer.[123,124] In the DAS of transient absorption experiments of the C51A/Y343F double mutant, the strong 490 nm feature is not observed (Fig. 6.11 (b)), which is in full agreement with its assignment to the Tyr343 cation radical.

A minimal reaction scheme, concerning the fraction of the enzyme that gives rise to a product state with a 3 ps lifetime, is depicted in Scheme 6.1. After the decay of the main 1.1 ps and 3 ps phases a small phase remains, which corresponds to $\sim 3\%$ in the bleaching area. The spectrum of this long-lived phase is reminiscent of that of the 3 ps phase and may reflect a very small fraction of the protein in which the product state is long- lived, although the low amplitude prohibits firm assignment.
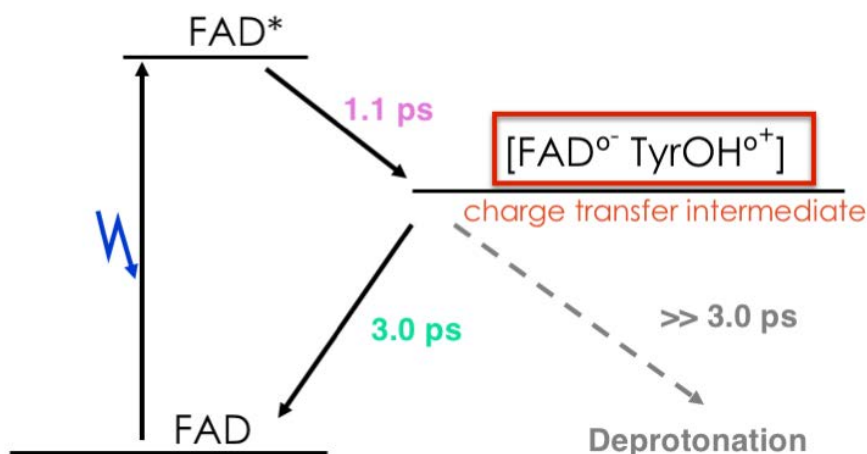
Scheme 6.1. *Proposed Minimal Charge-Transfer Pathway in C51A TrmFO.*

6.3   Identification of the TyrOH$^{\bullet+}$ intermediate

To determine the spectrum of TyrOH$^{\bullet+}$, the 3 ps phase from Fig. 6.11 (a) was modeled as a sum of FAD$^{\bullet-}$ *minus* FAD$_{ox}$ and TyrOH$^{\bullet+}$ *minus* TyrOH. As a model spectrum for FAD$^{\bullet-}$, the published steady state FAD$^{\bullet-}$ spectrum of an insect cryptochrome[83] was taken. The steady state FAD$_{ox}$ absorption spectrum of TrmFO C51A has been measured
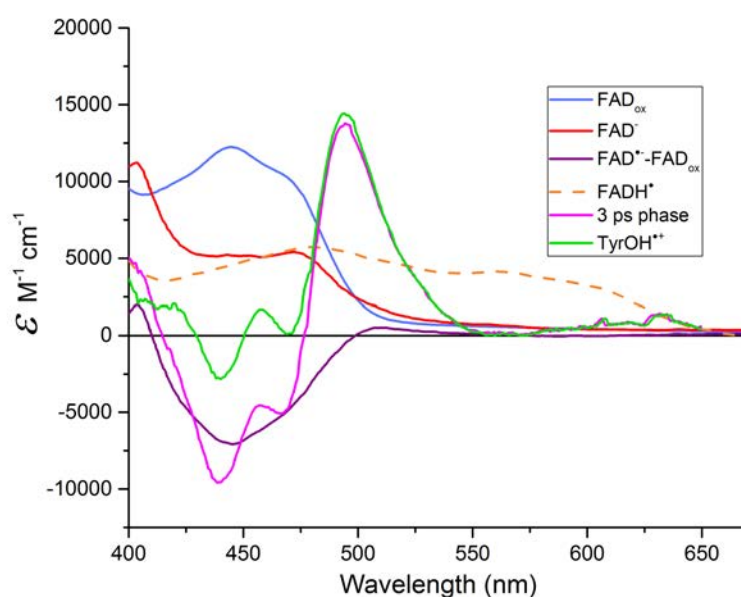
Figure 6.13: *Spectrum of TyrOH[•+] as calculated from the 3 ps DADS of Fig. 6.11 (a) using a model spectrum of FAD[•−83] and the measured FAD_{ox} steady-state spectrum. For comparison, a spectrum for the FADH[•] form of DNA photolyase from E. coli[89] has also been shown, which can be fully formed in steady state. In the red part of the spectrum, where it does not overlap with FAD_{ox}, this spectrum is similar to the FADH[•] spectrum of TrmFO.[125]*

(Fig. 6.2). TyrOH doesn't absorb in the visible range in its ground state. Therefore,

$$\varepsilon_{\text{TyrOH}^{\bullet+}} = b\text{DADS}_{3ps} - (\varepsilon_{\text{FAD}^{\bullet-}} - \varepsilon_{\text{FAD}_{\text{ox}}}) \tag{6.1}$$

where the variable b has been optimized so that the blue spectral region (<470 nm) is dominated by the flavin contributions and the TyrOH$^{\bullet+}$ spectrum in that region is minimal. However, small oscillations are observed in the deduced TyrOH$^{\bullet+}$ spectrum in that region. These can be attributed to the usage of the FAD$^{\bullet-}$ spectrum from insect cryptochrome which may vary from that of TrmFO.

At wavelengths >470 nm, the TyrOH$^{\bullet+}$ spectrum is smooth as the flavin forms absorb poorly (if at all) and hence contribute only modestly to the uncertainty of the spectrum. The TyrOH$^{\bullet+}$ spectrum modeled here consists of a $\sim$40 nm broad band with a maximum at 490 nm. This spectrum represents to our knowledge the first known spectrum of the tyrosyl cation radical in solution or in a polypeptide.[1]
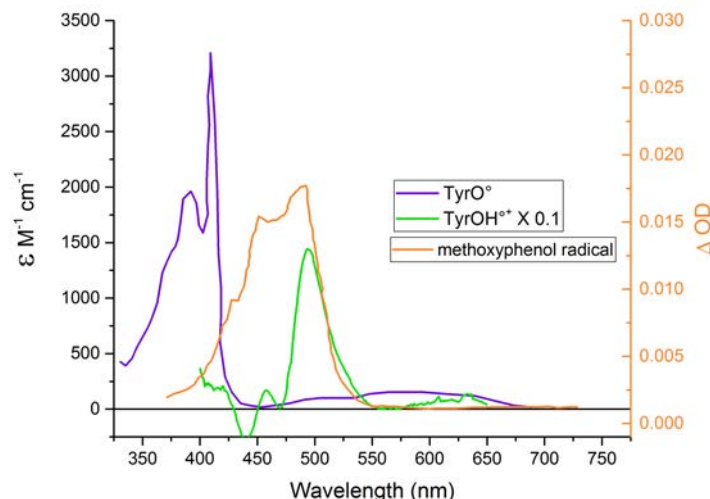
Figure 6.14: *Spectrum of TyrOH$^{\bullet+}$ as shown in Fig. 6.13 compared with the known spectrum of the TyrO$^{\bullet}$.[93,122] Also shown for reference is the spectrum of the methoxyphenol radical[126] which is close to the structure of TyrOH$^{\bullet+}$.*

Fig. 6.14 compares the calculated spectrum of TyrOH$^{\bullet+}$ with that of TyrO$^{\bullet}$.[93,122] The two are distinctly different with TyrO$^{\bullet}$ having a sharp peak at 400-410 nm and very weak contributions >470 nm. This comparison lays further weight to the assignment of the product state to TyrOH$^{\bullet+}$. Additionally, the TyrOH$^{\bullet+}$ spectrum corresponds well with the spectrum of the the structurally close methoxyphenol radical obtained by laser flash photolysis.[126]

Given the low pK$_a$(≈ -2) of tyrosyl, it might also be expected that deprotonation

occurs to a closely located proton acceptor. Hence, deprotonation of TyrOH$^{\bullet+}$ could compete with back electron transfer from TyrOH$^{\bullet+}$ to FAD$^{\bullet-}$. While Tyr343 is within hydrogen bonding distance of other residues,[1] the most prominent candidate for a proton acceptor would be the reduced flavin (pK$_a$ $\sim$8.3[127]): the distance between Tyr O and FAD N5 atoms is 3.9Å). The expected resultant FADH$^{\bullet}$ spectrum is shown in Fig. 6.13. As deduced from the lack of sizable tyrosyl deprotonation and of FADH$^{\bullet}$ formation, the rate constant of such a proton transfer reaction is $\ll (3\text{ps})^{-1}$.

Finally, the rate of proton transfer is expected to be sensitive to substitution of H$^+$ to D$^+$. Therefore, transient absorption experiments were also performed on TrmFO C51A by changing to a D$_2$O HEPES buffer. No changes were found in the transient spectra and the rate constants (not shown). This result is consistent with the above conclusion that proton transfer does not play a role in the C51A reaction scheme (Scheme 6.1).

Altogether, the above results demonstrate that not only is the intermediate TyrOH$^{\bullet+}$ formed and observed, it decays very fast in 3 ps and can be formed without concomitant proton transfer.

6.4 Dipole moment directions from anisotropy experiments

The transient absorption experiments described above were performed under isotropic conditions (pump polarized at magic angle with respect to the probe). In order to gain insight in the orientation of the involved dipole moments, we also performed transient anisotropy experiments on C51A TrmFO as described in chapter 5. Here we will focus on the results from the DADS of the 3 ps phase corresponding to the FAD$^{\bullet-}$ *plus* TyrOH$^{\bullet+}$ *minus* FAD$_{\text{ox}}$ spectrum.

The direction and spectral properties of the transition dipole moments of FMN in flavodoxin crystals have been determined by steady state polarization spectroscopy by *Eaton et. al.* in 1975.[116] Using this work as a reference, under our excitation conditions (pump centred at 390 nm), both the (lowest-lying) α- and the β-transitions are excited (see Fig. 6.3), but the α-transition is predominantly excited. The two transitions make a small angle ($\sim 20°$). Our finding (Fig. 6.15) of two regions where the anisotropies are both almost constant but have two distinct values justifies the decomposition of Fig. 6.13 with little spectral overlap between TyrOH$^{\bullet+}$ and the two FAD forms.

The anisotropy in the bleaching region in Fig. 6.15 is close to 0.4 which corresponds to pumping and probing parallel transitions. In this region, the bleaching of the FAD_{ox} α-transition contributes to the signal as well as the induced absorption of $FAD^{\bullet-}$ (Fig. 6.1). The constant r value of $\sim$0.4 in this region confirms that the FAD_{ox} α-transition is excited predominantly and indicates that the probed $FAD^{\bullet-}$ transition is near-parallel to this α-transition.

The other distinct anisotropy region at 0.24 ± 0.04 in Fig. 6.15 corresponds to the spectral region assigned to the $TyrOH^{\bullet+}$ absorption band. This anisotropy corresponds to a $31° \pm 5°$ angle between the excited FAD_{ox} α- transition and the probed $TyrOH^{\bullet+}$ transition.

Given the evidence that the 450 nm band is not due to a "hot" vibrational state of FAD (*c.f.* ref [128]) as seen from the distinct anisotropy bands in Fig. 6.15, it can be concurred that the spectral peak at $\sim$ 490nm in the 3 ps phase (see Fig. 6.12) corresponds to a different species than FAD_{ox}.

The transition dipole moments in neutral TyrOH have already been studied through linear dichroism spectroscopy in combination with quantum mechanical calculations.[129] The L_a transition is parallel to the symmetry axis in the plane of the molecule (Fig. 6.16). Assuming the orientation of the transitions determined for the isoalloxazine as seen by Eaton *et al.*[116] are the same in TrmFO, the direction of the FAD α-transition is depicted in Fig. 6.16 in the wt crystal structure (PDB:3G5Q). Our result that the angle between the FAD α-transition and the $TyrOH^{\bullet+}$ transition is $31°$ leads to a cone of possible angles for the latter transition. In addition, assuming that the $TyrOH^{\bullet+}$ transition lies within the phenol plane, this cone is reduced to two possible orientations of the transition. They both lie closer to the symmetry axis corresponding to the lowest (UV) L_b transition of neutral TyrOH[129] rather than the perpendicular L_a transition (Fig. 6.16). The most likely candidate is the one that makes a small angle of $23°$ with the symmetry axis (solid yellow line in Fig. 6.16). This can be explored further with theoretical studies of the $TyrOH^{\bullet+}$ transition in TrmFO C51A. Such studies may help to reach a firm assignment on which of these orientations corresponds to the 490 nm $TyrOH^{\bullet+}$ band.

6.5 Secondary quencher of fluorescence

As mentioned in Section 6.2.1, when the primary quencher Tyr343 is mutated, the fluorescence decay of C51A/Y343F slows down but remains faster than the open form of free FAD in solution[121] indicating the presence of a secondary quencher. On
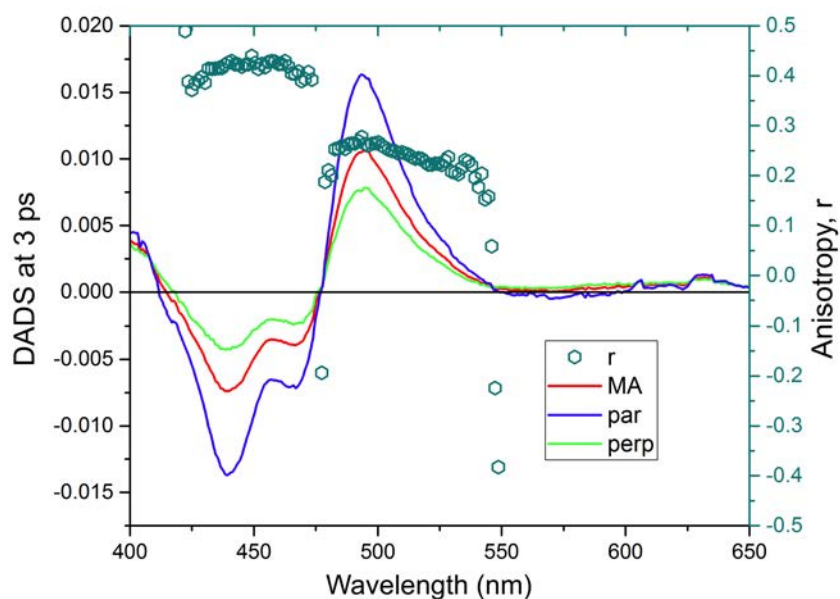
Figure 6.15: *Anisotropy spectrum (r) calculated from the DADS of the 3 ps phases obtained under polarized excitation conditions overlaid with the 3 ps phase from the DADS from Fig. 6.11 (a) obtained under magic angle polarization.*
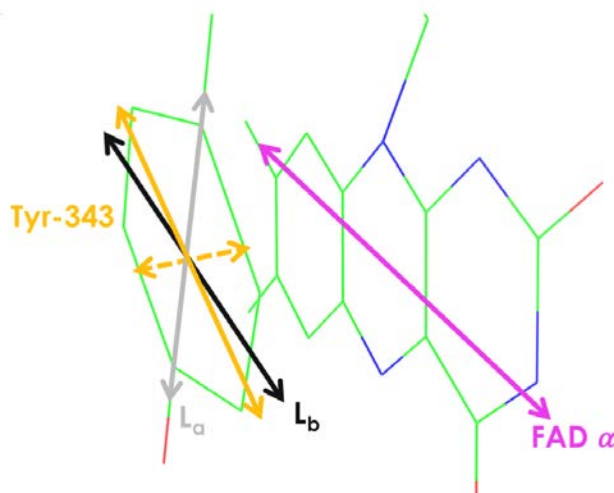
Figure 6.16: *Possible orientations of the TyrOH$^{\bullet+}$ transition in the tyrosine plane (yellow) deduced from the transient anisotropy experiments of Fig. 6.15. The lowest α transition dipole in FAD[116] and the ground-state L_a and L_b transitions of TyrOH$^{\bullet+}$[129] are also represented.*
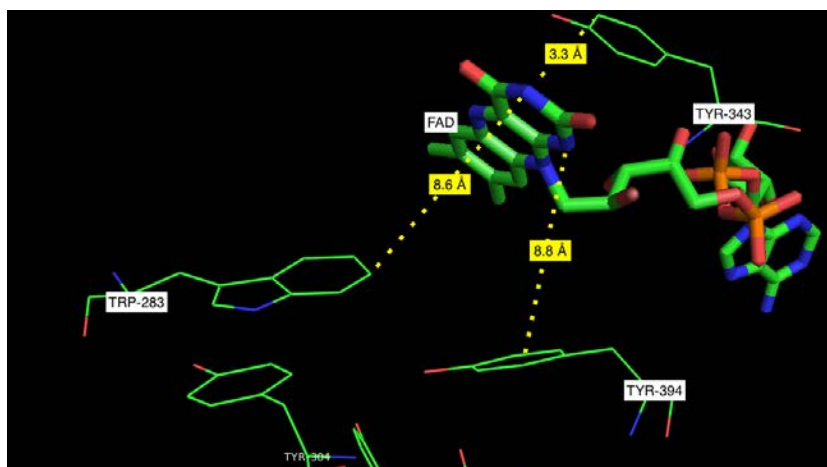
Figure 6.17: *Prospective secondary quenchers of FAD* fluorescence as visualized using
the wt TrmFO crystal structure (PDB:3G5Q). Trp283 (8.6Åclosest distance from FAD)
and Tyr394 (8.8 Å closest distance from FAD) are seen to be the next closest redox active
amino acid residues. Another possibility has been proposed to be Trp214 which lies on a
flexible loop.*
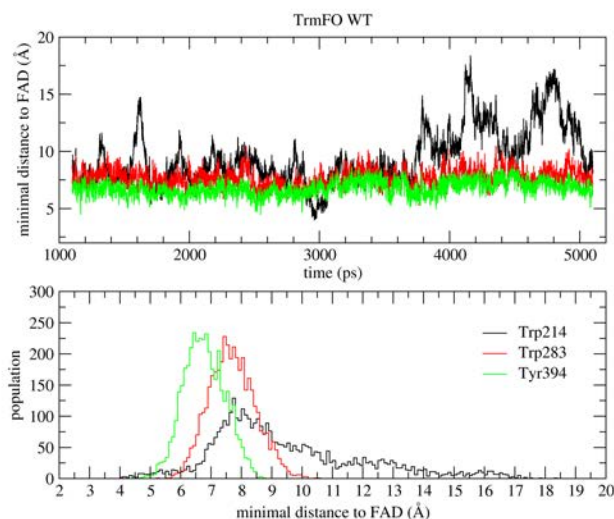
Figure 6.18: *Distance variations (upper) and distribution (lower) of residues Trp214,
Trp283 and Tyr394 to the FAD extracted from molecular dynamics simulations of wt
TrmFO.*
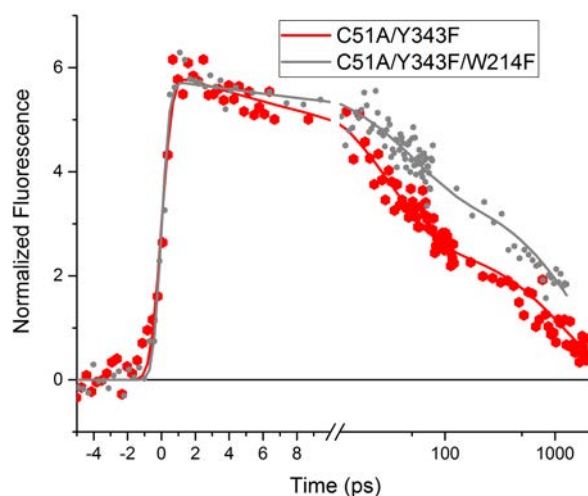
Figure 6.19: *Fluorescence decay of C51A/Y343 compared with that of C51A/Y343F/W214F at 520 nm. Both measurements were performed using CS_2 as Kerr medium.*

Figure 6.20: *Decay associated spectra (DAS) of triple mutant C51A/Y343F/W214F. W214 proves to be a candidate for future studies on the secondary quencher as the fastest DAS phase here is slower than that of C51A, but yet faster than free FAD solution.*

examining the crystal structure (Fig. 6.17), Trp283 (8.6 Åclosest distance from FAD) and Tyr394 (8.8 Å closest distance from FAD) are seen to be the next closest redox active amino acid residues. Additionally, wt TrmFO also contains a highly flexible loop which c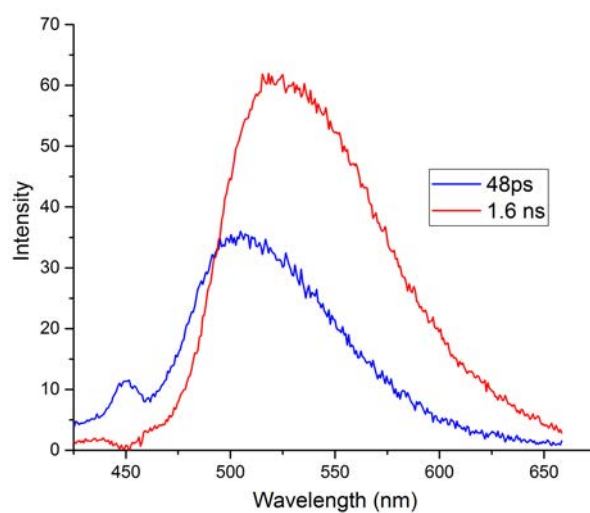annot be visualized in the crystal structure. The Trp214 situated on this flexible loop was examined as a potential secondary quencher of FAD* fluorescence in TrmFO. Using molecular dynamics simulations on wt TrmFO (in collaboration with Jean-Christophe Lambry at LOB), the distances between the potential secondary quenchers and FAD were modelled (Fig. 6.18). Although the average distance of Trp214 to FAD appears higher than that of Trp283 and Tyr394, these results confirm the freedom of motion of Trp214 as its distance distribution is very broad (spanning 13Å) and includes FAD-Trp214 distances below 5 Å. Furthermore, we note that the average distances of Trp283 and Tyr394 to the isoalloxazine ring in the equilibrated system are somewhat lower than those in the crystal structure.

To explore the role of Trp214 as a secondary fluorescence quencher, the triple mutant C51A/Y343F/W214F was made and studied. Its fluorescence kinetics are compared with the double mutant C51A/Y343F in Fig. 6.19. To ensure a fair comparison between the two, data recorded only using CS_2 as Kerr medium have been used as data for the highly fluorescent C51A/Y343F/W214F was recorded only using CS_2 Kerr medium. As seen in Fig. 6.19, the fluorescence decay of this triple mutant was slower than C51A/Y343F indicating that Trp214 may be one of the secondary quenchers.

On global analysis of the fluorescence data of C51A/Y343F/W214F, two phases of 48 ps and 1.6 ns were obtained. As in C51A/Y343F, the faster of the two phases in Fig. 6.20 is blue shifted compared to the other, with a peak at 500 nm. The time constants of the DAS fit from C51A/Y343F are 30 ps, 0.4 ns and a long-lived phase (excluding the 1.6 ps relaxation phase retrieved with suprasil as a Kerr medium, Fig. 6.8(c). On comparison, the 30 ps phase becomes slower in the triple mutant (to 48 ps) and lower in relative amplitude, suggesting the involvement of Trp214 as a secondary quencher of FAD* fluorescence, but not as exclusively.

The results above describe the preliminary investigation of the secondary quencher of FAD* quenching in TrmFO, suggesting the involvement of Trp214. However, other residues, in particular Trp283 and Tyr394 presumably also contribute to the quenching observed in the C51A/Y343F mutant. To better elucidate the secondary quenching mechanism, further experiments with proteins modified at these positions are required.

6.6 Flexibility studies on TrmFO C51A/Y343F

(a)   (b)
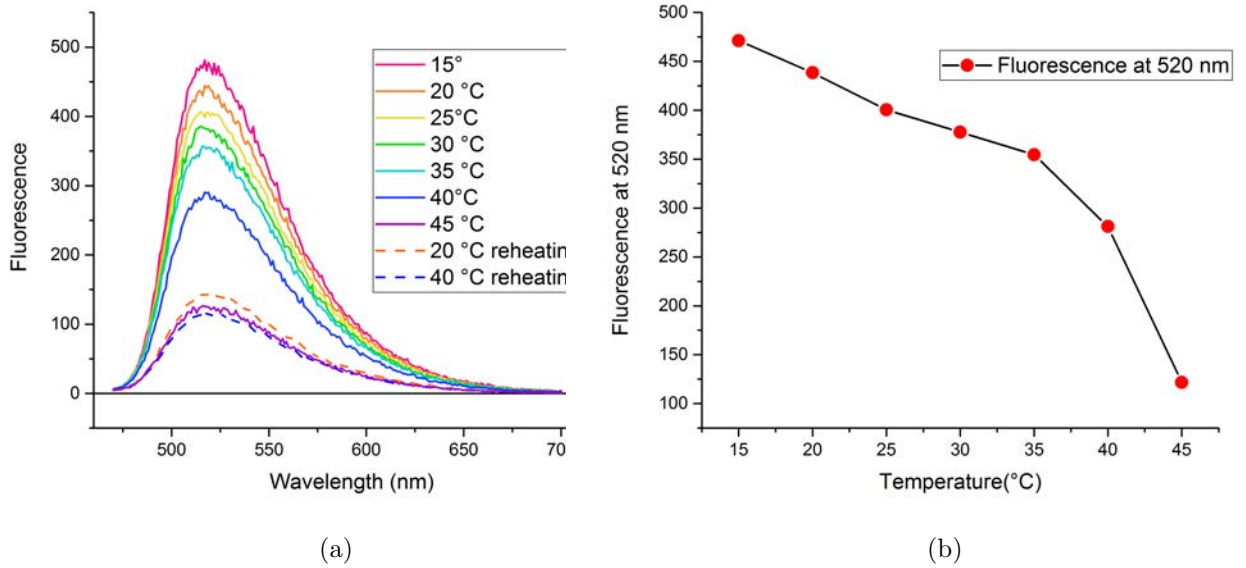
Figure 6.21: *(a) Evolution of steady state fluorescence of TrmFO C51A/Y343F with temperature. Spectra are recorded with polarizers in the excitation and emission beam set at magic angle to remove any polarization effects. The change appears irreversible: when lowering the temperature again the fluorescence remained low (20°C and 40°C reheating). (b) Maximum fluorescence of TrmFO C51A/Y343F at 520 nm as a function of temperature.*
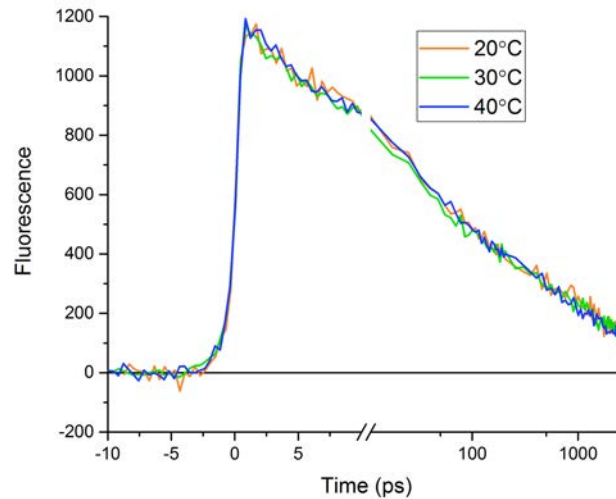
Figure 6.22: *Comparison of normalized fluorescence decays of TrmFO C51A/Y343F at different temperatures.*

As discussed in Section 6.1, the mutant C51A/Y343F has a slower fluorescence decay than C51A and it is multi exponential. This indicated that multiple

72

configurations of flavin-electron donor pairs coexist, like in the flexible enzyme ThyX from the hyperthermophile *Thermotoga maritima* which catalyzes a similar reaction[114] as TrmFO. In the study by Laptenok *et al.*[114] (see chapter 4), steady state ThyX fluorescence was observed to reversibly decrease as a function of increasing temperature. On performing a similar experiment on TrmFO C51A/Y343F, total fluorescence also decreased with increasing temperature. The fluorescence decrease rather than increase at higher temperatures indicated that the protein-bound FAD is not released at high temperatures ($\sim$ 40°) in TrmFO C51A/Y343F. However, the change appears irreversible: when lowering the temperature again, the fluorescence remained low (20°C and 40°C recooling, Fig. 6.21 (b)). Concomitantly, slow sample precipitation was also observed at higher temperatures. Qualitatively similar effects were observed when less extensive temperature ranges were investigated. These effects are assigned to protein degradation without flavin release upon warming, suggesting a low thermal stability of the mutant protein, notwithstanding the origin in thermophilic organism of the wild type protein.

On performing temperature-dependent time-resolved fluorescence measurements on C51A/Y343F, a remarkably invariable fluorescence decay was observed in the 20-40° range (Fig. 6.22). This indicates that the decrease of total fluorescence upon warming described above is not due to changes in fluorescence lifetime, but rather to flavin degradation into non-fluorescent species. The temperature-independence of the multi phasic fluorescence decay is unlike that observed in ThyX[114] and indicates that the distribution of donor-acceptor configurations sampled does not change during the time-period sampled. To further investigate the implications of this finding, a clearer identification of the effective residues of the quenching in the mutant is required.

Generally, the striking temperature-independence of Fig. 6.22 is in agreement with the reasoning in section 6.1 that in FAD* $\rightarrow$ FAD$^{\bullet-}$TyrOH$^{\bullet+}$, electron transfer occurs in a virtually barrierless regime (see also Mataga *et al* : ref [120]).

Chapter 7

Identification and characterization of TyrOH$^{\cdot+}$ of *wild type* Glucose Oxidase

Glucose oxidase (GOX) is a widely used flavoprotein in the food[130,131] and pharmaceutical industries[132] , in biofuel cells[133] as well as a major component of glucose biosensors[134] . GOX is a flavoprotein that catalyzes the oxidation of β-d-glucose at the hydroxyl group at the C1 position by using molecular oxygen as the electron acceptor to produce glucono-β-lactone and hydrogen peroxide. While glucose oxidase does not require photoactivation for its function, photoinduced electron transfer in wild type GOX has been relatively well studied before with ultrafast spectroscopic techniques[100,106,120,135,136] presumably related to its commercial availability.

Tyrosyl radicals have been suggested to be involved as an intermediate in electron transfer reactions in several systems, as discussed previously in chapter 3 but they have not been well characterized. Following the spectral characterization of TyrOH$^{\bullet+}$ in a TrmFO variant (chapter 6), we will present evidence in this chapter for its involvement in the photo-induced electron transfer pathway in GOX from *Aspergillus niger*.

7.1   Wild type glucose oxidase from *Aspergilus niger*

GOX is a homodimeric enzyme, with an FAD molecule bound non-covalently at the active site of each subunit. The two subunits of GOX from *Aspergillus niger* that is studied here have a molecular mass of 80 kDa each. In the vicinity of the isoalloxazine moiety of the FAD, there are five aromatic residues (shown in Fig. 7.1): Tyr515 (at 4.0 Å closest approach to the isoalloxazine of the FAD), Tyr68 (4.3 Å), Trp111 (7.0 Å), Tyr565 (8.3 Å) and Trp426 (8.4 Å). On photoexcitation of GOX, fluorescence
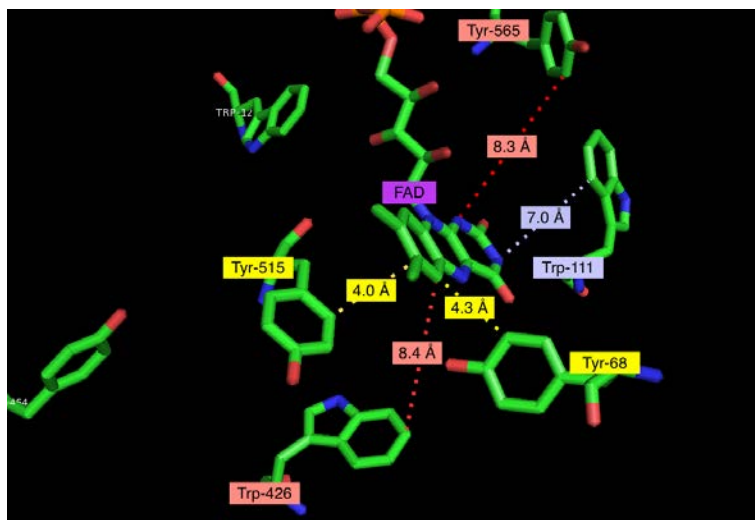
Figure 7.1: *Active site of GOX from Aspergillus niger as seen in the crystal structure PDB: 1CF3. The potential redox-active residues closest to the isoalloxazine ring of the FAD have been shown. The closest residues are Tyr515 (4.0 Å) and Tyr68 (4.3 Å) and are indicated in yellow, the next closest is Trp111 (7.0 Å) indicated in blue and subsequently, 565(8.3 Å) and Trp426(8.4 Å) indicated in red.*

quenching of the FAD molecule is expected to be due to its interactions with these residues. In particular, Tyr515 and Tyr68 are located at $\sim$4 Å from the isoalloxazine ring and appear as candidates to be primary electron donors, although no ring stacking configuration, as in TrmFO, occurs.

All studies reported in this chapter were performed on wild type GOX.

7.2 Previous studies on photochemistry of glucose oxidase

Mataga *et al.*,[107,120] were the first to report ultrafast data on GOX. Femtosecond upconversion experiments yielded flavin fluorescence decay time constants of 0.4 ps, 1.8 ps and 6.0 ps. Although these experiments do not allow investigating product states, the most close-lying Tyr residues Tyr515 and Tyr68, rather than the Trp residues were suggested to be involved in the barrierless ultrafast electron transfer reactions.

Zhong and Zewail,[106] by contrast, proposed that electron transfer can occur from both Tyr and Trp, since none of the surrounding redox-active residues stack completely with the FAD. In their single-wavelength time-resolved fluorescence and absorption measurements, they observed decay constants of $\sim$2 ps and $\sim$10 ps (fluorescence) and $\sim$1 ps, $\sim$10 ps, $\sim$30 ps and nanoseconds(absorption) which are close to our results(Section 7.4 and 7.5). They also attributed the $\sim$30 ps decay to FAD$^{\bullet-}$ - TrpH$^{\bullet+}$

and the longer nanosecond phase to the FAD$^{\bullet-}$ - TyrOH$^{\bullet+}$ decay. In view of the lower stability of the TyrOH$^{\bullet+}$ intermediate (as discussed in chapter 3), this may appear unlikely.

Fujiwara *et al.* studied photoinduced electron transfer in GOX using transient ultraviolet resonance Raman (UVRR) spectroscopy[136] with ∼3 ps resolution. Based on the intermediate bleaching of Trp-assignable bands (that are stronger than Tyr-assignable UVRR features) they proposed the involvement of Trp rather than Tyr as electron donor to FAD, although they did not explicitly rule out the possibility of the involvement of the two close-lying Tyr residues in electron transfer. They explained their findings by the less favourable driving force for tyrosine oxidation due to the higher oxidation potential of TyrOH/TyrOH$^{\bullet+}$[137] compared to TrpH/TrpH$^{\bullet+}$.[94] We note that TyrOH$^{\bullet+}$ has not yet been characterized by Raman spectroscopy and its signal could be weak making it difficult to observe and characterize by this method.

A strong motivation for our studies came from the study by Lukacs *et al.*[100] who performed time-resolved IR and visible absorption studies on GOX with full spectral resolution. The DADS obtained from the visible transient absorption measurements are shown in Fig. 7.2. The 3 ps phase was ascribed to excited state decay (in rough agreement with the multiphasic decay on the same timescale reported in the above-mentioned studies) and the 24 ps phase to a product state. The product state was reported to contain FAD$^{\bullet-}$ and an oxidized electron donor.

This quencher, responsible for the reduction of FAD*, was hypothesized to be TrpH$^{\bullet+}$ in this study. The 24 ps phase product state DADS was modelled, using the then-available model spectra, as FAD$^{\bullet-}$ *plus* TrpH$^{\bullet+}$ *minus* FAD$_{ox}$ (Fig. 7.2). However this model fits the experimental data rather unsatisfactorily, as TrpH$^{\bullet+}$ has a broader, red-shifted spectral signal.[98] On comparing this 24 ps DADS with the 3 ps DADS from TrmFO C51A(6.11 (a)), it is observed that both have a similar peak at ∼490 nm (reminiscent of the TyrOH$^{\bullet+}$ spectrum in section 6.3).

Altogether, the above studies give indications of the involvement of TyrOH$^{\bullet+}$ in FAD fluorescence quenching and electron transfer in GOX, although the spectral evolution appears more complex than in the TrmFO C51A system. We therefore reinvestigated GOX photochemistry. The results obtained from our studies, substantiating TyrOH$^{\bullet+}$ involvement, are detailed in the following sections.
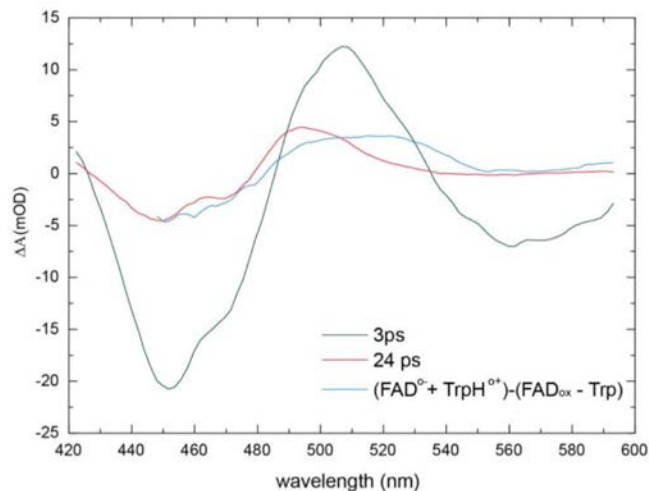
Figure 7.2: *DADS of glucose oxidase as reported by Lukacs et al..[100] The 24 ps phase has a spectra similar to that of the 3 ps phase in TrmFO C51A (Fig. 6.11 (a)), with an intense induced absorption peak $\sim$490 nm. The 24 ps phase was modelled with the TrpH$^{\bullet+}$ spectrum. This model, as claimed by the authors, is "not definitive".*
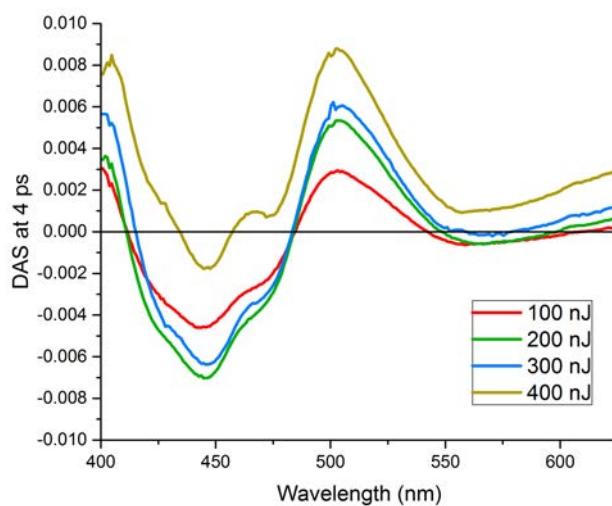
Figure 7.3: *Pump energy per pulse dependency on transient absorption signals of GOx. The pump energy per pulse was fixed at 150 nJ for all experiments to keep the signal in the linear regime.*

7.3 Pump energy dependency of GOX spectrum

Excitation for both transient fluorescence and absorption experiments was centred at 390 nm. On conducting preliminary transient absorption experiments on GOX, a signal dependency on the pump intensity was observed (Fig. 7.3). At pump energies per pulse > 200 nJ the signal saturated and additional non-linear signals were observed. For this reason, the pump energy was kept at 150 nJ per pulse to keep the signal in the linear regime.

7.4 Excited state kinetics from time-resolved fluorescence

<div align="center">(a)   (b)</div>
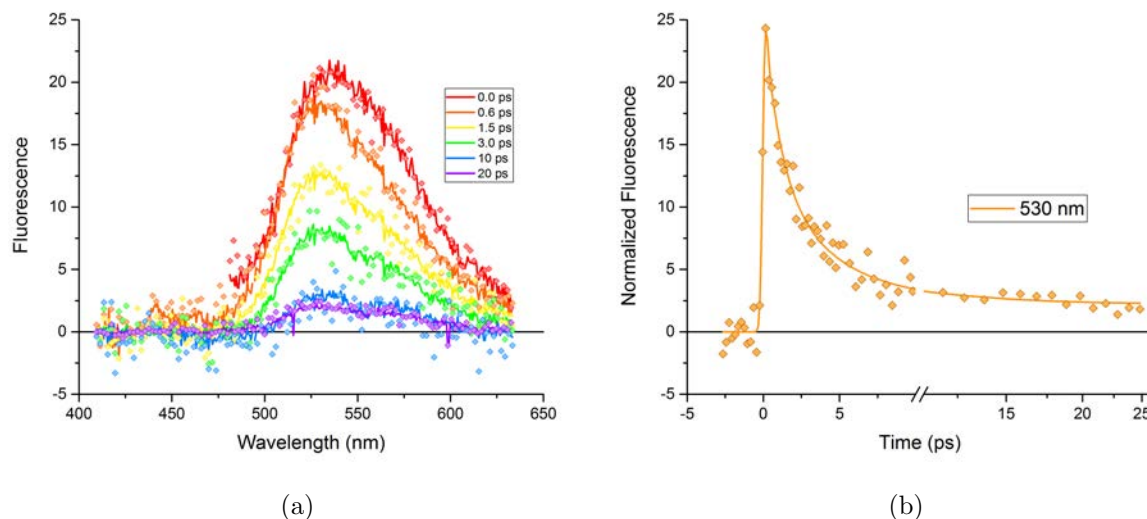
Figure 7.4: *Evolution of the fluorescence spectra(a) and the timetrace at 530 nm for the transient fluorescence spectra (b) of GOx on a lin-log scale.*

The fluorescence data were acquired using two Kerr media (Suprasil and CS$_2$) upto 25 ps. The first 10ps of data have been obtained with Suprasil and the remaining 15 ps with CS$_2$. Fig. 7.4 (a) shows the evolution of the spectra in time and Fig. 7.4 (b), the timetrace at 530 nm. The total fluorescence decays to approximately half after 2 ps and at 10 ps, most protein-bound FAD* decay is completed. The fluorescence remains constant from 10 ps onwards indicating the presence of a small amount of free FAD in solution, which has a longer fluorescence decay.

The global analysis fit indicates that, as reported in other work, the decay is modestly non-exponential in GOX. The time-constant parameters obtained from the fit were 1 ps ($\sim$ 70%), 4 ps and a minor long phase (longer than the timescale of the
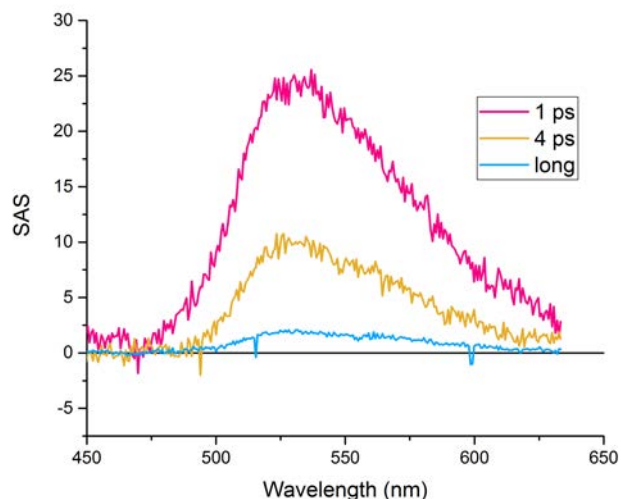
Figure 7.5: *Absolute SAS for GOx with time constants.*

experiment). This confirmed that the fluorescence decay of GOX bound-FAD is rapid and reflects conformational heterogeneity.

To visualize the product states formed, transient absorption experiments were performed.

7.5 Time-resolved absorption of GOX

| (a) | (b) |
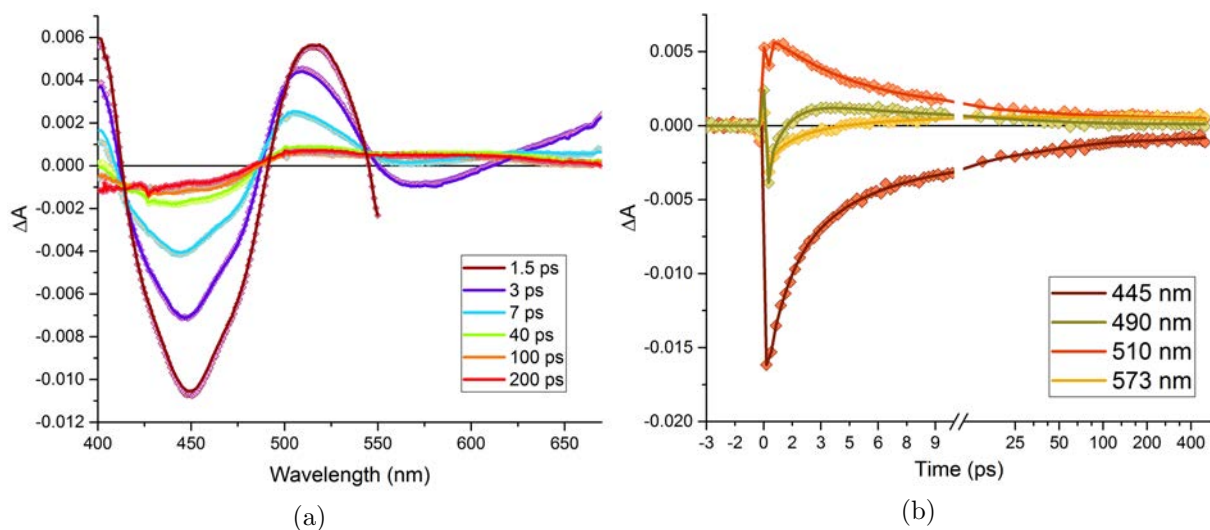
Figure 7.6: *Evolution of the GOX spectra in time (a) and timetraces as a function of wavelength (b). The time scale in 7.6 (b) is lin-log.*

The spectral evolution shown in Fig. 7.6 (a) shows that most of the stimulated

emission disappears by 7 ps, confirming that the protein-bound FAD* decays very fast. The 3 ps spectrum (purple) strongly resembles that of an excited state with distinct bands showing bleaching (450 nm) and stimulated emission (broad band from 550-600 nm). At the same time, the peak of the induced absorption band at $\sim$520 nm shifts towards the blue. The spectrum at 7ps shows a significantly diminished bleaching band and a $+\Delta A$ band peaking at 500 nm, which is significant in comparison with the bleaching band. This indicates that a product state, reminiscent of that in TrmFO C51A, may have formed by this stage in GOX. From 40 ps onwards, the spectra do not evolve much at >500 nm, and from 100 ps onwards over the whole spectral range, indicating the presence of a longer-lived product state.

The kinetics of Fig. 7.6 (b) highlight that the bleaching timetrace (at 445 nm) has a faster decay than the $+\Delta A$ timetrace at 510 nm, a feature that can be compared with Fig. 6.10 (a) for C51A TrmFO. The timetrace for stimulated emission(573 nm) evolves faster than that of bleaching (445 nm) and both are faster than the decay at 510 nm, leading us to believe that not only recombination occurs here but also that some product states formed.
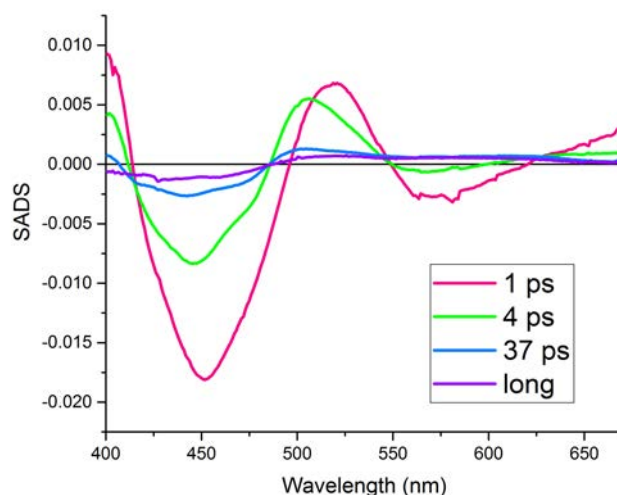

Figure 7.7: *Absolute species associated difference spectra (SADS) for GOX associated with the time constants 1 ps, 4 ps, 37 ps and a long phase.*

Using global analysis, a minimum of four parameters were required to satisfactorily fit the transient absorption data, of which two had a time constant <10 ps. The species associated decay spectra have been obtained using the same time constants as those retrieved from the fluorescence data (1 ps and 4 ps), in addition to a 37 ps and a long-lived phase as shown in Fig. 7.7. The 1 ps phase is dominant and has a characteristic excited state spectrum, in agreement with the fluorescence results. The

ratio of the product state peak to the bleaching evolves from the 1ps phase to the 4 ps phase, indicating the latter does not reflect a pure excited state. It is to be noted that the ratio of the amplitudes of the 4 ps phase and 1 ps phases are comparable for both fluorescence and (the stimulated emission region of) absorption, at 0.4 approximately.

Through deconvolution of the above SADS, we were able to construct and analyse the spectrum of the product states in GOX, as described below. In this analysis, the spectra for FAD$^{\bullet-}$ and FADH$^{\bullet}$ as described in the literature for glucose oxidase[138,139] have been used.

7.6 Characterization of product states
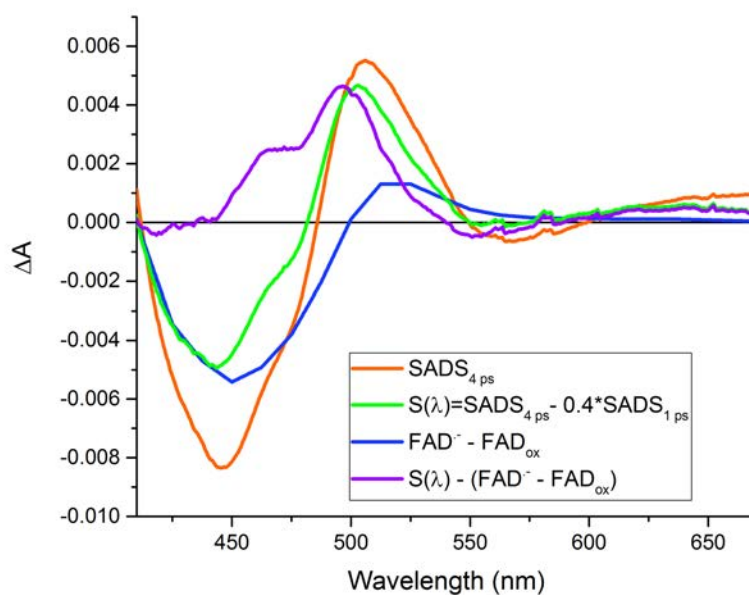
Figure 7.8: *Spectral deconvolution of the 4 ps phase of the GOX SADS. For the analysis, the excited state contribution (from the 1 ps phase) has been subtracted from the 4 ps SADS to obtain S(λ). The deconvolution has been performed with spectrum S(λ) and available model spectra. The choice of the scaling factor of (FAD$^{\bullet-}$-FAD$_{ox}$) spectrum with respect to S(λ) has been described in the text.*

Figs. 7.2 and Fig. 7.6(a) (3 ps spectrum) suggested the likelihood of involvement of TyrOH$^{\bullet+}$ in the electron transfer product states in photo-excited GOX. For characterization of the product state spectra in GOX, we performed spectral deconvolution of the 4 ps, 37 ps and long phases in the SADS of GOX.
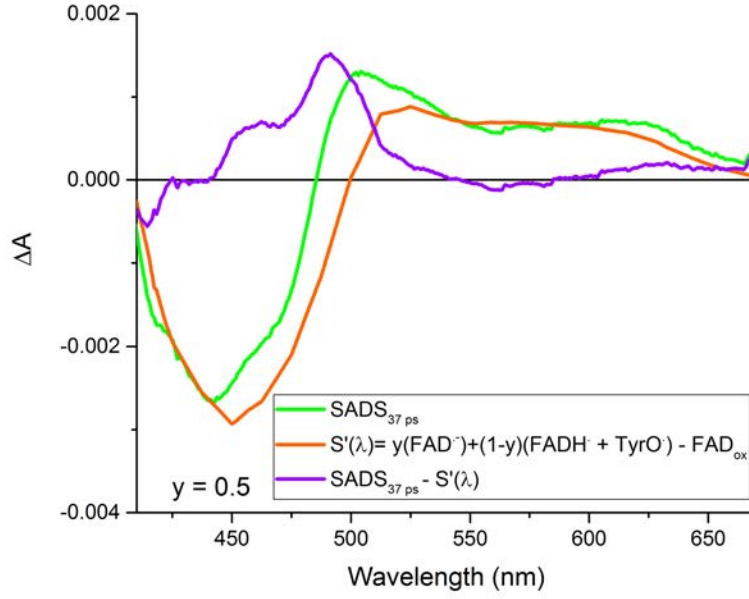
Figure 7.9: *Spectral deconvolution of the 37 ps phase of the GOX SADS. For ease of understanding, $S'(\lambda)$ has been shown as the spectrum containing all the model spectrum components and is shown for $y = 0.4$. The final model has been shown as $SADS_{37ps} - S'(\lambda)$ and it is this spectrum which has been used in Fig. 7.10.*

Fig. 7.8 shows the deconvolution of the 4ps phase SADS in GOX. On observing the total SADS in Fig. 7.7 , it is seen that some stimulated emission remains in the 4 ps phase. This led us to the hypothesis that the 4 ps phase is a mixture of FAD* (with the same spectrum as the 1ps phase) and the product states FAD$^{\bullet-}$ and TyrOH$^{\bullet+}$. The 1 ps phase was normalized on the stimulated emission part of the 4 ps phase and subtracted. The scaling factor here was 0.4. The scaling factor is also in accordance with the ratio between the 4 ps and 1 ps phases SAS observed from time-resolved fluorescence measurements (Fig. 7.5). The resulting spectrum $S(\lambda)$ (Fig. 7.8, green) is qualitatively similar to the spectrum assigned to FAD$^{\bullet-}$ TyrOH$^{\bullet+}$ in C51A TrmFO (Fig. 6.13). Consequently, we propose that the same state is formed in GOX. Similarly the TyrOH$^{\bullet+}$ spectrum in GOX was calculated from

$$S(\lambda) = \text{SADS}_{4\text{ps}} - 0.4 \times \text{SADS}_{1\text{ps}} \tag{7.1}$$

$$S(\lambda) = \alpha[\text{FAD}^{\bullet-} + \text{TyrOH}^{\bullet+} - \text{FAD}_{\text{ox}}] \tag{7.2}$$

Here, the scaling factor was taken such that the scaled extinction spectrum matches the bleaching on $S(\lambda)$ in the blue part of the spectrum (<460 nm). The resultant TyrOH$^{\bullet+}$ spectrum is comparable with that obtained from TrmFO C51A(section 6.3). We therefore conclude that TyrOH$^{\bullet+}$ is also formed in GOX.

The analysis of the 37 ps phase SAD(Fig. 7.9) appeared more complex. The peak around 500 nm indicates a remaining contribution of TyrOH$^{\bullet+}$. In addition, the broad absorption in the 550-650 nm range is indicative of a contribution of FADH$^{\bullet}$. This could be due to proton transfer from TyrOH$^{\bullet+}$ to FAD$^{\bullet-}$. Therefore, this SADS was modelled as

$$SADS_{37ps} = [0.5 \times (FAD^{\bullet-} + TyrOH^{\bullet+}) + (1 - 0.5)(FADH^{\bullet} + TyrO^{\bullet})] - FAD_{ox} \quad (7.3)$$

The factor 0.5 was taken to be the one which corresponds to an optimum fit in the 550 nm-650 nm range where only the FADH$^{\bullet}$ contribution is significant.
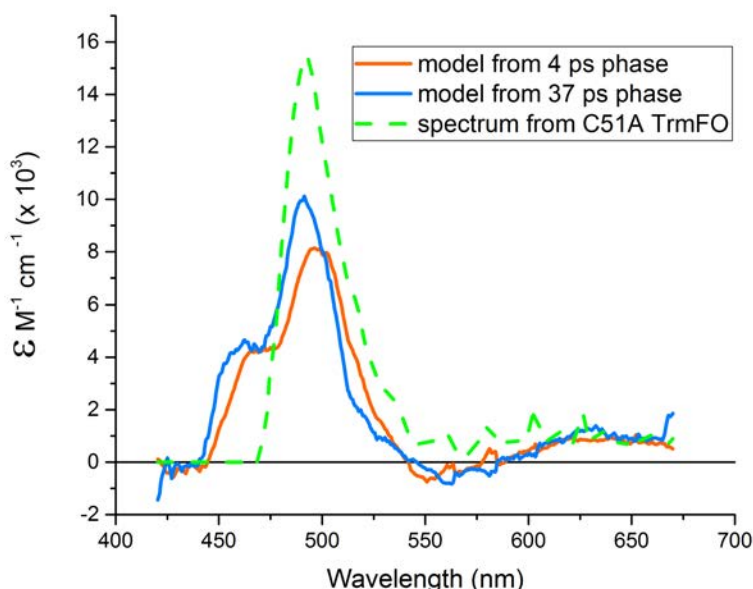
Figure 7.10: *Comparison of TyrOH$^{\bullet+}$ spectra obtained from GOX SADS deconvolution as well as from C51A TrmFO (section 6.3).*

Fig. 7.10 shows that the TyrOH$^{\bullet+}$ spectrum derived from the modelling of the 37 ps phase is very similar to that derived from the modelling of the 4 ps phase, implying consistency of the approach. The GOX spectra also compare well with that of TrmFO C51A (subsection 6.2.2) with the characteristic strong peak at ~490 nm and no significant spectral features on the red side. It appears that in the GOX spectrum, a fraction of the oscillator strength of the 490 nm band of the TrmFO spectrum is blue-shifted to ~460 nm. This may be due to a different protein environment. It cannot be excluded that the details of the assumptions underlying the modelling also
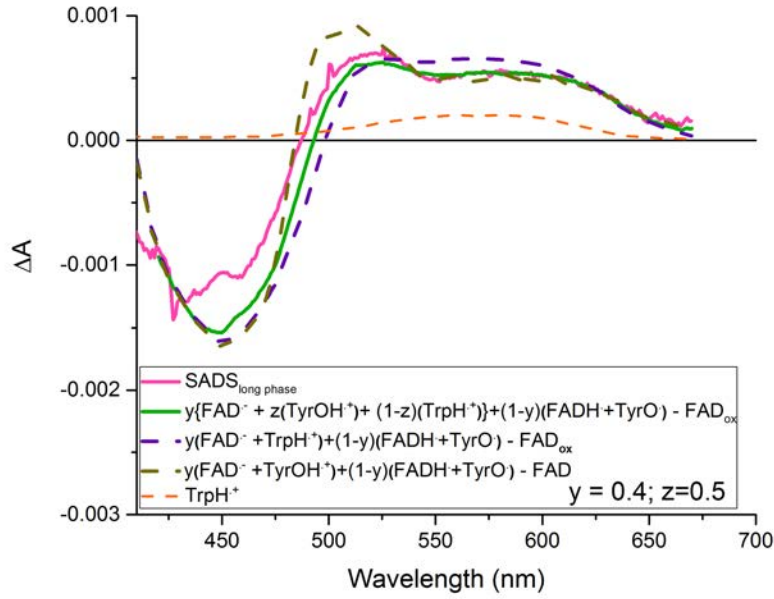
Figure 7.11: *Spectral deconvolution of the long phase in GOx SADS.*

contribute to this difference.

Finally, we address the SADS associated with the long-lived phase in GOX (Fig. 7.11). Comparing with the 37 ps SADS, here the TyrOH$^{\bullet+}$ peak at ∼500 nm has decreased with respect to the FADH$^{\bullet}$ feature. Hence, modelling with the same components as with the 37 ps phase did not yield satisfactory results. However, assuming that a fraction of the cation radical is transferred from Tyr to Trp allows modelling of the SADS of the long-lived phase

$$\text{SADS}_{\text{longphase}} = [y\{\text{FAD}^{\bullet-} + z(\text{TyrOH}^{\bullet+}) + (1-z)(\text{TrpH}^{\bullet+})\} + (1-y)(\text{FADH}^{\bullet} + \text{TyrO}^{\bullet}] - \text{FAD}_{\text{ox}} \tag{7.4}$$

Here, the TyrOH$^{\bullet+}$ spectrum used is the one which was calculated for the 37 ps phase (Fig. 7.9). The factor y (0.4) was determined from the ratio of the FADH$^{\bullet}$ induced absorption feature >620 nm (where TrpH$^{\bullet+}$ does not absorb) and the FAD$_{\text{ox}}$ bleaching and z(0.5) from adjusting the remainder of the spectrum. The modest deviations from the SADS spectrum in the 430 nm - 500 nm region may be due to changes in the TyrOH$^{\bullet+}$ spectrum.

Based on the spectral deconvolution performed, a minimal kinetic model (Scheme 7.1) was made to describe the electron transfer reactions in GOX. For simplicity, this scheme ignores the heterogeneity in the FAD* decay and focusses on the ∼1 ps component. According to this model, the product state FAD$^{\bullet-}$ and TyrOH$^{\bullet+}$ is formed

84

in 1.1 ps. Following this, it decays with an efficiency of ∼50% to a mixture of states of FAD$^{\bullet-}$ *plus* TyrOH$^{\bullet+}$ and FADH$^{\bullet}$ *plus* TyrO$^{\bullet}$ with an equilibrium constant K$_2$≈1 between those states. Charge recombination, with a similar intrinsic rate of ($\sim 8ps^{-1}$), competes with the formation of this mixture of states. After this stage, the system evolves into a different mixture of states with a ∼57% yield, again in competition with charge recombination (intrinsic rate $\sim 86ps^{-1}$). This mixture contains the same states as the initial mixture, but with an equilibrium constant K$_{31}$=1.5. In addition, the TyrOH$^{\bullet+}$ is itself in equilibrium with TrpH$^{\bullet+}$ with an equilibrium constant K$_{32}$=1. The products remaining after the second forward reaction are a mixture of radicals which decay on a longer timescale than the experiment.

This scheme is reminiscent of the charge stabilization scheme associated with photolyase and cryptochrome photoactivation,[99,140] where hopping of the positive charge between different residues occurs in competition with charge recombination and sometimes proton transfer. Similarly in GOX, the FAD is surrounded by several Tyr residues (Tyr68, 515 and Tyr565) which could each be involved in the charge transfer pathway. A similar mechanism involving different residues is possible here. For instance, the initial step likely involves the closest-lying 515 and/or Tyr68, and further steps may involve 565 and Trp426. The latter states that appear mixtures of states can be considered as in pseudo-equilibrium: the equilibration between these states occurs faster than their formation time. Within the framework of this scheme, an interpretation of the different steps as equilibration involving only one residue (for instance by proton transfer for reaction 2) appears unlikely, as this reaction would be incomplete. However, more subtle equilibrations involving protein relaxations are, in principle, also possible. To identify the role of each residue as an electron transfer candidate more precisely, experiments will have to be performed on mutants of GOX where each such residue would be substituted by a redox-inactive Phe residue.

The important conclusion from this work is that a spectrum characteristic of TyrOH$^{\bullet+}$ is required to comprehensively describe the spectral evolution of GOX using femtosecond absorption spectroscopy. This spectrum (Fig. 7.10) has a characteristic band ∼490 nm. The spectral feature in the blue region ∼450-475 nm is different from the one observed in TrmFO C51A. This difference in the TyrOH$^{\bullet+}$ spectrum can be characteristic for the GOX environment as spectral features for radical ion intermediates are known differ slightly from one protein system to another.
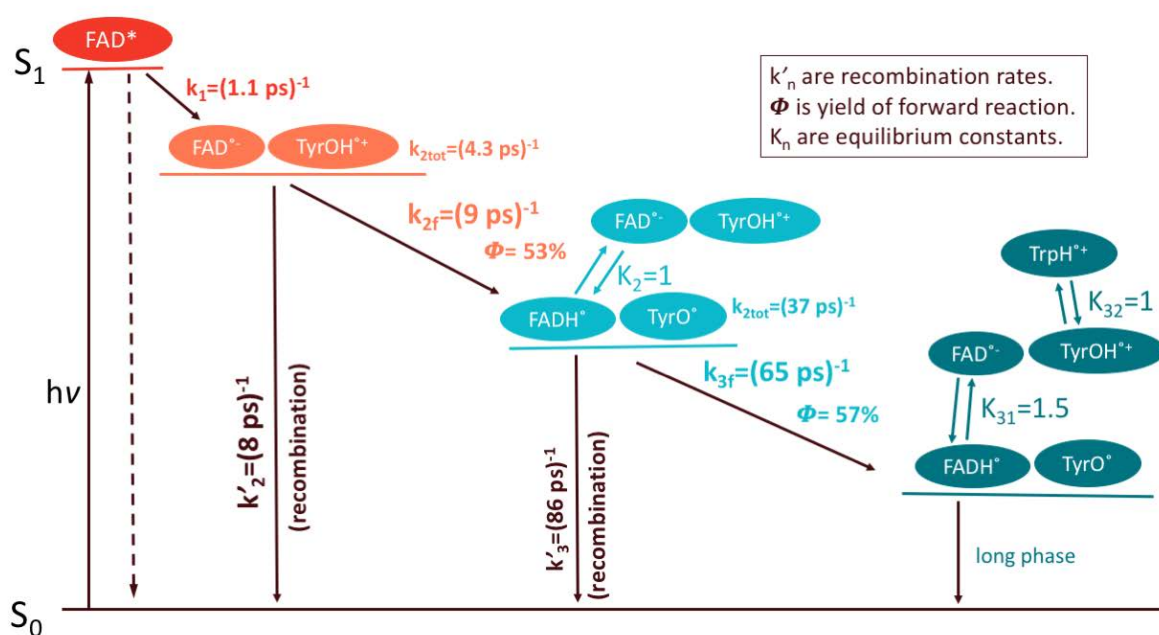
Scheme 7.1. *Scheme displaying the electron transfer pathway in GOX. k_i are forward reaction rates and k_i' are recombination rates. The efficiency ϕ for each step has been indicated*

Chapter 8

Conclusions and perspectives

In this thesis, properties of charge transfer reactions involving flavin and amino acid radicals in proteins have been investigated. The functioning of biochemical processes widely relies on charge transfer reactions. Such reactions often intrinsically occur on timescales faster than those of the interaction between protein and substrates. Short-lived intermediates can therefore be difficult to monitor in real time. However, in biochemical systems where the reactions can be triggered by light, ultrafast optical methods are well-suited to the study of charge transfer intermediates. We have used femtosecond time-resolved absorption and fluorescence spectroscopy to study charge transfer in flavoproteins and the subsequent intermediates formed.

As the rate of electron transfer is strongly distance-dependent, electron transfer in proteins often proceeds through a chain of redox components[23] connecting the catalytic site(s) and bridge components. Here, the charge can "hop" from one catalytic site to another within or between proteins. Typical catalytic site components include cofactors like chlorophyll, heme or flavins; furthermore, bridge components include redox-active amino acid side-chains: tyrosine and tryptophan.

Flavins are among the most versatile redox cofactors as they can undergo $1e^-/2e^-$ transfer, proton transfer and/or hydride transfer. Additionally, the extinction coefficients of flavin redox states in flavoproteins are comparable to those of known tyrosine and tryptophan intermediates. This makes flavoproteins ideal systems to observe intermediates of tyrosine and tryptophan during charge transfer, even when they are not naturally light-active. Both neutral and cationic tryptophanyl radicals, as well as the neutral tyrosyl radical[96] had been identified using pulse radiolysis as well as photolysis. Tryptophan radicals have been observed to be formed both independently or via concerted electron and proton transfer (PCET) whereas tyrosyl cation was speculated to not form outside PCET as the $TyrOH^{\bullet+}$ radical cation is highly unstable ($pK_a = -2$) and remained uncharacterized.

In our work, we focused on the flavoproteins methyl transferase TrmFO from *Thermus thermophilus* and glucose oxidase (GOX) from *Aspergillus niger*. Both systems harbour aromatic amino acids in close proximity to the FAD cofactor. Using the TrmFO C51A mutant (to avoid complications due to a highly fluorescent FAD-cysteine adduct partly forming in wild type TrmFO), our time-resolved fluorescence studies on TrmFO C51A showed only one rapidly decaying component with a time constant of ∼1.2 ps. The rapid quenching of FAD* fluorescence could be attributed to near barrierless electron transfer from the nearby redox-active Tyr343 residue, which has an edge-to-edge distance of 3.3Åfrom FAD.

Time-resolved absorption experiments on the same system revealed, apart from a ∼1.2 ps phase reflecting FAD* decay, a second phase with a time constant of ∼3 ps. This finding indicates that, at least in a fraction of the proteins, a product state is formed which decays slower than it is formed. The difference spectrum associated with this phase, assigned to recombination of $FAD^{\bullet-}$ and a radical form of the quencher Tyr343, has a sharp peak at ∼490 nm. The spectrum, being markedly different from the one known for $TyrO^{\bullet}$, was attributed to the species $FAD^{\bullet-} TyrOH^{\bullet+}$ This constitutes the first attribution of a $TyrOH^{\bullet+}$ species and implies that it can exist, albeit briefly, without concomitant deprotonation.[1]

On performing spectral deconvolution, we characterized the absolute spectrum of $TyrOH^{\bullet+}$ in TrmFO. This spectrum has a relatively strong characteristic band at ∼490 nm, and resembles the spectrum of the analogous methoxyphenol radical (see Figure 6.14). Additionally, we calculated the dipole moment directions for the transition using polarization photoselection. The anisotropy (r) spectrum of the 3 ps phase contained two highly distinct bands - one at r ∼ 0.4 covering the bleaching of the FAD ground state and another at $r = 0.24 \pm 0.04$ which covers the spectral band of the assigned $TyrOH^{\bullet+}$ intermediate. This corresponded to an angle of 31° ± 5°between the excited FADox transition and the probed $TyrOH^{\bullet+}$ transition. This finding allows to set limits to the orientation of the transition dipole in the molecular frame of the phenol plane. Yet, precise assignment of the transition dipole must await theoretical-chemistry studies of the $TyrOH^{\bullet+}$ radical.

On a different level, the very finding of two distinct anisotropy values constitutes an important confirmation of the interpretation in terms of two different molecules. In this context, it has very recently been suggested that the band we assigned to $TyrOH^{\bullet+}$ might actually reflect vibrationally hot flavin.[128] The anisotropy results contradict this suggestion.

Based on the findings in TrmFO, the photochemistry of the model flavoprotein

glucose oxidase (GOX) was reinvestigated with the aim to identify transient tyrosine radicals. The FAD_{ox} in the active site of GOX is surrounded by several Tyr and Trp residues at varying distances, the closest-lying being two tyrosines Tyr515 (4.0 Å) and Tyr68 (4.3 Å). While several studies had already been performed on the photochemistry of GOX, our interest was stimulated by the one by Lukacs et al.,[100] the only study with full spectral resolution. This paper showed transient absorption measurements containing a band which had a similar spectrum as the 3 ps band in TrmFO C51A, which could not be very adequately described with the then-available model spectra.

The spectral evolution is far more complex in GOX than in C51A TrmFO, with multiphasic FAD_{ox}^* decay (dominated by ~1 ps and ~4 ps phases) partly taking place on similar time scales as product state evolution. Product state evolution occurred with 4 ps, 37 ps phases and a long phase. The 4 ps phase was modelled using FAD_{ox} and $FAD^{\bullet-}$ (after removal of the 1 ps excited state contribution). The 37 ps phase was modelled using FAD_{ox}, $FAD^{\bullet-}$, $FADH^{\bullet}$ and $TyrO^{\bullet}$ model spectra. Yet, for the 4 ps and 37 ps phases an additional contribution with a spectral component strongly resembling that of the $TyrOH^{\bullet+}$ spectra obtained in TrmFO was required, with the characteristic peak near 490 nm. A comprehensive model of the involvement of Tyr and Trp radicals in light-induced charge separation and subsequent charge recombination processes in GOX could thus be elaborated, taking into account all spectral features and incorporating both electron and proton transfer. Importantly, this study emphasized, in a different protein system, the transient population of $TyrOH^{\bullet+}$, up to a timescale of tens of picoseconds.

The role of individual residues in the charge transfer processes in GOX could not be inferred from the complex data and will require additional experiments associating site-directed mutagenesis and spectroscopy. Such experiments are foreseen in collaboration with the laboratory of Dr. Andras Lukacs (University of Pecs, Hungary).

Altogether, $TyrOH^{\bullet+}$ was visualized and spectrally characterized in both TrmFO C51A and in GOX. Due to the close proximity between the photoexcitable flavin and tyrosine residues in these systems we have been able to show that $TyrOH^{\bullet+}$ can be formed without concomitant proton transfer. Tyrosines play an important role as redox relays in a wide range of biological redox reactions (sometimes in chains containing also tryptophan residues[141]), notably including ribonucleotide reductase, photosystem II, certain photolyases and are also suggested to play an important role in the photochemistry of certain BLUF domains. Hitherto in such systems only deprotonated tyrosine radicals ($TyrO^{\bullet}$) have been experimentally identified as intermediates. Our results indicate that these are not necessarily formed by concomitant electron and proton transfer, but that the build-up of sizeable populations of the real cation

precursors of these states may be limited by the intrinsic formation time.

The present studies revealing and characterizing the TyrOH$^{\bullet+}$ intermediate were limited to TrmFO C51A and GOX; in the latter system a complex analysis is required. As a perspective, other relatively simple systems will be characterized to investigate the properties of this intermediate, and also to investigate whether stabilization of the radical by deprotonation can be observed, rather than recombination as in TrmFO C51A. The flavoprotein ferredoxin-NADP+ oxidoreductase (FNR) from *Bacillus subtilis* is particularly interesting as it contains a tyrosine residue very close to the FAD isoalloxazine ring and a crystal structure is available (closest ring-to-ring distance 3.4 Å, PDB: 3LXZ135) of the WT form where FAD fluorescence is strongly quenched.[142] Time-resolved studies on this FNR, in collaboration with Dr. Daisuke Seo (Kanazawa University, Japan) are in progress in the laboratory.

Finally, the very initial aim of this thesis was to study active site flexibility of the multi-substrate enzyme TrmFO using amino acid-FAD* electron transfer rates as conformational markers. Initial mutagenesis studies did not yet allow to identify unique electron-donor residues suitable for such studies. Extension of this approach, guided by molecular dynamics simulations may help to construct TrmFO variants allowing studies of functionally relevant conformational flexibility.

References

(1) Nag, L.; Sournia, P.; Myllykallio, H.; Liebl, U.; Vos, M. H. Identification of the TyrOH•+ Radical Cation in the Flavoenzyme TrmFO. *Journal of the American Chemical Society* **Aug. 2017**, *139*, 11500–11505.

(2) McConnell, I.; Li, G.; Brudvig, G. W. Energy Conversion in Natural and Artificial Photosynthesis. *Chemistry & Biology* **May 2010**, *17*, 434–447.

(3) Brzezinski, P.; Larsson, G. Redox-driven proton pumping by heme-copper oxidases. *Biochimica et Biophysica Acta (BBA) - Bioenergetics* **Aug. 2003**, *1605*, 1–13.

(4) Johnsen, S.; Lohmann, K. J. Magnetoreception in animais. *Physics today* **2008**, *61*, 29–35.

(5) Weber, S. Light-driven enzymatic catalysis of DNA repair: a review of recent biophysical studies on photolyase. *Biochimica et Biophysica Acta (BBA) - Bioenergetics* **Feb. 2005**, *1707*, 1–23.

(6) Lötzbeyer, T.; Schuhmann, W.; Schmidt, H.-L. Minizymes. A new strategy for the development of reagentless amperometric biosensors based on direct electron-transfer processes. *Bioelectrochemistry and Bioenergetics* **Apr. 1997**, *42*, 1–6.

(7) Alstrum-Acevedo, J. H.; Brennaman, M. K.; Meyer, T. J. Chemical Approaches to Artificial Photosynthesis. 2. *Inorganic Chemistry* **Oct. 2005**, *44*, 6802–6827.

(8) Hambourger, M.; Moore, G. F.; Kramer, D. M.; Gust, D.; Moore, A. L.; Moore, T. A. Biology and technology for photochemical fuel production. *Chemical Society Reviews* **2009**, *38*, 25–35.

(9) Sutin, N Electron Exchange Reactions. *Annual Review of Nuclear Science* **Dec. 1962**, *12*, 285–328.

(10) Page, C. C.; Moser, C. C.; Chen, X.; Dutton, P. L. Natural engineering principles of electron tunnelling in biological oxidation–reduction. *Nature* **Nov. 1999**, *402*, 47–52.

(11) Michaelis, L, *The Enzymes-Chemistry and Mechanism of Action, Vol. 2, Part 1, eds JR Sumner and K. Myrback*; New York, NY: Academic Press: 1951.

(12)   Chance, B.; Williams, G. R. The respiratory chain and oxidative phosphorylation., eng *Advances in enzymology and related subjects of biochemistry* **1956**, *17*, 65–134.

(13)   Gray, H. B.; Winkler, J. R. Electron tunneling through proteins. *Quarterly Reviews of Biophysics* **Aug. 2003**, *36*, 341–372.

(14)   Marcus, R. A. On the Theory of OxidationReduction Reactions Involving Electron Transfer. I. *The Journal of Chemical Physics* **May 1956**, *24*, 966–978.

(15)   Marcus, R.; Sutin, N. Electron transfers in chemistry and biology. *Biochimica et Biophysica Acta (BBA) - Reviews on Bioenergetics* **Aug. 1985**, *811*, 265–322.

(16)   Marcus, R. A. Chemical and Electrochemical Electron-Transfer Theory. *Annual Review of Physical Chemistry* **Oct. 1964**, *15*, 155–196.

(17)   Halpern, J. Mechanisms of electron transfer and related processes in solution. *Quarterly Reviews, Chemical Society* **1961**, *15*, 207–236.

(18)   Taube, H. In *Advances in Inorganic Chemistry and Radiochemistry*, Emeléus, H., Sharpe, A., Eds.; Academic Press: Jan. 1959; Vol. 1, pp 1–53.

(19)   Hush, N. S. Adiabatic theory of outer sphere electron-transfer reactions in solution. *Transactions of the Faraday Society* **1961**, *57*, 557–580.

(20)   Dogonadze, R.; Kuznetsov, A.; Levich, V. Theory of hydrogen-ion discharge on metals: Case of high overvoltages. *Electrochimica Acta* **May 1968**, *13*, 1025–1044.

(21)   Hopfield, J. J. Electron Transfer Between Biological Molecules by Thermally Activated Tunneling. *Proceedings of the National Academy of Sciences* **Sept. 1974**, *71*, 3640.

(22)   De la Lande, A.; Gillet, N.; Chen, S.; Salahub, D. R. Progress and challenges in simulating and understanding electron transfer in proteins. *Archives of Biochemistry and Biophysics* **Sept. 2015**, *582*, 28–41.

(23)   Page, C Mechanism for electron transfer within and between proteins. *Current Opinion in Chemical Biology* **Oct. 2003**, *7*, 551–556.

(24)   Stubbe, J.; Nocera, D. G.; Yee, C. S.; Chang, M. C. Y. Radical Initiation in the Class I Ribonucleotide Reductase: Long-Range Proton-Coupled Electron Transfer? *Chemical Reviews* **June 2003**, *103*, 2167–2202.

(25)   Lambert, C.; Nöll, G.; Schelter, J. Bridge-mediated hopping or superexchange electron-transfer processes in bis(triarylamine) systems. *Nature Materials* **Sept. 2002**, *1*, 69.

(26)   Isied, S. S.; Ogawa, M. Y.; Wishart, J. F. Peptide-mediated intramolecular electron transfer: long-range distance dependence. *Chemical Reviews* **May 1992**, *92*, 381–394.

(27) Warren, J. J.; Ener, M. E.; Vlček, A.; Winkler, J. R.; Gray, H. B. Electron hopping through proteins. *Coordination chemistry reviews* **Nov. 2012**, *256*, 2478–2487.

(28) Jortner, J.; Bixon, M.; Langenbacher, T.; Michel-Beyerle, M. E. Charge transfer and transport in DNA. *Proceedings of the National Academy of Sciences* **Oct. 1998**, *95*, 12759.

(29) Davis, W. B.; Ratner, M. A.; Wasielewski, M. R. Dependence of electron transfer dynamics in wire-like bridge molecules on donor–bridge energetics and electronic interactions. *Chemical Physics* **Aug. 2002**, *281*, 333–346.

(30) Jovanovic, S. V.; Harriman, A.; Simic, M. G. Electron-transfer reactions of tryptophan and tyrosine derivatives. *The Journal of Physical Chemistry* **Apr. 1986**, *90*, 1935–1939.

(31) Harriman, A. Further comments on the redox potentials of tryptophan and tyrosine. *The Journal of Physical Chemistry* **Nov. 1987**, *91*, 6102–6104.

(32) Stubbe, J.; van der Donk, W. A. Protein Radicals in Enzyme Catalysis. *Chemical Reviews* **Apr. 1998**, *98*, 705–762.

(33) Tommos, C.; Skalicky, J. J.; Pilloud, D. L.; Wand, A. J.; Dutton, P. L. De Novo Proteins as Models of Radical Enzymes. *Biochemistry* **July 1999**, *38*, 9495–9507.

(34) Hosseinzadeh, P.; Lu, Y. Design and fine-tuning redox potentials of metalloproteins involved in electron transfer in bioenergetics. *Biodesign for Bioenergetics - the design and engineering of electron transfer cofactors, proteins and protein networks* **May 2016**, *1857*, 557–581.

(35) Blankenship, R. E. Origin and early evolution of photosynthesis. *Photosynthesis Research* **Aug. 1992**, *33*, 91–111.

(36) Rappaport, F.; Diner, B. A. Primary photochemistry and energetics leading to the oxidation of the (Mn)4Ca cluster and to the evolution of molecular oxygen in Photosystem II. *The Role of Manganese in Photosystem II* **Feb. 2008**, *252*, 259–272.

(37) Pilet, E.; Jasaitis, A.; Liebl, U.; Vos, M. H. Electron transfer between hemes in mammalian cytochrome c oxidase. *Proceedings of the National Academy of Sciences of the United States of America* **Nov. 2004**, *101*, 16198–16203.

(38) Sancar, A. Structure and function of DNA photolyase. *Biochemistry* **Jan. 1994**, *33*, 2–9.

(39) Sorigué, D. et al. An algal photoenzyme converts fatty acids to hydrocarbons. *Science* **Sept. 2017**, *357*, 903.

(40) Lukacs, A.; Eker, A. P. M.; Byrdin, M.; Brettel, K.; Vos, M. H. Electron Hopping through the 15 Å Triple Tryptophan Molecular Wire in DNA Photolyase Occurs within 30 ps. *Journal of the American Chemical Society* **Nov. 2008**, *130*, 14394–14395.

(41) Byrdin, M.; Villette, S.; Espagne, A.; Eker, A. P. M.; Brettel, K. Polarized Transient Absorption To Resolve Electron Transfer between Tryptophans in DNA Photolyase. *The Journal of Physical Chemistry B* **June 2008**, *112*, 6866–6871.

(42) Byrdin, M.; Eker, A. P. M.; Vos, M. H.; Brettel, K. Dissection of the triple tryptophan electron transfer chain in Escherichia coli DNA photolyase: Trp382 is the primary donor in photoactivation. *Proceedings of the National Academy of Sciences* **July 2003**, *100*, 8676.

(43) Byrdin, M.; Villette, S.; Eker, A. P. M.; Brettel, K. Observation of an Intermediate Tryptophanyl Radical in W306F Mutant DNA Photolyase from Escherichia coli Supports Electron Hopping along the Triple Tryptophan Chain. *Biochemistry* **Sept. 2007**, *46*, 10072–10077.

(44) Briggs, W. R.; Huala, E. Blue-Light Photoreceptors in Higher Plants. *Annual Review of Cell and Developmental Biology* **Nov. 1999**, *15*, 33–62.

(45) Van der Horst, M. A.; Hellingwerf, K. J. Photoreceptor Proteins, "Star Actors of Modern Times": A Review of the Functional Dynamics in the Structure of Representative Members of Six Different Photoreceptor Families. *Accounts of Chemical Research* **Jan. 2004**, *37*, 13–20.

(46) Rizzini, L.; Favory, J.-J.; Cloix, C.; Faggionato, D.; O'Hara, A.; Kaiserli, E.; Baumeister, R.; Schäfer, E.; Nagy, F.; Jenkins, G. I.; Ulm, R. Perception of UV-B by the Arabidopsis UVR8 Protein. *Science* **Apr. 2011**, *332*, 103.

(47) Huala, E.; Oeller, P. W.; Liscum, E.; Han, I.-S.; Larsen, E.; Briggs, W. R. Arabidopsis NPH1: A Protein Kinase with a Putative Redox-Sensing Domain. *Science* **Dec. 1997**, *278*, 2120.

(48) Crosson, S.; Moffat, K. Structure of a flavin-binding plant photoreceptor domain: Insights into light-mediated signal transduction. *Proceedings of the National Academy of Sciences of the United States of America* **Mar. 2001**, *98*, 2995–3000.

(49) Swartz, T. E.; Corchnoy, S. B.; Christie, J. M.; Lewis, J. W.; Szundi, I.; Briggs, W. R.; Bogomolni, R. A. The Photocycle of a Flavin-binding Domain of the Blue Light Photoreceptor Phototropin. *Journal of Biological Chemistry* **Sept. 2001**, *276*, 36493–36500.

(50)   Kennis, J. T. M.; Crosson, S.; Gauden, M.; van Stokkum, I. H. M.; Moffat, K.; van Grondelle, R. Primary Reactions of the LOV2 Domain of Phototropin, a Plant Blue-Light Photoreceptor. *Biochemistry* **Apr. 2003**, *42*, 3385–3392.

(51)   Crosson, S.; Rajagopal, S.; Moffat, K. The LOV Domain Family: Photoresponsive Signaling Modules Coupled to Diverse Output Domains. *Biochemistry* **Jan. 2003**, *42*, 2–10.

(52)   Christie, J. M.; Salomon, M.; Nozue, K.; Wada, M.; Briggs, W. R. LOV (light, oxygen, or voltage) domains of the blue-light photoreceptor phototropin (nph1): Binding sites for the chromophore flavin mononucleotide. *Proceedings of the National Academy of Sciences* **July 1999**, *96*, 8779.

(53)   Gomelsky, M.; Klug, G. BLUF: a novel FAD-binding domain involved in sensory transduction in microorganisms. *Trends in Biochemical Sciences* **Oct. 2002**, *27*, 497–500.

(54)   Gomelsky, M.; Hoff, W. D. Light helps bacteria make important lifestyle decisions. *Trends in Microbiology* **Sept. 2011**, *19*, 441–448.

(55)   Fiedler, B.; Börner, T.; Wilde, A. Phototaxis in the Cyanobacterium Synechocystis sp. PCC 6803: Role of Different Photoreceptors. *Photochemistry and Photobiology* **Apr. 2007**, *81*, 1481–1488.

(56)   Ntefidou, M.; Iseki, M.; Watanabe, M.; Lebert, M.; Häder, D.-P. Photoactivated Adenylyl Cyclase Controls Phototaxis in the Flagellate Euglena gracilis. *Plant Physiology* **Dec. 2003**, *133*, 1517.

(57)   Masuda, S.; Bauer, C. E. AppA Is a Blue Light Photoreceptor that Antirepresses Photosynthesis Gene Expression in Rhodobacter sphaeroides. *Cell* **Sept. 2002**, *110*, 613–623.

(58)   Braatsch, S.; Gomelsky, M.; Kuphal, S.; Klug, G. A single flavoprotein, AppA, integrates both redox and light signals in Rhodobacter sphaeroides. *Molecular Microbiology* **July 2002**, *45*, 827–836.

(59)   Tschowri, N.; Busse, S.; Hengge, R. The BLUF-EAL protein YcgF acts as a direct anti-repressor in a blue-light response of Escherichia coli. *Genes & Development* **Feb. 2009**, *23*, 522–534.

(60)   Mussi, M. A.; Gaddy, J. A.; Cabruja, M.; Arivett, B. A.; Viale, A. M.; Rasia, R.; Actis, L. A. The Opportunistic Human Pathogen Acinetobacter baumannii Senses and Responds to Light. *Journal of Bacteriology* **Dec. 2010**, *192*, 6336.

(61)   Brust, R. et al. Ultrafast Structural Dynamics of BlsA, a Photoreceptor from the Pathogenic Bacterium Acinetobacter baumannii. *The Journal of Physical Chemistry Letters* **Jan. 2014**, *5*, 220–224.

(62) Fukushima, Y.; Okajima, K.; Shibata, Y.; Ikeuchi, M.; Itoh, S. Primary Intermediate in the Photocycle of a Blue-Light Sensory BLUF FAD-Protein, Tll0078, of Thermosynechococcus elongatus BP-1. *Biochemistry* **Apr. 2005**, *44*, 5149–5158.

(63) Penzkofer, A.; Stierl, M.; Hegemann, P.; Kateriya, S. Photo-dynamics of the BLUF domain containing soluble adenylate cyclase (nPAC) from the amoeboflagellate Naegleria gruberi NEG-M strain. *Chemical Physics* **Aug. 2011**, *387*, 25–38.

(64) Masuda, S.; Hasegawa, K.; Ishii, A.; Ono, T.-a. Light-Induced Structural Changes in a Putative Blue-Light Receptor with a Novel FAD Binding Fold Sensor of Blue-Light Using FAD (BLUF); Slr1694 of Synechocystis sp. PCC6803. *Biochemistry* **May 2004**, *43*, 5304–5313.

(65) Mathes, T.; Götze, J. P. A proposal for a dipole-generated BLUF domain mechanism. *Frontiers in Molecular Biosciences* **2015**, *2*, 62.

(66) Gil, A. A.; Laptenok, S. P.; Iuliano, J. N.; Lukacs, A.; Verma, A.; Hall, C. R.; Yoon, G. E.; Brust, R.; Greetham, G. M.; Towrie, M.; French, J. B.; Meech, S. R.; Tonge, P. J. Photoactivation of the BLUF Protein PixD Probed by the Site-Specific Incorporation of Fluorotyrosine Residues. *Journal of the American Chemical Society* **Oct. 2017**, *139*, 14638–14648.

(67) Lukacs, A.; Brust, R.; Haigney, A.; Laptenok, S. P.; Addison, K.; Gil, A.; Towrie, M.; Greetham, G. M.; Tonge, P. J.; Meech, S. R. BLUF Domain Function Does Not Require a Metastable Radical Intermediate State. *Journal of the American Chemical Society* **Mar. 2014**, *136*, 4605–4615.

(68) Maeda, K.; Robinson, A. J.; Henbest, K. B.; Hogben, H. J.; Biskup, T.; Ahmad, M.; Schleicher, E.; Weber, S.; Timmel, C. R.; Hore, P. J. Magnetically sensitive light-induced reactions in cryptochrome are consistent with its proposed role as a magnetoreceptor. *Proceedings of the National Academy of Sciences* **Mar. 2012**, *109*, 4774.

(69) Aubert, C.; Vos, M. H.; Mathis, P.; Eker, A. P. M.; Brettel, K. Intraprotein radical transfer during photoactivation of DNA photolyase. *Nature* **June 2000**, *405*, 586.

(70) Chaves, I.; Pokorny, R.; Byrdin, M.; Hoang, N.; Ritz, T.; Brettel, K.; Essen, L.-O.; van der Horst, G. T. J.; Batschauer, A.; Ahmad, M. The Cryptochromes: Blue Light Photoreceptors in Plants and Animals. *Annual Review of Plant Biology* **June 2011**, *62*, 335–364.

(71) Solov'yov, I.; Hore, P. J.; Ritz, T.; Schulten, K. Chemical compass for bird navigation., eng *Quantum Effects in Biology* **2014**, ed. by Mohseni Omar, Y. E. G. P. M. B. M., 218–236.

(72) Solov'yov, I. A.; Mouritsen, H.; Schulten, K. Acuity of a Cryptochrome and Vision-Based Magnetoreception System inBirds. *Biophysical Journal* **July 2010**, *99*, 40–49.

(73) Minnihan, E. C.; Nocera, D. G.; Stubbe, J. Reversible, Long-Range Radical Transfer in E. coli Class Ia Ribonucleotide Reductase. *Accounts of Chemical Research* **Nov. 2013**, *46*, 2524–2535.

(74) Geng, J.; Dornevil, K.; Davidson, V. L.; Liu, A. Tryptophan-mediated charge-resonance stabilization in the bis-Fe(IV) redox state of MauG. *Proceedings of the National Academy of Sciences* **June 2013**, *110*, 9639–9644.

(75) Winkler, J. R.; Gray, H. B. Long-Range Electron Tunneling. *Journal of the American Chemical Society* **Feb. 2014**, *136*, 2930–2939.

(76) Bacher, A.; Illarionov, B.; Eisenreich, W.; Fischer, M. In *Flavins and Flavoproteins: Methods and Protocols*, Weber, S., Schleicher, E., Eds.; Springer New York: New York, NY, 2014, pp 65–78.

(77) Macheroux, P.; Kappes, B.; Ealick, S. E. Flavogenomics–a genomic and structural view of flavin-dependent proteins. *The FEBS Journal* **June 2011**, *278*, 2625–2634.

(78) Blyth, A. W. LVI.—The composition of cows' milk in health and disease. *Journal of the Chemical Society, Transactions* **1879**, *35*, 530–539.

(79) Maria Barile; Teresa Anna Giancaspero; Carmen Brizio; Concetta Panebianco; Cesare Indiveri; Michele Galluccio; Lodovica Vergani; Ivano Eberini and Elisabetta Gianazza Biosynthesis of Flavin Cofactors in Man: Implications in Health and Disease. *Current Pharmaceutical Design* **2013**, *19*, 2649–2675.

(80) Schramm, M.; Wiegmann, K.; Schramm, S.; Gluschko, A.; Herb, M.; Utermöhlen, O.; Krönke, M. Riboflavin (vitamin B2) deficiency impairs NADPH oxidase 2 (Nox2) priming and defense against Listeria monocytogenes. *European Journal of Immunology* **Nov. 2013**, *44*, 728–741.

(81) Derrien, M.; Veiga, P. Rethinking Diet to Aid Human–Microbe Symbiosis. *Trends in Microbiology* **Feb. 2017**, *25*, 100–112.

(82) Conrad, K. S.; Manahan, C. C.; Crane, B. R. Photochemistry of flavoprotein light sensors. *Nature Chemical Biology* **Sept. 2014**, *10*, 801.

(83) Liu, B.; Liu, H.; Zhong, D.; Lin, C. Searching for a photocycle of the cryptochrome photoreceptors. *Current Opinion in Plant Biology* **Oct. 2010**, *13*, 578–586.

(84) Edwards, A. M. In *Flavins and Flavoproteins: Methods and Protocols*, Weber, S., Schleicher, E., Eds.; Springer New York: New York, NY, 2014, pp 3–13.

(85) Porra, R.; Thompson, W.; Kriedemann, P. Determination of accurate extinction coefficients and simultaneous equations for assaying chlorophylls a and b extracted with four different solvents: verification of the concentration of chlorophyll standards by atomic absorption spectroscopy. *Biochimica et Biophysica Acta (BBA) - Bioenergetics* **Aug. 1989**, *975*, 384–394.

(86) Antonini, E.; Brunori, M. Hemoglobin and Myoglobin in Their Reactions with Ligands. *North-Holland, Amsterdam* **1971**, *178*, 296.

(87) Kritsky, M. S.; Telegina, T. A.; Vechtomova, Y. L.; Buglak, A. A. Why Flavins Are not Competitors of Chlorophyll in the Evolution of Biological Converters of Solar Energy. *International Journal of Molecular Sciences* **Jan. 2013**, *14*, 575–593.

(88) Proshlyakov, D. A.; Pressler, M. A.; DeMaso, C.; Leykam, J. F.; DeWitt, D. L.; Babcock, G. T. Oxygen Activation and Reduction in Respiration: Involvement of Redox-Active Tyrosine 244. *Science* **Nov. 2000**, *290*, 1588.

(89) Aubert, C.; Mathis, P.; Eker, A. P.; Brettel, K. Intraprotein electron transfer between tyrosine and tryptophan in DNA photolyase from Anacystis nidulans. *Proceedings of the National Academy of Sciences* **1999**, *96*, 5423–5427.

(90) Warren, J. J.; Tronic, T. A.; Mayer, J. M. The Thermochemistry of Proton-Coupled Electron Transfer Reagents and its Implications. *Chemical reviews* **Dec. 2010**, *110*, 6961–7001.

(91) Rao, P. S.; Hayon, E. Correlation between ionization constants of organic free radicals and electrochemical properties of parent compounds. *Analytical Chemistry* **Mar. 1976**, *48*, 564–568.

(92) Dixon, W. T.; Murphy, D. Kinetic effects in the electron spin resonance spectra of some semiquinones. *Journal of the Chemical Society, Faraday Transactions 2: Molecular and Chemical Physics* **1976**, *72*, 135–142.

(93) Butler, J.; Land, E. J.; Prütz, W. A.; Swallow, A. Charge transfer between tryptophan and tyrosine in proteins. *Biochimica et Biophysica Acta (BBA) - Protein Structure and Molecular Enzymology* **July 1982**, *705*, 150–162.

(94) DeFelippis, M. R.; Murthy, C. P.; Broitman, F.; Weinraub, D.; Faraggi, M.; Klapper, M. H. Electrochemical properties of tyrosine phenoxy and tryptophan indolyl radicals in peptides and amino acid analogs. *The Journal of Physical Chemistry* **1991**, *95*, 3416–3419.

(95) Dongare, P.; Maji, S.; Hammarström, L. Direct Evidence of a Tryptophan Analogue Radical Formed in a Concerted ElectronProton Transfer Reaction in Water. *Journal of the American Chemical Society* **Feb. 2016**, *138*, 2194–2199.

(96) Gräslund, A.; Sahlin, M.; Sjöberg, B.-M. The tyrosyl free radical in ribonucleotide reductase. *Environmental health perspectives* **1985**, *64*, 139.

(97)   Irebo, T.; Reece, S. Y.; Sjödin, M.; Nocera, D. G.; Hammarström, L. Proton-Coupled Electron Transfer of Tyrosine Oxidation: Buffer Dependence and Parallel Mechanisms. *Journal of the American Chemical Society* **Dec. 2007**, *129*, 15462–15464.

(98)   Müller, P.; Bouly, J.-P.; Hitomi, K.; Balland, V.; Getzoff, E. D.; Ritz, T.; Brettel, K. ATP Binding Turns Plant Cryptochrome Into an Efficient Natural Photoswitch. *Scientific Reports* **May 2015**, *4*, DOI: `10.1038/srep05175`.

(99)   Brazard, J.; Usman, A.; Lacombat, F.; Ley, C.; Martin, M. M.; Plaza, P.; Mony, L.; Heijde, M.; Zabulon, G.; Bowler, C. SpectroTemporal Characterization of the Photoactivation Mechanism of Two New Oxidized Cryptochrome/Photolyase Photoreceptors. *Journal of the American Chemical Society* **Apr. 2010**, *132*, 4935–4945.

(100)   Lukacs, A.; Zhao, R.-K.; Haigney, A.; Brust, R.; Greetham, G. M.; Towrie, M.; Tonge, P. J.; Meech, S. R. Excited State Structure and Dynamics of the Neutral and Anionic Flavin Radical Revealed by Ultrafast Transient Mid-IR to Visible Spectroscopy. *The Journal of Physical Chemistry B* **May 2012**, *116*, 5810–5818.

(101)   Laptenok, S. P.; Bouzhir-Sima, L.; Lambry, J.-C.; Myllykallio, H.; Liebl, U.; Vos, M. H. Ultrafast real-time visualization of active site flexibility of flavoenzyme thymidylate synthase ThyX. *Proceedings of the National Academy of Sciences* **May 2013**, *110*, 8924–8929.

(102)   Finer-Moore, J. S.; Santi, D. V.; Stroud, R. M. Lessons and Conclusions from Dissecting the Mechanism of a Bisubstrate Enzyme: Thymidylate Synthase Mutagenesis, Function, and Structure. *Biochemistry* **Jan. 2003**, *42*, 248–256.

(103)   Myllykallio, H. An Alternative Flavin-Dependent Mechanism for Thymidylate Synthesis. *Science* **July 2002**, *297*, 105–107.

(104)   Urbonavicius, J. Identification of a novel gene encoding a flavin-dependent tRNA:m5U methyltransferase in bacteria–evolutionary implications. *Nucleic Acids Research* **July 2005**, *33*, 3955–3964.

(105)   Sournia, P. La méthylation flavine-dépendante d'acides nucléiques : aspects évolutifs, métaboliques, biochimiques et spectroscopiques., Thèse de doctorat dirigée par Liebl, Ursula et Myllykallio, Hannu Biologie Paris Saclay 2016, Ph.D. Thesis, 2016.

(106)   Zhong, D.; Zewail, A. H. Femtosecond dynamics of flavoproteins: charge separation and recombination in riboflavine (vitamin B2)-binding protein and in glucose oxidase enzyme. *Proceedings of the National Academy of Sciences* **2001**, *98*, 11867–11872.

(107) Mataga, N.; Chosrowjan, H.; Shibata, Y.; Tanaka, F. Ultrafast Fluorescence Quenching Dynamics of Flavin Chromophores in Protein Nanospace. *The Journal of Physical Chemistry B* **Sept. 1998**, *102*, 7081–7084.

(108) Laptenok, S. P.; van Stokkum, I. H. M.; Borst, J. W.; van Oort, B.; Visser, A. J. W. G.; van Amerongen, H. Disentangling Picosecond Events That Complicate the Quantitative Use of the Calcium Sensor YC3.60. *The Journal of Physical Chemistry B* **Mar. 2012**, *116*, 3013–3020.

(109) Van Stokkum, I. H. M.; Van Oort, B.; Van Mourik, F.; Gobets, B.; Van Amerongen, H. In *Biophysical Techniques in Photosynthesis*, Aartsma, T. J., Matysik, J., Eds.; Springer Netherlands: Dordrecht, 2008, pp 223–240.

(110) Cannizzo, A.; Bräm, O.; Zgrablic, G.; Tortschanoff, A.; Oskouei, A. A.; van Mourik, F.; Chergui, M. Femtosecond fluorescence upconversion setup with broadband detection in the ultraviolet. *Optics Letters* **Dec. 2007**, *32*, 3555–3557.

(111) Zhang, X.-X.; Würth, C.; Zhao, L.; Resch-Genger, U.; Ernsting, N. P.; Sajadi, M. Femtosecond broadband fluorescence upconversion spectroscopy: Improved setup and photometric correction. *Review of Scientific Instruments* **June 2011**, *82*, 063108.

(112) Arzhantsev, S.; Maroncelli, M. Design and Characterization of a Femtosecond Fluorescence Spectrometer Based on Optical Kerr Gating. *Applied Spectroscopy* **Feb. 2005**, *59*, 206–220.

(113) Nakamura, R.; Kanematsu, Y. Femtosecond spectral snapshots based on electronic optical Kerr effect. *Review of Scientific Instruments* **Feb. 2004**, *75*, 636–644.

(114) Laptenok, S. P.; Nuernberger, P.; Lukacs, A.; Vos, M. H. In, Engelborghs, Y., Visser, J. A., Eds.; Humana Press: Totowa, NJ, 2014, pp 321–336.

(115) Van Stokkum, I. H.; Larsen, D. S.; van Grondelle, R. Global and target analysis of time-resolved spectra. *Biochimica et Biophysica Acta (BBA) - Bioenergetics* **July 2004**, *1657*, 82–104.

(116) Eaton, W. A.; Hofrichter, J.; Makinen, M. W.; Andersen, R. D.; Ludwig, M. L. Optical spectra and electronic structure of flavine mononucleotide in flavodoxin crystals. *Biochemistry* **May 1975**, *14*, 2146–2151.

(117) Nishimasu, H.; Ishitani, R.; Yamashita, K.; Iwashita, C.; Hirata, A.; Hori, H.; Nureki, O. Atomic structure of a folate/FAD-dependent tRNA T54 methyltransferase. *Proceedings of the National Academy of Sciences* **May 2009**, *106*, 8180–8185.

(118) Hamdane, D.; Bruch, E.; Un, S.; Field, M.; Fontecave, M. Activation of a Unique Flavin-Dependent tRNA-Methylating Agent. *Biochemistry* **Dec. 2013**, *52*, 8949–8956.

(119) Hamdane, D.; Argentini, M.; Cornu, D.; Golinelli-Pimpaneau, B.; Fontecave, M. FAD/Folate-Dependent tRNA Methyltransferase: Flavin as a New Methyl-Transfer Agent. *Journal of the American Chemical Society* **Dec. 2012**, *134*, 19739–19745.

(120) Mataga, N.; Chosrowjan, H.; Shibata, Y.; Tanaka, F.; Nishina, Y.; Shiga, K. Dynamics and Mechanisms of Ultrafast Fluorescence Quenching Reactions of Flavin Chromophores in Protein Nanospace. *The Journal of Physical Chemistry B* **Nov. 2000**, *104*, 10667–10677.

(121) Van den Berg, P. A. W.; Feenstra, K. A.; Mark, A. E.; Berendsen, H. J. C.; Visser, A. J. W. G. Dynamic Conformations of Flavin Adenine Dinucleotide: Simulated Molecular Dynamics of the Flavin Cofactor Related to the Time-Resolved Fluorescence Characteristics. *The Journal of Physical Chemistry B* **Aug. 2002**, *106*, 8858–8869.

(122) Bensasson, R.; Land, E.; Truscott, T. In *Flash Photolysis and Pulse Radiolysis*; Pergamon: 1983, pp 135–163.

(123) Hammarström, L. Towards artificial photosynthesis: ruthenium–manganese chemistry mimicking photosystem II reactions. *Current Opinion in Chemical Biology* **Dec. 2003**, *7*, 666–673.

(124) Mayer, J. M. Proton-coupled electron transfer: A Reaction Chemist's View. *Annual Review of Physical Chemistry* **Apr. 2004**, *55*, 363–390.

(125) Hamdane, D.; Guérineau, V.; Un, S.; Golinelli-Pimpaneau, B. A Catalytic Intermediate and Several Flavin Redox States Stabilized by Folate-Dependent tRNA Methyltransferase from *Bacillus subtilis*. *Biochemistry* **June 2011**, *50*, 5208–5219.

(126) Gadosy, T. A.; Shukla, D.; Johnston, L. J. Generation, Characterization, and Deprotonation of Phenol Radical Cations [1]. *The Journal of Physical Chemistry A* **Nov. 1999**, *103*, 8834–8839.

(127) Miura, R. Versatility and specificity in flavoenzymes: Control mechanisms of flavin reactivity. *The Chemical Record* **2001**, *1*, 183–194.

(128) Kundu, M.; He, T.-F.; Lu, Y.; Wang, L.; Zhong, D. Short-Range Electron Transfer in Reduced Flavodoxin: Ultrafast Nonequilibrium Dynamics Coupled with Protein Fluctuations. *The Journal of Physical Chemistry Letters* **June 2018**, *9*, 2782–2790.

(129) Fornander, L. H.; Feng, B.; Beke-Somfai, T.; Nordén, B. UV Transition Moments of Tyrosine. *The Journal of Physical Chemistry B* **Aug. 2014**, *118*, 9247–9257.

(130) Rasiah, I. A.; Sutton, K. H.; Low, F. L.; Lin, H.-M.; Gerrard, J. A. Crosslinking of wheat dough proteins by glucose oxidase and the resulting effects on bread and croissants. *Food Chemistry* **2005**, *89*, 325 –332.

(131) Crueger, A.; Crueger, W. In *Microbial Enzymes and Biotechnology*, Fogarty, W. M., Kelly, C. T., Eds.; Springer Netherlands: Dordrecht, 1990, pp 177–226.

(132) Afseth, J.; Rølla, G. Clinical Experiments with a Toothpaste Containing Amyloglucosidase and Glucose Oxidase. *Caries Research* **1983**, *17*, 472–475.

(133) Chen, T.; Barton, S. C.; Binyamin, G.; Gao, Z.; Zhang, Y.; Kim, H.-H.; Heller, A. A Miniature Biofuel Cell. *Journal of the American Chemical Society* **2001**, *123*, 8630–8631.

(134) Bankar, S. B.; Bule, M. V.; Singhal, R. S.; Ananthanarayan, L. Glucose oxidase — An overview. *Biotechnology Advances* **2009**, *27*, 489 –501.

(135) Akiya, K.; Noriaki, I.; Noboru, M.; Fumio, T. Picosecond laser photolysis studies of fluorescence quenching mechanisms of flavin: A direct observation of indole-flavin singlet charge transfer state formation in solutions and flavoenzymes. *Photochemistry and Photobiology* **1982**, *37*, 495–502.

(136) Fujiwara, A.; Mizutani, Y. Photoinduced electron transfer in glucose oxidase: a picosecond time-resolved ultraviolet resonance Raman study. *Journal of Raman Spectroscopy* **Nov. 2008**, *39*, 1600–1605.

(137) Tommos, C.; Babcock, G. T. Proton and hydrogen currents in photosynthetic water oxidation. *Biochimica et Biophysica Acta (BBA) - Bioenergetics* **2000**, *1458*, 199 –219.

(138) Pan, J.; Byrdin, M.; Aubert, C.; Eker, A. P. M.; Brettel, K.; Vos, M. H. Excited-State Properties of Flavin Radicals in Flavoproteins: Femtosecond Spectroscopy of DNA Photolyase, Glucose Oxidase, and Flavodoxin. *The Journal of Physical Chemistry B* **July 2004**, *108*, 10160–10167.

(139) Massey, V.; Matthews, R. G.; Foust, G. P.; Howell, L. G.; Williams, C. H.; Zanetti, G.; Ronchi, S. In *Pyridine Nucleotide-Dependent Dehydrogenases: Proceedings of an Advanced Study Institute held at the University of Konstanz, Germany*, Sund, H., Ed.; Springer Berlin Heidelberg: Berlin, Heidelberg, 1970, pp 393–411.

(140) Liu, Z.; Tan, C.; Guo, X.; Li, J.; Wang, L.; Sancar, A.; Zhong, D. Determining complete electron flow in the cofactor photoreduction of oxidized photolyase. *Proceedings of the National Academy of Sciences* **Aug. 2013**, *110*, 12966–12971.

(141) Gray, H. B.; Winkler, J. R. Hole hopping through tyrosine/tryptophan chains protects proteins from oxidative damage. *Proceedings of the National Academy of Sciences* **Sept. 2015**, *112*, 10920–10925.

(142) Seo, D.; Naito, H.; Nishimura, E.; Sakurai, T. Replacement of Tyr50 stacked on the si-face of the isoalloxazine ring of the flavin adenine dinucleotide prosthetic group modulates Bacillus subtilis ferredoxin-NADP+ oxidoreductase activity toward NADPH. *Photosynthesis Research* **Aug. 2015**, *125*, 321–328.

Appendix A

# Identification of the TyrOH$^{\cdot+}$ Radical Cation in the Flavoenzyme TrmFO

Identification of the TyrOH•+ Radical Cation in the Flavoenzyme TrmFO

Lipsa Nag, Pierre Sournia, Hannu Myllykallio, Ursula Liebl, and Marten H. Vos*

LOB, Ecole Polytechnique, CNRS, INSERM, Université Paris-Saclay, Palaiseau 91128 Cedex, France

S Supporting Information

ABSTRACT: Tyrosine (TyrOH) and tryptophan radicals play important roles as intermediates in biochemical charge-transfer reactions. Tryptophanyl radicals have been observed both in their protonated cation form and in their unprotonated neutral form, but to date, tyrosyl radicals have only been observed in their unprotonated form. With a genetically modified form of the flavoenzyme TrmFO as a suitable model system and using ultrafast fluorescence and absorption spectroscopy, we characterize its protonated precursor TyrOH•+, and we show this species to have a distinct visible absorption band and a transition moment that we suggest to lie close to the phenol symmetry axis. TyrOH•+ is formed in ~1 ps by electron transfer to excited flavin and decays in ~3 ps by charge recombination. These findings imply that TyrOH oxidation does not necessarily induce its concerted deprotonation. Our results will allow disentangling of photoproduct states in flavoproteins in often-encountered complex situations and more generally are important for understanding redox chains relying on tyrosyl intermediates.
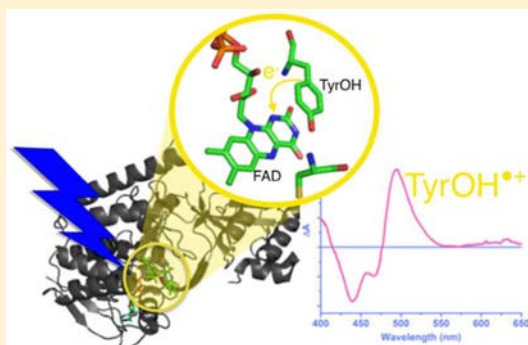
INTRODUCTION

Charge-transfer reactions are ubiquitous in protein biochemistry. They almost invariably involve specialized cofactor molecules. In numerous cases they also involve amino acid residues that are integral parts of the protein structure, in particular the aromatic residues tyrosine and tryptophan.[1,4] Examples include photolyase,[6] class 1a ribonucleotide reductase,[7] MauG,[8] and photosystem II.[9] In these systems, tryptophan and tyrosine radicals act as reaction intermediates. Resting tyrosine and tryptophan are protonated at physiological pH. The transiently formed tryptophanyl and tyrosyl radicals are typically above their pKa, and long-lived oxidation of these residues is associated with their deprotonation (proton-coupled electron transfer), either concertedly or sequentially.

For tryptophanyl (pKa ~ 4),[10] it has been shown (in DNA photolyase) that both the protonated (TrpH•+) and the deprotonated (Trp•) radicals can be formed sequentially and at different time scales.[1] In a Trp-analogue-containing model compound in aqueous solution, the latter species was inferred to be formed by concerted proton and electron transfer.[11] Altogether, formation of Trp• can, but does not necessarily, occur via synchronous electron/proton transfer.[4]

The situation is different for the tyrosyl radical. Its pKa is thought to be as low as ~−2,[12] and hence the protonated tyrosyl radical (TyrOH•+), if it can be formed at all, presumably is highly unstable. Probably for this reason this form has not been directly observed as a reaction intermediate[13,14] and has not been spectroscopically characterized. For instance in the extensively studied photoactive protein system involving tyrosyl intermediates, photosystem II, tyrosine Z acts as a secondary electron donor to the photooxidized chlorophyll dimer P$_{680}$.[15] This electron transfer occurs concomitant with tyrosine deprotonation (to a different acceptor) on the nanosecond time scale.[16−20] For tyrosine-containing photoactivatable model compounds in aqueous solution, a stepwise mechanism with electron transfer preceding proton transfer has been invoked, but here, the rate of tyrosyl deprotonation is much faster than that of electron transfer,[21] and spectroscopically no intermediates are observed.

In flavoproteins, photoreduction of excited flavin by electron transfer from nearby tyrosine or tryptophan residues is an efficient fluorescence quenching mechanism.[22,23] This property is naturally exploited by cryptochrome blue light sensors[24] and has also been used as a sensitive probe of the conformational dynamics in active sites of flavoenzymes that are not naturally light-active.[25,26] Here flavin excited-state lifetimes can be shortened to the picosecond time scale or less, providing opportunities to characterize short-lived radical product states by transient absorption spectroscopy. The formed radicals of aromatic residues absorb in the visible wavelength range. Full spectral studies have been used to determine the formation of protonated and unprotonated tryptophanyl radicals, in particular in photolyase and cryptochrome.[1,27] Here we present a full spectral investigation of a flavoprotein system that harbors an efficient tyrosine quencher. In this system the short-lived tyrosyl radical is initially generated in the protonated cation form, and we determine its spectral properties.

The flavoenzyme TrmFO is found in many bacteria; it is implicated in the post-transcriptional formation of m^{5}U$_{54}$ in tRNAs and is required for structural stabilization of these crucial RNA molecules. In this methylation reaction, the methylene from the C$_2$H$_4$folate is transferred to tRNAs (or in some cases to rRNA) via an intermediate of the N5 of the NADPH-reduced FAD cofactor.[28,29] Figure 1 shows the active
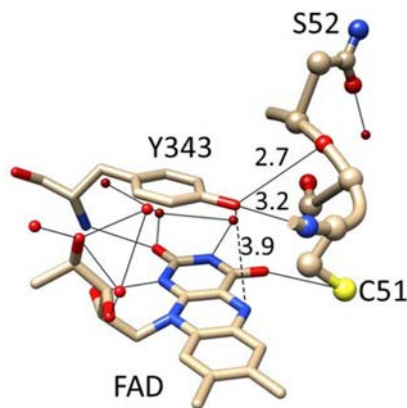

Figure 1. Structure of the active site of wild-type TrmFO (pdb 3G5Q). Red dots represent O atoms of structural water molecules. The thin dotted lines represent possible hydrogen-bonding interactions, using the standard relaxed hydrogen-bond constraints criteria of Chimera.[31] The dashed line represents the distance between the Tyr343 O and the flavin N5 atoms. Distances are in Å.

site of the *Thermus thermophilus* enzyme, the only TrmFO for which a structure is determined.[30] The residues closest to the isoalloxazine ring of the FAD cofactor are Tyr343 (ring-to-ring distance 3.3 Å) and Cys51. Tyr343 is in an apolar environment and shielded from the cleft forming the substrate binding site (a water-rich area in the crystal structure) by the isoalloxazine ring. The Tyr343 OH group is in possible hydrogen-bonding interaction distance with the backbone of Ser 52 and Cys 51, but not with structural waters. The present study focuses on the interaction between FAD and the very closeby Tyr343, using a genetically modified version of this enzyme.

■ EXPERIMENTAL SECTION

The gene encoding TrmFO from *Thermus thermophilus* was codon optimized for expression in *E. coli* and cloned into a pQE80L expression vector (Qiagen). The protein (molecular mass 48,9 kDa) was expressed in *E. coli* BL21 DE3 after induction with 1 mM isopropyl-β-D-thiogalactopyranoside. *Tt*TrmFO was purified by affinity chromatography on Ni-TED columns (Protino Ni-TED, Macherey Nagel) and eluted with 50 mM NaH$_2$PO$_4$, 300 mM NaCl, and 250 mM imidazole, pH 8.0, followed by imidazole removal on Econo-Pac 10DG desalting columns (BIO-RAD). Site-directed mutants were constructed using the QuikChange II site-directed mutagenesis kit (Agilent), following the manufacturer's instructions and using the following primers: C51A: forward 5′-CGGGTGTTGAAGGCTGGCTGGAATCTGCGGCG-3′; reverse 5′-CGCCGCAGATTCCAGCCAGCCTTCAAC ACCCG-3′; Y343F: forward 5′-CCCAGGCTGTTGCTGGCGACGATCTCAGCGAA-3′; reverse 5′-TTCGCT GAGATCGTCGCCAGCAACAGCCTGGG-3′. All purified proteins were suspended in 50 mM Hepes buffer, pH 8.0, containing up to 250 mM NaCl. For all time-resolved experiments, the proteins were kept under air atmosphere in a quartz cell of 1 mm path length, at a temperature of 20 °C. The optical density of the samples was ~0.15 and ~0.3 at the absorption maximum near 450 nm for the

transient fluorescence and transient absorption experiments, respectively.

Steady-state absorption and fluorescence spectra were taken at room temperature using a Shimadzu UV–vis 1700 spectrometer and a Cary Eclipse fluorometer, respectively.

The setup for time-resolved fluorescence employs a Kerr gate and has been described before.[25,32] Briefly, the excitation pulse centered at 390 nm is obtained by frequency-doubling, using a BBO crystal, part of the 780 nm pulse from the Ti:sapphire laser/amplifier system (Quantronix Integra-C) operating at 1 kHz. The remaining 780 nm beam is led through a motorized delay-line and focused into the Kerr medium where it spatially overlapped the fluorescence from the sample. The Kerr medium used was either Suprasil (response time ~200 fs), benzene (response time ~300 fs), or CS$_2$ (response time 1 ps), depending on the desired time resolution. For the C51A experiments, only Suprasil was used. Transient fluorescence spectra were measured on time windows up to 24 ps for C51A and 2 ns for C51A/Y343F. Multicolor time-resolved absorption spectra were performed on an instrument operating at 500 Hz as described,[33] with pump pulses centered at 390 nm (as for the time-resolved fluorescence experiments) and continuum broadband probe pulses. The excitation power was adapted such that the pump beam excited <10% of the sample at each laser shot. All time-resolved data were analyzed using the Glotaran package for global analysis.[34]

■ RESULTS AND DISCUSSION

In purified TrmFO in solution, a highly fluorescent Cys51-FAD adduct is formed that is thought to be a dormant reaction intermediate that can be activated by binding of tRNA.[35] In heterologously expressed *Bacillus subtilis* TrmFO at physiological pH, this adduct dissociates within hours after purification.[36] In the purified *T. thermophilus* enzyme, we found that by contrast the adduct is stable and does not convert to regular oxidized FAD (FAD$_{ox}$), even at elevated temperatures. Cys51 was therefore replaced by alanine to allow studying the interaction between FAD$_{ox}$ and the nearby Tyr343 residue.

Figure 2 shows the steady-state spectra of the C51A *Tt*TrmFO mutant. The absorption spectrum is characteristic of oxidized flavoproteins[37] with bands centered at ~450 and 370 nm. The fluorescence is centered at ~520 nm, as also characteristic of FAD$_{ox}$, but has a low intensity. Consistently the fluorescence fully decays, with a single exponential, in 1.2 ps (Figure 3 and Figures S1 and S2). To test whether this very
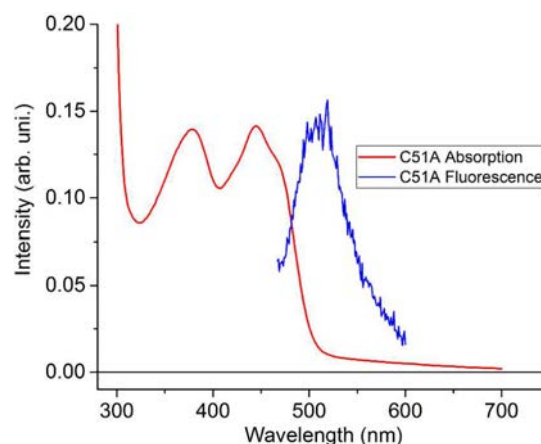

Figure 2. Steady-state absorption and fluorescence spectra of the C51A mutant of *T. thermophilus* TrmFO. The spectra are typical of FAD$_{ox}$ containing proteins.
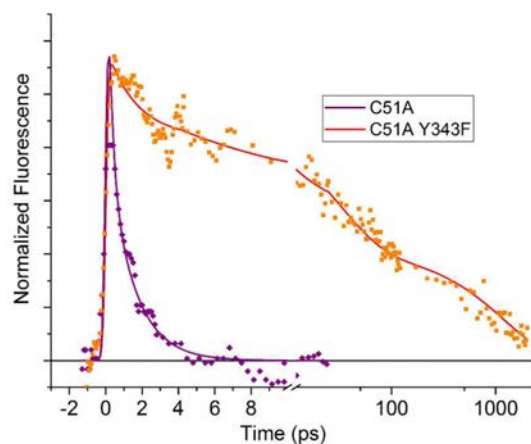
Figure 3. Fluorescence decay at 520 nm in *Tt*TrmFO mutants C51A and C51A/Y343F. Solid lines are fits. The time axis is linear up to 10 ps and logarithmic thereafter. The decay of the C51A mutant is distinctly faster than that of C51A/Y343F TrmFO.

efficient fluorescence quenching is due to the nearby Tyr343 residue, we investigated the C51A/Y343F mutant protein, where this residue is replaced by the redox-inactive phenylalanine. This modification results in a much stronger fluorescence, and the corresponding slower decay (Figure 3) is dominated by slower phases with time constants of 30 ps, 0.4 ns, and >2 ns (Figure S2). The finding that mutation of Tyr343 strongly slows down the fluorescence decay demonstrates that in the C51A *Tt*TrmFO mutant protein, Tyr343 is the main electron donor to excited FAD.

Full transient spectra and the global analysis of the fluorescence data are shown in Figures S1 and S2. In the C51A/Y343F protein, the decay is slower than that in the C51A protein (see above), but still predominantly faster than expected for nonquenched unstacked FAD (a few nanoseconds).[38,39] This indicates that an electron donor other than Tyr343 can also donate electrons to excited FAD, but less efficiently. Furthermore, the fluorescence decay in C51A/Y343F *Tt*TrmFO is multiphasic (see above), indicating that multiple configurations of flavin-electron donor pairs coexist, as is the case in the flexible enzyme ThyX, which catalyzes a similar reaction.[25] Consistent with these assessments, in *Tt*TrmFO, the next-nearest potential electron donor, Trp214, is located on a flexible loop. Further studies aimed at characterizing the protein dynamics of the active site environment in *Tt*TrmFO, including on mutant proteins modified in position 214 assessing the involvement of this residue in the quenching of C51A/Y343F mutant fluorescence, will be presented elsewhere.

To characterize the photoproducts of the C51A *Tt*TrmFO protein, we performed transient absorption spectroscopy. Figure 4 shows time traces at selected wavelengths. The kinetics at 450 nm (peak of the ground-state absorption) and at 568 nm (in the stimulated emission region) are dominated by a phase of ~1 ps. The time constant of this phase is similar to that of the fluorescence decay, and therefore this phase can be assigned to FAD* decay. At 500 nm, however, an induced absorption that decays substantially slower is observed, indicating the presence of a distinct product state.

A full analysis of the data in terms of decay associated spectra (DAS) is given in Figure 5, and the corresponding species associated difference spectra are shown in Figure S3. Two
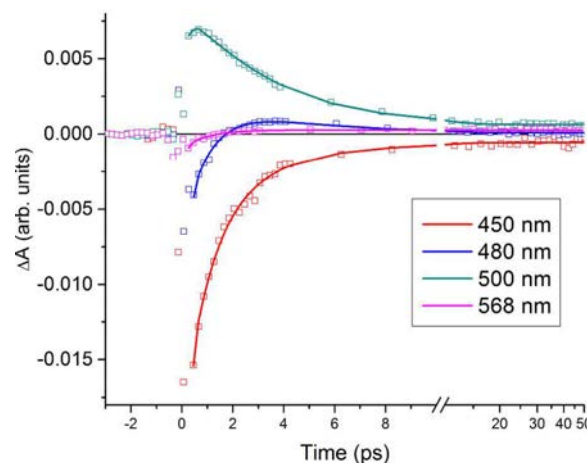

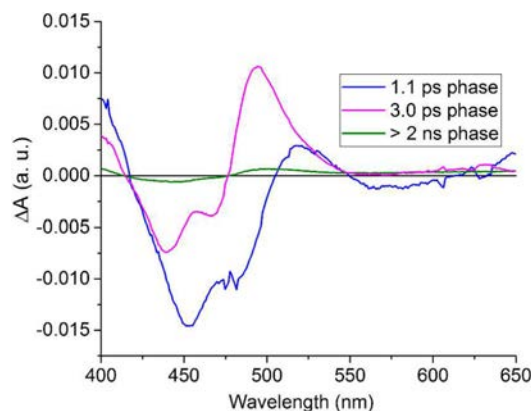**Figure 4.** Kinetics of time-resolved absorption in C51A *Tt*TrmFO at selected wavelengths.

Figure 5. Decay associated spectra obtained from the global analysis of transient absorption data from the C51A *Tt*TrmFO mutant protein.

distinct kinetic phases, with time constants of 1.1 and 3.0 ps, are required to fit the data. The 1.1 ps phase, ascribed to decay of the excited-state FAD*, contains bleaching features in the FAD$_{ox}$ absorption region and further negative absorption above 550 nm that is assigned to stimulated emission, as well as induced absorption features around 400 and 520 nm that are assigned to excited-state absorption. As explained in Figure S3, the FAD* decay in 1.1 ps gives rise to the product state decaying partly very fast and partly in 3.0 ps. The remaining work concerns the latter fraction. The 3.0 ps phase lacks stimulated emission features. It contains a strong induced absorption band centered at 490 nm that has significantly higher amplitude than the corresponding bleaching band at 450 nm. The 490 nm band is much larger and very uniquely shaped compared to any absorption expected for the anionic and neutral flavoquinone forms FAD$^{\bullet-}$ and FADH$^{\bullet}$ in this region (see Figure 6). As Tyr343 is the electron donor responsible for quenching FAD*, we assign it to a tyrosyl radical. As the tyrosine is protonated in the neutral state (TyrOH), the initial photoproduct is expected to be TyrOH$^{\bullet+}$, but if deprotonation occurs along with electron transfer, then TyrO$^{\bullet}$ will be formed. The latter state has been spectrally well characterized and absorbs at 400−410 nm.[4,40] We therefore assign the feature at 490 nm to TyrOH$^{\bullet+}$ and infer that in this protein system, the tyrosyl cation radical can be formed as a distinct species without
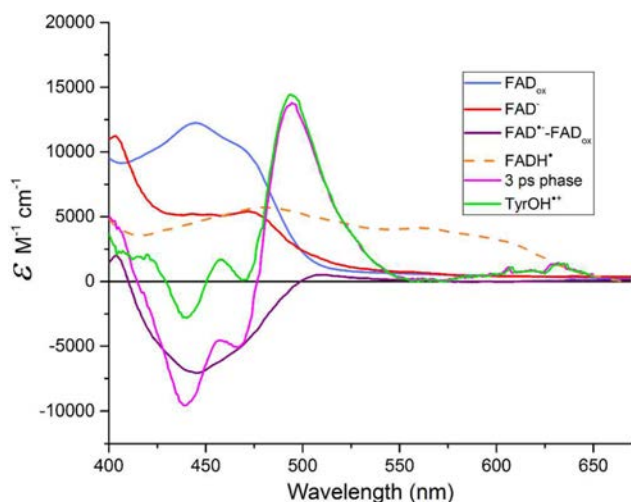
Figure 6. Spectrum of TyrOH$^{\bullet+}$ calculated from the 3 ps DAS of Figure 5 and model spectra for FAD$^{\bullet-}$ and FAD$_{ox}$ as described in the text. For comparison, a spectrum for the FADH$^{\bullet}$ form of DNA photolyase from *E. coli*[1] is also shown, that can be fully formed in steady state. In the red part of the spectrum, where it does not overlap with FAD$_{ox}$, this spectrum is similar to the FADH$^{\bullet}$ spectrum of TrmFO.[3]

concomitant deprotonation. In the DAS of transient absorption experiments of the C51A/Y343F double mutant, the strong 490 nm feature is not observed (Figure S4), which is in full agreement with its assignment to the Tyr343 cation.

Finally, a very small (∼3% of the initial signal in the bleaching area) long-lived phase remains. Its spectrum is reminiscent of that of the 3 ps phase and may reflect a very small fraction of the protein in which the product state is long-lived, although the low amplitude prohibits firm assignment.

A minimal reaction scheme for the C51A protein is depicted in Scheme 1. The rate constants are tabulated in Table 1. To

Scheme 1. Proposed Minimal Charge-Transfer Pathway in C51A TrmFO[a]
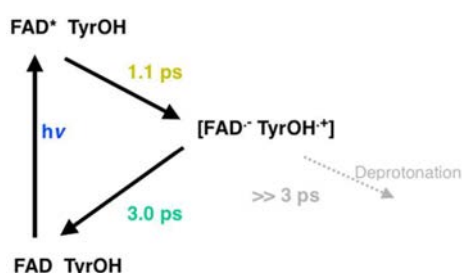
[a]Thick solid arrows correspond to the observed reactions, and the dotted grey line to (non-observed) potential tyrosine deprotonation.

Table 1. Values of Main Experimentally Determined Rate Constants and Angles for C51A TrmFO

k (FAD*TyrOH → FAD$^{\bullet-}$TyrOH$^{\bullet+}$)	0.9 ps^{-1}
k (FAD$^{\bullet-}$TyrOH$^{\bullet+}$ → FADTyrOH)	0.3 ps^{-1}
k (TyrOH$^{\bullet+}$ → TyrO$^{\bullet}$)	≪0.3 ps^{-1}
φ (FADα, TyrOH$^{\bullet+}$)	31 ± 5°

obtain a more quantitative characterization of the TyrOH$^{\bullet+}$ absorption band, we decomposed the 3 ps DAS in terms of the

sum of (FAD$^{\bullet-}$ *minus* FAD$_{ox}$) and (TyrOH$^{\bullet+}$ *minus* TyrOH) spectra (Figure 6). To this end, we used the ground-state absorption spectrum of C51A *Tt*TrmFO (Figure 2) and, as stable FAD$^{\bullet-}$ cannot be generated in TrmFO, the published steady-state FAD$^{\bullet-}$ spectrum of an insect cryptochrome[41] as a model for *Tt*TrmFO FAD$^{\bullet-}$. TyrOH does not absorb in the visible spectral region. Here, the only adjustable parameter is the scaling factor b of the DAS spectrum:

$$\varepsilon_{\text{TyrOH}^{\bullet+}} = b(\text{DAS}_{3\text{ps}}) - (\varepsilon_{\text{FAD}^{\bullet-}} - \varepsilon_{\text{FADox}}) \qquad (1)$$

where b was chosen such that the blue spectral region (<470 nm) is dominated by the flavin contributions and the TyrOH$^{\bullet+}$ spectrum is minimal, a choice confirmed by the polarization experiments described below. In this blue region, the modeled TyrOH$^{\bullet+}$ spectrum (Figure 6, green) displays some remaining features that we ascribe to the differences in the FAD$^{\bullet-}$ spectrum between the cryptochrome and TrmFO; the details of flavin spectra are known to be very sensitive to their protein environment. At longer wavelengths, where the flavin forms absorb weakly or not at all and do not give rise to uncertainty, the TyrOH$^{\bullet+}$ spectrum is smooth. The thus modeled TyrOH$^{\bullet+}$ spectrum consists of a ∼40 nm broad band with a maximum at 490 nm. This spectrum represents to our knowledge the first known spectrum of the tyrosyl cation radical in solution or in a polypeptide. This assessment is in general agreement with bands in the same spectral region assigned by Gadosy et al. to various methoxy-phenoxyl cation radicals generated by a photoinduced oxidation reaction in neat acetonitrile.[42]

The transient absorption experiments described above were performed under isotropic conditions (pump polarized at magic angle with respect to the probe). In order to gain insight in the orientation of the involved dipole moments, we also performed transient anisotropy experiments. In such experiments, transient spectra are measured with the pump and probe pulses polarized parallel ($\Delta A_{//}$) and perpendicular ($\Delta A_{\perp}$). For pumping and probing single transitions, the anisotropy r:

$$r = (\Delta A_{//} - \Delta A_{\perp})/(\Delta A_{//} + 2\Delta A_{\perp}) \qquad (2)$$

can vary between −0.2 and 0.4 and is related to the angle ϕ between the pumped and probed transition as[43]

$$r = (3\cos^2 \varphi - 1)/5 \qquad (3)$$

For situations where spectral regions with signals arising from different overlapping transitions are probed, more complex and wavelength-dependent anisotropies can occur, including with values outside the (−0.2 to 0.4) interval.[44]

In principle, the experimentally determined anisotropy has a somewhat lower amplitude than the real anisotropy due to finite sample absorption and excitation intensity. Under our experimental conditions using a sample near the optically thin limit and <10% excitation energy, the deviation is estimated <∼3% (cf. ref 45); hence substantially smaller than the variation in anisotropy used to discuss the results (see below).

Comparing with steady-state polarization spectroscopy of flavodoxin crystals,[2] under our excitation conditions, while both the (lowest-lying) α and the β transitions are excited, the α transition is predominantly excited. The two transitions make a small angle (∼20°).[2] Figure S5 shows the 3.0 ps DAS obtained under different polarization conditions and Figure 7 the corresponding anisotropies. The anisotropy in the bleaching area is almost constant and close to 0.40, the value expected for pumping and probing identical or parallel transitions. This
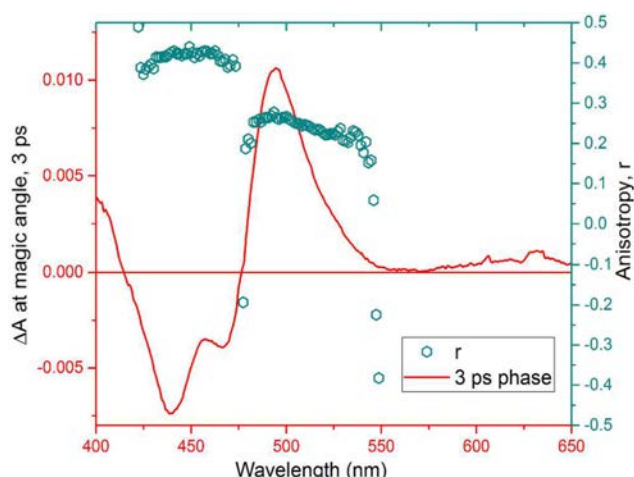
Figure 7. Anisotropy (r) spectrum overlaid with the isotropic 3 ps DAS of the C51A mutant. The mean r in the region of bleaching (425−475 nm) is 0.40 ± 0.03 and that in the product-state absorption (480−530 nm) 0.24 ± 0.04.

finding is consistent with the notion that the lowest (α) FAD_{ox} transition is predominantly excited and probed here and indicates that the probed $FAD^{\bullet-}$ transition is near-parallel to this transition. The anisotropy in the $TyrOH^{\circ+}$ absorption band area is also almost constant, but markedly lower at 0.24 ± 0.04. The finding of two regions where the anisotropies are both almost constant but have two distinct values justifies the decomposition of Figure 6 with little spectral overlap between the $TyrOH^{\bullet+}$ and the two FAD forms. The anisotropy determined from the $TyrOH^{\bullet+}$ spectral region corresponds to an angle between the excited FAD_{ox} α transition and the probed $TyrOH^{\bullet+}$ transition of 31° ± 5°. On analyzing the *Tt*TrmFO crystal structure and assuming that the $TyrOH^{\bullet+}$ transition lies in the phenol plane, this finding predicts two possible orientations of the transition that both lie closer to the symmetry axis corresponding to the lowest (UV) L_b transition of neutral TyrOH[5] than to the perpendicular L_a transition (Figure 8). One makes a small angle of 23° with the symmetry axis; we suggest this to be the most likely candidate. It will be interesting to compare this experimental assessment with theoretical studies of the $TyrOH^{\bullet+}$ transition. Such studies may help to reach a firm assignment on which of these orientations corresponds to the 490 nm $TyrOH^{\bullet+}$ band.

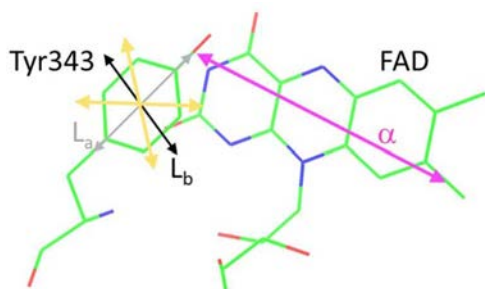**Figure 8.** Possible orientations of the $TyrOH^{\bullet+}$ transition in the tyrosine plane (yellow) deduced from the transient anisotropy experiments of Figure 7. The lowest α transition dipole in FAD[2] and the ground-state L_a and L_b transitions of TyrOH[5] are also represented.

CONCLUSIONS

Thus far, in experiments on chemical and biochemical systems on the nanosecond and longer time scales, only deprotonated tyrosyl intermediates have been identified.[4,13,46−48] Our results demonstrate that on the picosecond time scale, tyrosine can be oxidized without concomitant deprotonation. The $TyrOH^{\bullet+}$ photoproduct is short-lived: it decays in ∼3 ps, in a vast majority by charge recombination of the radical pair formed. Given the low pK_a of tyrosyl, it might also be expected that deprotonation occurs to a closely located proton acceptor. The most prominent candidate for this would be the reduced flavin (pK_a ∼ 8.3,[49] distance between Tyr O and FAD N5 atoms is 3.9 Å). As we do not observe sizable tyrosyl deprotonation and $FADH^{\bullet}$ formation in our experiments, our findings indicate that such a proton-transfer reaction has a rate constant of ≪3 ps^{-1}.

In many protein systems, tyrosine is thought to play a functional role as a redox intermediate.[50] Such intermediates may be difficult to characterize in many cases due to experimental rate limitations in their formation. However, our results demonstrate that for tyrosines located close to potential redox partners, protonated tyrosyl radicals should be considered as separate intermediate species. Concerning flavoproteins, tyrosyl radicals are thought to play an important role in several blue-light sensing systems. For instance in BLUF proteins, involved in light-sensing of photosynthetic bacteria through electron and glutamine-mediated proton transfer to the flavin, a tyrosine residue in the vicinity of FAD is thought to play a crucial role in the formation of the signaling state. However, the mechanism of this highly complex process that contains branched reaction schemes is subject to intense debate.[51−55] We foresee that knowledge of the here-determined spectrum of the $TyrOH^{\bullet+}$ state will help to experimentally elucidate the mechanism.

Altogether, our results demonstrating the formation of the $TyrOH^{\bullet+}$ state as a real but short-lived redox intermediate in a protein system and determining its spectroscopic characteristics provide a unique basis for disentangling electron- and proton-transfer reaction pathways in tyrosine-incorporating redox chains.

ASSOCIATED CONTENT

Ⓢ Supporting Information

The Supporting Information is available free of charge on the ACS Publications website at DOI: 10.1021/jacs.7b04586.

Five supporting figures (PDF)

AUTHOR INFORMATION

Corresponding Author

*marten.vos@polytechnique.edu

ORCID Ⓘ

Marten H. Vos: 0000-0003-0493-4831

Notes

The authors declare no competing financial interest.

REFERENCES

(1) Aubert, C.; Vos, M. H.; Mathis, P.; Eker, A. P. M.; Brettel, K. *Nature* **2000**, *405*, 586−590.

(2) Eaton, W. A.; Hofrichter, J.; Makinen, M. W.; Andersen, R. D.; Ludwig, M. L. *Biochemistry* **1975**, *14*, 2146−2151.

(3) Hamdane, D.; Guérineau, V.; Un, S.; Golinelli-Pimpaneau, B. *Biochemistry* **2011**, *50*, 5208−5219.

(4) Butler, J.; Land, E. J.; Prütz, W. A.; Swallow, A. J. *Biochim. Biophys. Acta, Protein Struct. Mol. Enzymol.* **1982**, *705*, 150−162.

(5) Fornander, L. H.; Feng, B.; Beke-Somfai, T.; Nordén, B. *J. Phys. Chem. B* **2014**, *118*, 9247−9257.

(6) Lukacs, A.; Eker, A. P. M.; Byrdin, M.; Brettel, K.; Vos, M. H. *J. Am. Chem. Soc.* **2008**, *130*, 14394−14395.

(7) Minnihan, E. C.; Nocera, D. G.; Stubbe, J. *Acc. Chem. Res.* **2013**, *46*, 2524−2535.

(8) Geng, J.; Dornevil, K.; Davidson, V. L.; Liu, A. *Proc. Natl. Acad. Sci. U. S. A.* **2013**, *110*, 9639−9644.

(9) Dempsey, J. L.; Winkler, J. R.; Gray, H. B. *Chem. Rev.* **2010**, *110*, 7024−7039.

(10) Solar, S.; Getoff, N.; Surdhar, P. S.; Armstrong, D. A.; Singh, A. *J. Phys. Chem.* **1991**, *95*, 3639−3643.

(11) Dongare, P.; Maji, S.; Hammarström, L. *J. Am. Chem. Soc.* **2016**, *138*, 2194−2199.

(12) Dixon, W. T.; Murphy, D. *J. Chem. Soc., Faraday Trans. 2* **1976**, *72*, 1221−1230.

(13) Warren, J. J.; Winkler, J. R.; Gray, H. B. *FEBS Lett.* **2012**, *586*, 596−602.

(14) Pagba, C. V.; Chi, S.-H.; Perry, J.; Barry, B. A. *J. Phys. Chem. B* **2015**, *119*, 2726−2736.

(15) Barry, B. A.; Babcock, G. T. *Proc. Natl. Acad. Sci. U. S. A.* **1987**, *84*, 7099−7103.

(16) Reece, S. Y.; Hodgkiss, J. M.; Stubbe, J.; Nocera, D. G. *Philos. Trans. R. Soc., B* **2006**, *361*, 1351−1364.

(17) Mayer, J. M. *Annu. Rev. Phys. Chem.* **2004**, *55*, 363−390.

(18) Hammarström, L. *Curr. Opin. Chem. Biol.* **2003**, *7*, 666−673.

(19) Weinberg, D. R.; Gagliardi, C. J.; Hull, J. F.; Murphy, C. F.; Kent, C. A.; Westlake, B. C.; Paul, A.; Ess, D. H.; McCafferty, D. G.; Meyer, T. J. *Chem. Rev.* **2012**, *112*, 4016−4093.

(20) Barry, B. A. *J. Photochem. Photobiol., B* **2011**, *104*, 60−71.

(21) Irebo, T.; Reece, S. Y.; Sjödin, M.; Nocera, D. G.; Hammarström, L. *J. Am. Chem. Soc.* **2007**, *129*, 15462−15464.

(22) Mataga, N.; Chosrowjan, H.; Shibata, Y.; Tanaka, F.; Nishina, Y.; Shiga, K. *J. Phys. Chem. B* **2000**, *104*, 10667−10677.

(23) Zhong, D.; Zewail, A. H. *Proc. Natl. Acad. Sci. U. S. A.* **2001**, *98*, 11867−11872.

(24) Chaves, I.; Pokorny, R.; Byrdin, M.; Hoang, N.; Ritz, T.; Brettel, K.; Essen, L.-O.; van der Horst, G. T. J.; Batschauer, A.; Ahmad, M. *Annu. Rev. Plant Biol.* **2011**, *62*, 335−364.

(25) Laptenok, S. P.; Bouzhir-Sima, L.; Lambry, J.-C.; Myllykallio, H.; Liebl, U.; Vos, M. H. *Proc. Natl. Acad. Sci. U. S. A.* **2013**, *110*, 8924−8929.

(26) Yang, H.; Luo, G.; Karnchanaphanurach, P.; Louie, T.-M.; Rech, I.; Cova, S.; Xun, L.; Xie, X. S. *Science* **2003**, *302*, 262−266.

(27) Brazard, J.; Usman, A.; Lacombat, F.; Ley, C.; Martin, M. M.; Plaza, P.; Mony, L.; Heijde, M.; Zabulon, G.; Bowler, C. *J. Am. Chem. Soc.* **2010**, *132*, 4935−4945.

(28) Hamdane, D.; Argentini, M.; Cornu, D.; Myllykallio, H.; Skouloubris, S.; Hui-Bon-Hoa, G.; Golinelli-Pimpaneau, B. *J. Biol. Chem.* **2011**, *286*, 36268−36280.

(29) Urbonavicius, J.; Skouloubris, S.; Myllykallio, H.; Grosjean, H. *Nucleic Acids Res.* **2005**, *33*, 3955−3964.

(30) Nishimasu, H.; Ishitani, R.; Yamashita, K.; Iwashita, C.; Hirata, A.; Hori, H.; Nureki, O. *Proc. Natl. Acad. Sci. U. S. A.* **2009**, *106*, 8180−8185.

(31) Pettersen, E. F.; Goddard, T. D.; Huang, C. C.; Couch, G. S.; Greenblatt, D. M.; Meng, E. C.; Ferrin, T. E. *J. Comput. Chem.* **2004**, *25*, 1605−1612.

(32) Laptenok, S. P.; Nuernberger, P.; Lukacs, A.; Vos, M. H. In *Methods in Molecular Biology, Fluorescence Spectroscopy and Microscopy: Methods and Protocols*; Engelborghs, Y., Visser, A. J. W. G., Eds.; Humana Press: New York, 2014; p 321−336, Vol. *1076*.

(33) Lambry, J.-C.; Stranava, M.; Lobato, L.; Martinkova, M.; Shimizu, T.; Liebl, U.; Vos, M. H. *J. Phys. Chem. Lett.* **2016**, *7*, 69−74.

(34) Snellenburg, J. J.; Laptenok, S. P.; Seger, R.; Mullen, K. M.; van Stokkum, I. H. M. *J. Stat. Software* **2012**, *49*.

(35) Hamdane, D.; Bruch, E.; Un, S.; Field, M.; Fontecave, M. *Biochemistry* **2013**, *52*, 8949−8956.

(36) Hamdane, D.; Argentini, M.; Cornu, D.; Golinelli-Pimpaneau, B.; Fontecave, M. *J. Am. Chem. Soc.* **2012**, *134*, 19739−19745.

(37) Ghisla, S.; Massey, V.; Lhoste, J.-M.; Mayhew, S. G. *Biochemistry* **1974**, *13*, 589−597.

(38) Brazard, J.; Usman, A.; Lacombat, F.; Ley, C.; Martin, M. M.; Plaza, P. *J. Phys. Chem. A* **2011**, *115*, 3251−3262.

(39) Kao, Y.-T.; Saxena, C.; He, T.-F.; Guo, L.; Wang, L.; Sancar, A.; Zhong, D. *J. Am. Chem. Soc.* **2008**, *130*, 13132−13139.

(40) Bensasson, R.; Land, E. J.; Truscott, T. *Flash Photolysis and Pulse Radiolysis: Contributions to the Chemistry of Biology and Medicine*; Pergamon Press: Oxford, 1983.

(41) Liu, B.; Liu, H.; Zhong, D.; Lin, C. *Curr. Opin. Plant Biol.* **2010**, *13*, 578−586.

(42) Gadosy, T. A.; Shukla, D.; Johnston, L. J. *J. Phys. Chem. A* **1999**, *103*, 8834−8839.

(43) Parson, W. W. *Modern Optical Spectroscopy*; Springer: Berlin, 2007.

(44) Byrdin, M.; Villette, S.; Espagne, A.; Eker, A. P. M.; Brettel, K. *J. Phys. Chem. B* **2008**, *112*, 6866−6871.

(45) Lim, M. *Bull. Korean Chem. Soc.* **2002**, *23*, 865−872.

(46) Sjödin, M.; Styring, S.; Wolpher, H.; Xu, Y.; Sun, L.; Hammarström, L. *J. Am. Chem. Soc.* **2005**, *127*, 3855−3863.

(47) Aubert, C.; Mathis, P.; Eker, A. P. M.; Brettel, K. *Proc. Natl. Acad. Sci. U. S. A.* **1999**, *96*, 5423−5427.

(48) Martinez-Rivera, M. C.; Berry, B. W.; Valentine, K. G.; Westerlund, K.; Hay, S.; Tommos, C. *J. Am. Chem. Soc.* **2011**, *133*, 17786−17795.

(49) Miura, R. *Chem. Rec.* **2001**, *1*, 183−194.

(50) Winkler, J. R.; Gray, H. B. *J. Am. Chem. Soc.* **2014**, *136*, 2930−2939.

(51) Mathes, T.; van Stokkum, I. H. M.; Stierl, M.; Kennis, J. T. M. *J. Biol. Chem.* **2012**, *287*, 31725−31738.

(52) Fujisawa, T.; Takeuchi, S.; Masuda, S.; Tahara, T. *J. Phys. Chem. B* **2014**, *118*, 14761−14773.

(53) Gauden, M.; van Stokkum, I. H. M.; Key, J. M.; Lührs, D. C.; van Grondelle, R.; Hegemann, P.; Kennis, J. T. M. *Proc. Natl. Acad. Sci. U. S. A.* **2006**, *103*, 10895−10900.

(54) Lukacs, A.; Brust, R.; Haigney, A.; Laptenok, S. P.; Addison, K.; Gil, A.; Towrie, M.; Greetham, G. M.; Tonge, P. J.; Meech, S. R. *J. Am. Chem. Soc.* **2014**, *136*, 4605−4615.

(55) Goyal, P.; Hammes-Schiffer, S. *Proc. Natl. Acad. Sci. U. S. A.* **2017**, *114*, 1480−1485.

F

Titre : Dynamique interne des flavoprotéines étudiées par spectroscopie femtoseconde

Mots clés : spectroscopie femtoseconde, protéine, tyrosine, absorption, fluoresence, optique

Résumé : Le transfert de charges dans les protéines s'effectue souvent par la formation d'intermédiaires radicalaires. On pense que les radicaux acides aminés de la tyrosine (TyrOH) et du tryptophane jouent un rôle important en tant qu'intermédiaires dans les réactions de transfert de charge intra et interprotéine. Les radicaux tryptophanyles ont déjà été caractérisés à la fois sous la forme neutre et sous la forme cationique protonnée. Par contre, les radicaux tyrosyles n'ont été caractérisés que sous la forme neutre déprotonnée.

Dans ce travail, les radicaux d'acides aminés et de flavines dans les protéines ont été étudiés par spectroscopie femtoseconde. Nous avons caractérisé des intermédiaires formés lors de réactions de transfert de charge non fonctionnelles dans les flavoprotéines. Les états excités et les états produit formés dans les formes sauvages et modifiés de la flavoenzyme méthyltransférase TrmFO de Thermus thermophilus ont été étudiés. Un état produit transitoire observé dans le mutant C51A a permis la toute première caractérisation du radical tyrosyle protonné TyrOH$^{\bullet+}$. Nous avons observé que cette espèce a une bande d'absorption visible distincte à environ 490 nm et un moment de transition suggéré proche de l'axe de symétrie du phénol. TyrOH$^{\bullet+}$ est formé dans 1 ps par transfert d'électrons à la flavine excitée et disparait par recombinaison de charges en 3 ps.

Ensuite, l'intermédiaire TyrOH$^{\bullet+}$ a été caractérisé dans les photoproduits complexes de la flavoprotéine prototypique glucose oxydase (GOX) d'Aspergilus niger. Il a été observé que son empreint spectral (absorption 490 nm) est similaire à celui de l'intermédiaire dans C51A TrmFO. Notamment, la visualisation du radical TyrOH$^{\bullet+}$ protonné dans TrmFO C51A et dans GOX suggère la possibilité de sa formation intermédiaire en tant que précurseur du TyrO$^{\bullet}$ dans des réactions biochimiques fonctionnelles. Enfin, dans TrmFO, la construction de variantes spécifiques par la mutagenèse dirigée a été entamée afin d'étudier la flexibilité du site actif en utilisant les taux de transfert d'électrons comme marqueurs conformationnels. D'autres travaux expérimentaux et de modélisation seront nécessaires pour atteindre cet objectif.

Title : Internal dynamics of flavoproteins studied using femtosecond spectroscopy

Keywords : femtosecond spectroscopy, proteins, tyrosine, absorption, fluorescence, optics

Abstract : Charge transfer in proteins often proceeds via formation of radical intermediates. The amino acid radicals of tyrosine (TyrOH) and tryptophan are thought to play important roles as intermediates in intra- and interprotein charge transfer reactions. Tryptophanyl radicals have been characterized before in both neutral and the cation protonated forms. However, tyrosyl radicals have been characterized only in the neutral deprotonated form.

In this work, amino acid and flavin radicals in proteins have been investigated using femtosecond spectroscopy. We have characterized intermediates formed in non-functional charge transfer reactions in flavoproteins. Excited states and product states formed in the wild type and mutant forms of the methyltransferase flavoenzyme TrmFO from Thermus thermophilus were investigated. A transient product state observed in the mutant C51A led to the first-ever characterization of the protonated tyrosyl radical TyrOH$^{\bullet+}$. We observed this speciesto have a distinct visible absorption band at 490 nm and a transition moment that is suggested to lie close to the phenol symmetry axis. TyrOH$^{\bullet+}$ is formedin 1 ps by electron transfer to excited flavin and decays in 3 ps bycharge recombination.

Subsequently, the TyrOH$^{\bullet+}$ intermediate was characterized in the complex photoproducts of the prototypical flavoprotein glucose oxidase (GOX) from Aspergilus niger. It was observed to have a similar spectral signal (absorption 490 nm) as the intermediate in C51A TrmFO. Importantly, the visualization of protonated TyrOH$^{\bullet+}$ radical in TrmFO C51A and GOX suggests the possibility of its intermediate formation as a precursor of TyrO$^{\bullet}$ in functional biochemical reactions. Finally, in TrmFO the construction of specific variants with site-directed mutagenesis was initiated to study active-site flexibility using electron transfer rates as conformational markers. Further experimental and modeling work is required to pursue this goal.